DE-FC26-07NT43096

Computational Modeling and Assessment Of Nanocoatings for Ultra Supercritical Boilers

Task 3 Technical Report

Processing of Advanced MCrAl Nanocoating Systems

August 14, 2009

Electric Power Research Institute
Project Managers—David W. Gandy, John P. Shingledecker
davgandy@epri.com, jshingledecker@epri.com

Principal Investigators
Southwest Research Institute
Foster Wheeler North America
Applied Films

CITATIONS

This report was prepared by:

Southwest Research Institute®
6220 Culebra Road
San Antonio, TX 78238

Principal Investigators
N. S. Cheruvu
R. Wei

ABSTRACT

Forced outages and boiler unavailability in conventional coal-fired fossil power plants is most often caused by fireside corrosion of boiler waterwalls. Industry-wide, the rate of wall thickness corrosion wastage of fireside waterwalls in fossil-fired boilers has been of concern for many years. It is significant that the introduction of nitrogen oxide (NO_x) emission controls with staged burners systems has increased reported waterwall wastage rates to as much as 120 mils (3 mm) per year. Moreover, the reducing environment produced by the low-NO_x combustion process is the primary cause of accelerated corrosion rates of waterwall tubes made of carbon and low alloy steels. Improved coatings, such as the MCrAl nanocoatings evaluated here (where M is Fe, Ni, and Co), are needed to reduce/eliminate waterwall damage in subcritical, supercritical, and ultra-supercritical (USC) boilers. The first two tasks of this six-task project-jointly sponsored by EPRI and the U.S. Department of Energy (DE-FC26-07NT43096)-have focused on computational modeling of an advanced MCrAl nanocoating system and evaluation of two nanocrystalline (iron and nickel base) coatings, which will significantly improve the corrosion and erosion performance of tubing used in USC boilers. The computational model results showed that about 40 wt.% is required in Fe based nanocrystalline coatings for long-term durability, leading to a coating composition of Fe-25Cr-40Ni-10 wt.% Al. In addition, the long term thermal exposure test results further showed accelerated inward diffusion of Al from the nanocrystalline coatings into the substrate. In order to enhance the durability of these coatings, it is necessary to develop a diffusion barrier interlayer coating such TiN and/or AlN. The third task "***Process Advanced MCrAl Nanocoating Systems"*** of the six-task project-jointly sponsored by the Electric Power Research Institute, EPRI and the U.S. Department of Energy (DE-FC26-07NT43096)- has focused on processing of advanced nanocrystalline coating systems and development of diffusion barrier interlayer coatings. Among the diffusion interlayer coatings evaluated, the TiN interlayer coating was found to be the optimum one. This report describes the research conducted under the Task 3 workscope.

EXECUTIVE SUMMARY

Fireside corrosion of boiler waterwalls continues to be the number one issue resulting in forced outages and boiler unavailability for conventional coal-fired fossil power plants. Several types of coatings and weld overlays have been used to extend the service life of boiler tubes. The coatings and weld overlays offered protection for only a limited time 1 to 8 years in subcritical boilers. Accelerated and sever fireside corrosion in ultra-supercritical (USC) boiler waterwalls is anticipated to be a primary concern since these boilers operate at a much higher temperature and pressure (760°C @ 35 MPa) then subcritical (538°C @ <22 MPa) or supercritical (565°C @ 24 MPa) boilers. Improved coatings or claddings are desperately needed by the industry to reduce/eliminate waterwall damage by mitigating fireside corrosion. As such, highly reliable coatings are desirable for USC alloys to mitigate corrosion while maintaining the improved strength.

The MCrAl-type coatings have been successfully used for oxidation and sulfidation protection of hot section components of gas turbines that operate at a much higher temperature. The MCrAl-type coatings exhibit excellent oxidation and corrosion resistance at the operating metal temperatures for up to a least 950°C. The performance of the MCrAl coatings can be significantly enhanced by depositing the coatings using advanced processing techniques that produce nanoscale microstructure. Short-term results published in the literature show that the corrosion and oxidation resistance of nanocrystalline coatings is significantly better than the conventional coatings with the same chemical composition. For a given Cr or Al concentration, nanoscale coatings exhibit 5 to 10 times longer life than the conventional coatings since the critical Cr or Al concentration required for the formation of a protective oxide layer, chromia (Cr_2O_3) or alumina (Al_2O_3) is expected to be significantly lower in the nanocrystalline coatings as compared to the conventional coatings. However, the chemical composition and processing parameters need to be optimized for these advanced coatings either by the trial and error method or using computational methods. Since the trial and error method is costly and time consuming, it is appropriate to use computer simulation methods to speed up the nanocrystalline coating development.

Last year under Task 1, computational modeling efforts have been undertaken to design and assess potential Fe-Cr-Ni-Al systems to produce stable nanocrystalline coatings that form a protective, continuous scale of Al_2O_3 or Cr_2O_3. Phase diagram computation was performed using Thermo-Calc® software to generate pseudo-ternary phase diagrams for the design of Fe-Cr-Ni-Al nanocrystalline coatings. The computational results identified a new series of Fe-Cr-Ni-Al nanocrystalline coatings that maintain long-term stability by forming a diffusion barrier layer at the coating/substrate interface.

Under Task 2, long-term cyclic oxidation tests were performed on Fe-18Cr-8Ni-xAl (where x = 0, 4, 10 wt.%) and Ni-20Cr-xAl (where x = 4, 7, 10 wt.%) coated and uncoated samples. The Fe-18Cr-8Ni-xAl nanocrystalline coatings were applied on 304 L stainless steel and P91 steel samples and Ni-20Cr-xAl coatings were applied on 304 SS and Haynes 230 substrate samples. The Fe-based coatings were tested at a peak temperature of 750°C, while the Ni-based coatings tested at two peak temperatures, 750°C and 1010°C. The results of these tests demonstrated that nanocrystalline coatings showed significant improvement in cyclic oxidation resistance. Following cyclic oxidation testing, metallurgical analysis results showed that for long-term durability, the nanocrystalline coatings should contain at least 7 wt.% Al and the coating fine grain structure accelerated the kinetics of inward and outward diffusion of Al, suggesting that a diffusion barrier interlayer coating is required to increase the durability of these coatings.

In the initial stages of Task 3, the emphasis was placed on understanding the influence of the deposition parameters on the microstructure of the coating. The critical parameters for the deposition include the deposition time, magnetron power for each target, worktable bias voltage (ion energy delivered to the film surface), and discharge current and the worktable bias current (both for the ion flux). A set of experiments were conducted and the samples coated were evaluated for microstructure, coating adhesion, and toughness. Based on these results, the process parameters of bias voltage of Vb = 60V with discharge current of Ib = 15A were selected for deposition of advanced coatings.

Considering the computation model results and the reliable MCrAl type coatings used for the hot section parts of a gas turbine, two iron base (Fe-Cr-Ni), a nickel base (Ni-Cr-Co), and a cobalt base (Co-Cr-Ni) MCr systems with 10 wt.% Al were selected for further evaluation. For deposition of these advanced coatings, four different MCr (310SS, Haynes 120, Haynes 160, and Haynes 188) targets were procured. The advanced coatings were deposited using the selected process parameters described above. Detailed metallurgical evaluations of as coated samples revealed coating defects such as cracking and “cauliflower –like looking” nodules with interface delamination. A new deposition method, High Power Impulse Magnetrons Sputtering (HIPIMS), was used to investigate whether this process produces crack free dense coatings. This process produced crack free coatings, but the coatings were found to be extremely brittle. Several coating trials were conducted by controlling the process parameters of plasma enhanced magnetron sputtering process (PEMS). These deposition trials showed that crack free coatings can be produced using low deposition rates. The effect of deposition rates and bias voltage (bombardment) on formation of nodules on the surface of the coating is being investigated.

Three ceramic coatings, TiN, TiSiCN and AlN, were selected for evaluation as the barrier interlayer coating. Long-term cyclic oxidation tests were performed at 750º and 1010ºC and the results showed that the thermal cycling did not lead to the diffusion interlayer coating spallation. However long-term thermal exposure resulted in disintegration of AlN interlayer.
In contrast, the TiN and the TiSiCN showed no degradation after long-term exposure at both temperatures. Among the three interlayer coatings evaluated, the TiN inter layer coating was considered to be the optimum one for both iron and nickel base coating systems. The coating process optimization study is being conducted for depositing TiN on the substrate alloys.

PROJECT TASKS AND GOALS

The goal of this project is to improve the reliability and availability of fossil-fired USC boilers and oxy-fuel combustor systems by developing advanced nanostructured coatings that are optimized utilizing science-based computational methodologies and validated via experimental verification and testing in simulated boiler environments in three different coal conditions and temperatures. The objective of the project is to develop and demonstrate nanostructured coatings through computational modeling methods that will significantly improve corrosion and oxidation performance of tubing used in ultra-supercritical boiler applications.

To achieve these goals, six tasks have been identified for this project. Each task is listed below along with the objective for that task:

Task 1. Computational Modeling of MCrAl Systems – Potential MCrAl nanostructured coating compositions will be selected through computational modeling using: A0 a full-potential linear-augmented planewave code (WIENK) to predict energy formation, b) CALPHAD and Thermo-Calc to develop pseudo-ternary phase diagrams, c) a grain growth model to examine nanostructure phase stability, and d) a fracture mechanics-based model to predict tensile ductility, fracture toughness, and interface toughness of MCrAl coatings.

Task 2. Establishment of Baseline Coating Data – Conventional coatings and existing nanocoatings will be procured and evaluated via metallurgical, thermal fatigue, bond strength, and erosion testing for comparison with advanced nanostructured coatings selected under Task 1.

Task 3. Process Advanced MCrAl Nanocoating Systems – Selected nanostructured coatings will be applied on up to four USC substrate alloys, evaluated via metallurgical, thermal fatigue, bond strength, and erosion testing, and then compared to the conventional coatings evaluated in Task 2. Results will be compared to computational model predictions.

Task 4. Fireside Corrosion Testing – Accelerated laboratory tests will be performed on the conventional and advanced nanostructured coated specimens produced in Tasks 2 and 3 at three temperatures under three different coal conditions. The exposed coated specimens will be characterized to assess the extent of corrosion attack.

Task 5. Computational Modeling and Validation – Computational modeling will be used to validate the phases predicted for select alloy compositions. Additionally, heat transfer characteristics of each coating/alloy substrate combination will be evaluated with the objective of offering improved heat transfer over conventional coatings/weld overlays. Coating life model will be developed based on Al and/or Cr depletion.

Task 6. Nanostructured Coatings Mock-Up Demonstration – Nanostructured coatings will be applied to waterwall panels using state-of-the-art magnetron sputtering equipment. Following application of the coating, metallurgical analysis will be performed to assess the quality of the coating and its bond strength.

This report provides the results of Tasks 3 generated through July, 2009.

BACKGROUND

Fireside corrosion of waterwalls continues to be the number one issue resulting in forced outages and boiler unavailability for conventional coal-fired fossil power plants. The rate of wall thickness corrosion wastage of fireside waterwalls in fossil fired boilers has been a concern for many years. The introduction of nitrogen oxide (NO_x) emission controls with the staged burners systems increased waterwall wastage rates of 120 mils (3 mm) a year have been reported [1]. The cause of accelerated corrosion rates of waterwall tubes made of carbon and low alloy steels is the reducing environment produced by the low NO_x combustion process. The extent of corrosion attack of is shown in Figure 1. Improved coatings or claddings to mitigate fireside corrosion are desperately needed by the industry to reduce/eliminate waterwall damage in sub and supercritical boilers.

Figure 1
Photographs of waterwall and a cross section of tubes showing the extent of corrosion and wall-thickness wastage.

Several studies conducted by EPRI have shown [2-4] that the corrosion deposits on the waterwalls of coal fired sub- and super-critical boilers predominantly contain iron sulfide (FeS) and alkali chloride. The deposition of FeS and alkali chloride will occur under reducing conditions. Under such conditions protective oxide scale Fe_3O_4 will not form on the waterwall

tubes, but promotes the formation of less protective FeS-rich scale. The formation of FeS scale or deposits will lead to pronounced subsequent corrosion under oxidizing or reducing environments. The cause of corrosion is usually the formation of alkali iron trisulfates on the tube surfaces. The presence of the low melting point alkali aluminum sulfates also causes this type of corrosion.

It is well known that the presence of deposits and cyclic operating environment accelerate corrosion rates. Laboratory tests conducted by EPRI and others [2-4] showed that low alloy steel samples when covered with deposits containing FeS, fly ash, and unburned carbon exhibited significantly higher corrosion rates compared to deposit free samples. In addition, cyclic-operating conditions where the boiler environment alternates between the oxidation and reducing conditions further increase corrosion rates. Mathematical models were developed using the laboratory data for predicting the corrosion rates for the boiler tubes [3].

Earlier EPRI field survey showed that the corrosion rates in sub-critical boilers are much lower compared to those in super-critical boilers. Typical wastage rates for subcritical and supercritical boilers are 20 mils/yr and 40-100 mils, respectively (3). The higher operating metal temperatures in super-critical boiler tubes increased corrosion rates by a factor of two to five.

Austenitic stainless steels typically exhibit poor sulfidation or coal ash corrosion resistance. Thus, reliable sulfidation and oxidation resistant coatings are required for improved durability of USC boiler tubes under aggressive operating conditions. To ameliorate the adverse effects of corrosion, such as forced outages and costly premature waterwall replacements, surface protective technologies, such as weld overlays and thermal spray coatings have been used in sub and supercritical boilers. It is well known that the oxidation and sulfidation resistance of steels and superalloys increases with their chromium (Cr) content. Small amounts of silicon (Si) and aluminum additions to Cr containing steels are beneficial. The published results (3) showed that minimum 12 wt.% Cr is required for the onset of reduction in corrosion rates. The corrosion loss becomes almost insignificant when the Cr content in the steel exceeded 20 wt.%.

Since it is not cost effective to use high chromium stainless steels as waterwall tubes, two major surface modification technologies have been developed and are commercially available: weld overlays and thermal spray coatings. Primarily Ni Cr and Fe-Cr thermal spray coatings are used in the industry. Thermal spray coatings and weld overlays were field tested in Hatfield's Ferry #2 supercritical boiler (5). The field test results showed that claddings containing at least 25 wt.% Cr provided excellent corrosion protection. This minimum Cr requirement is consistent with recent results generated by Foster Wheeler/EPRI under a DOE- sponsored program. Additions of Cr (20 to 25 wt.%) to both stainless steel and nickel alloys provide excellent coal ash corrosion resistance. At these higher chromium levels, both steels and Fe-based coatings are susceptible to embrittlement after service exposure at operating temperature around 450°C. The embrittlement leads to loss of toughness and ductility. Thus, addition of 20 to 25 wt.% Cr to Fe base coatings is not a viable option.

The field test results also have shown that the coatings exhibited relatively short life ranging 1 to 8 years in sub-critical boilers [6,7]. The post-service metallurgical evaluations of the coated boiler tubes showed that the coating failure was due to sulfidation attack penetrating in to the

substrate leading to coating debonding/spalling. The coating life variability (1 to 8 years) was attributed to variations in the pre-coating surface preparations and coating application procedures [6]. In addition, field experience suggests that thermal spray (Fe-Cr) coatings are more appropriate for application in sub-critical boilers rather than supercritical boilers. Supercritical boiler waterwall tubes operate around 425°C. Reliable performance of these coatings in USC boiler environments is questionable. Hence there is a need to optimize chemistry of the coatings for application of USC boilers and to enhance their durability.

Iron-aluminum (Fe-Al) alloys have been considered as coatings for the protection of waterwall tubes in coal fired USC boilers because these alloys exhibit excellent corrosion resistance in a wide range of high temperature environments. Published results [7,8,] have also shown that increasing the aluminum content increases the corrosion resistance of the Fe-Al alloy in a high temperature environment containing oxygen and sulfur. For good corrosion protection in oxygen and sulfur bearing environments, it has been shown that the Fe-Al alloy should contain approximately 10 wt.% aluminum. Aluminum helps to from a passive protective layer, Al_2O_3, which acts as a barrier between the corrosive gas and the substrate material. Chromium additions up to 5 wt.% have also been shown to improve the corrosion resistance of Fe-Al alloy or aluminides. It was reported that FeAlCr overlay compositions out performed Ni-based in long-term testing [9,10-12]. The Fe 10 wt.% Al-5Cr alloy is reported to be completely protective in simulated low NO_x for 2000 hours of exposure as shown in Figure 2 [11].

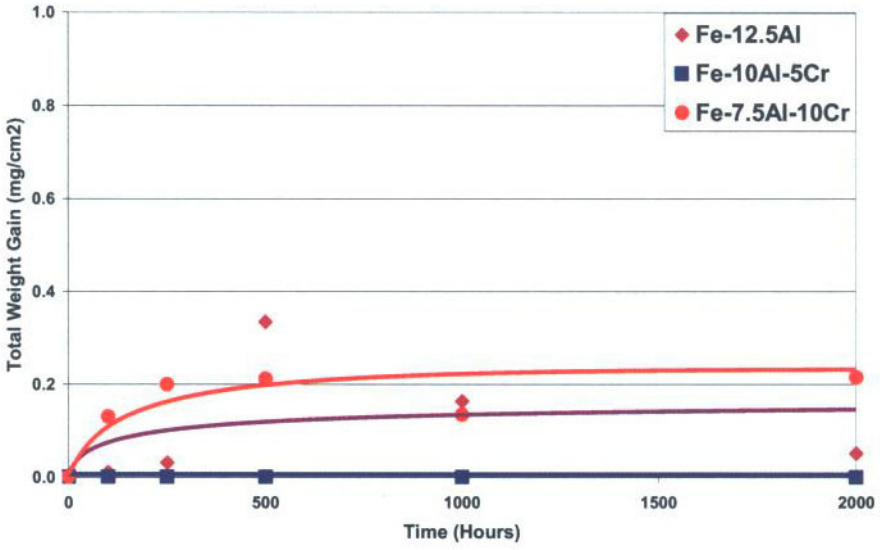

Figure 2
Corrosion behavior of Fe-Al (Cr) alloys in simulated low NO_x environment [11].

As mentioned earlier, it is not possible to add minimum required levels of about 25 wt.% Cr to the iron base coatings for service induced embrittlement reasons. However, higher amounts Cr can be added to a Ni-base system. Increased Cr concentration promotes the formation of a pure Cr_2O_3 protective layer without the presence of any other oxides of elements (like Fe, Ni, or Co, etc.). The pure Cr_2O_3 has a very low solubility in the molten phase. As a result, the presence of protective Cr_2O_3 surface layer exhibit superior coal ash corrosion resistance. The NiCrAl-type

coating have been successfully used for oxidation and sulfidation protection of hot section components of gas turbines [13] for over 30 years. Based on the field and laboratory results published in the literature MCrAl (where M is Fe, Ni or both) type coatings appeared to be the candidate coatings for USC boiler applications.

The performance of the MCrAl coatings can be significantly enhanced by depositing the coatings using advanced processing techniques that produce nanoscale microstructure. It has been shown [15,16] that nanocoatings performed significantly better than conventional coatings. The critical Cr_2O_3 and Al_2O_3 needed to form protective layer are significantly lower in nanostructured coatings as compared to the conventional coarse grained coatings. The critical Cr or Al concentration required for the formation of a protective Cr_2O_3 and Al_2O_3 layer is expected to be significantly lower in nanoscale coatings as compared to conventional coatings [15-17]. For a given Cr or Al concentration, nanoscale coatings exhibit longer life than the conventional coatings. However, the chemical composition and processing parameters need to be optimized for these advanced coatings either by trail and error method or using computational methods. Since the trail and error method is costly and time consuming, it is appropriate to use computer simulation methods to speed-up the nanostructured coating and process development.

CONTENTS

LIST OF FIGURES

LIST OF FIGURES (cont)

LIST OF FIGURES (cont)

LIST OF TABLES

1
TASK 3: PROCESS ADVANCED MCrAl NANOCOATING SYSTEM

Process Advanced Nanocoatings

Plasma enhanced magnetron sputter (PEMS) deposition technique was used to process advanced nanocrystalline coatings. PEMS is an advanced variation of conventional sputter deposition process, which falls into the family of physical vapor deposition (PVD). In the following sections, background on the principle of conventional magnetron sputtering, the discussion of the PEMS process, a brief summary of the process optimization study for the deposition of the advanced nanocrystalline-coatings, selection and application of advanced coatings for corrosion testing, process optimization studies to improve the quality of the as deposited coating, and development of diffusion barrier interlayer coatings are presented.

Conventional Magnetron Sputtering

In conventional magnetron sputter deposition (Figure 1.1a) parts are installed on a worktable inside a vacuum chamber between the magnetrons. In typical production deposition systems, four or even more magnetrons are used. A magnetron mainly consists of a solid metal plate commonly called target, which is used as the source of material for the coating to be formed on the parts, and magnets behind the target, which are arranged in such a way as to enhance the plasma production. After the vacuum system is pumped down, argon (Ar) gas is first fed into the vacuum chamber to reach a pressure of a few milli-torrs. When a negative voltage of a few hundreds of volts is applied to the magnetron, glow discharge plasma (designated as magnetron plasma) is generated. Plasma is defined generically as the discharged gas with ions, electrons and excited neutrals. The negatively biased voltage also draws Ar ions from the plasma to the target. The high energy ion bombardment (at a few hundred eV) results in sputtering of the target material. The sputtered atoms and clusters, a fraction of which are ionized in the plasma, arrive to the sample surface where rapid solidification occurs, thereby forming a metallic coating.

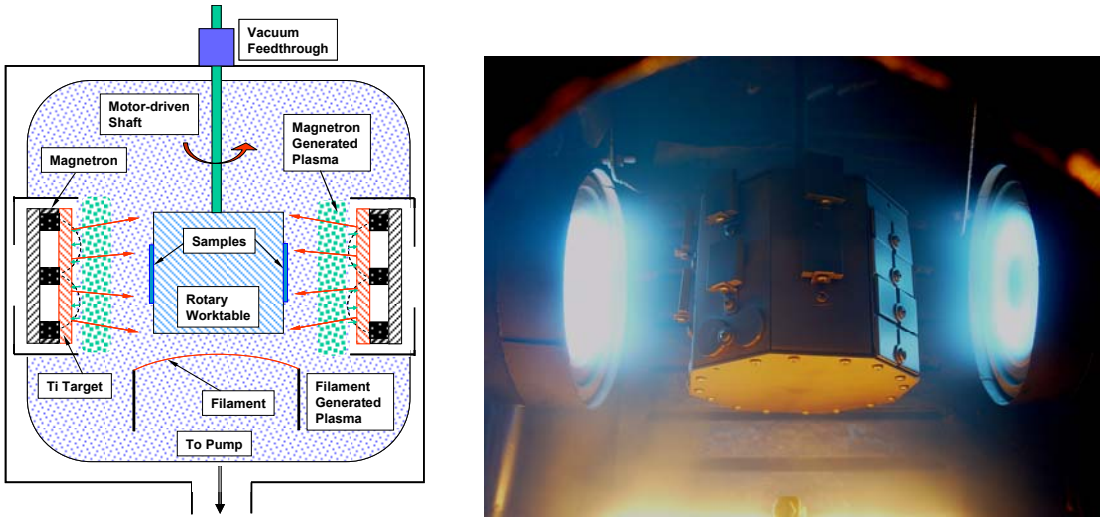

Figure 1.1
(a) SwRI PEMS system schematic and (b) a photograph of the PEMS process.

If the target material is made of only one element and all magnetrons used are of the same material, a single layered pure metallic coating of the target material will be deposited. If the target material is made of an alloy, a single-layered alloy coating will be obtained. Typically, the composition of the coating will be similar to that of the target(s). However, the microstructure of the coating (phases, grain size, etc) will be different from that of the target, which will be discussed in a later section. The coating typically exhibits a non-equilibrium structure. If the target material is made of an alloy but each magnetron has a different alloy target, a complex coating structure could be obtained. When the worktable rotates at a low speed, and/or if the deposition rate is high (high target power), a multi layered coating may be formed. Each layer corresponds to each target material. If the rotation speed is high, and/or if the deposition rate is low, the layered structure may not be distinguishable, while the coating contains all elements from all targets. During the deposition, a negative voltage is commonly applied to the worktable to draw ions from the plasma. Application of negative voltage densifies the coating. The ion bombardment will also increase the mixing of the depositing materials and further densifies the coating.

Because this deposition process is a non-equilibrium process, a new alloy with multi-elements or multi-layers that cannot be obtained from conventional metallurgy can be achieved. For instance, considering a simple binary alloy consisting of tungsten (W) and silver (Ag), it is difficult to obtain the alloy using conventional metallurgy methods because of the large difference in the melting point. But it can be done fairly easily using the deposition technique discussed above. As discussed above, when metallic atoms and clusters arrive at the surface, a solid film is formed due to rapid quenching. The film thus formed usually has a columnar structure with many voids because the surface temperature of the parts is typically very low, much lower than melting point of the target material. The atoms and clusters that have arrived at the surface do not have enough energy to diffuse, thereby shadowing the incoming atoms and clusters and forming voids. It has been observed during the film growth, if a high flux of ions at some energy levels is used to bombard the film, the coating can be densified.

Plasma Enhanced Magnetron Sputter (PEMS) Deposition

The development of the Southwest Research Institute® (SwRI®) PEMS technology is to produce a dense and defect free coating. In the PEMS system as shown in Figure 1.1a, a tungsten filament is introduced for the plasma enhancement. When the filament is heated the thermionic temperature via an AC power supply, electrons are emitted from the filament. By applying a positive DC voltage to the vacuum chamber wall with respect to the filament, the electrons will be accelerated to the chamber wall. Due to the presence of Ar, electron-neutral impact ionization occurs. Thus, a filament-plasma is generated, in addition to the magnetron plasma that is generated only in front of the magnetron.

Because the filament-plasma is generated from the entire volume of the vacuum chamber, the ion flux obtained at the part surface is much higher (about 25 times) than that obtained from the magnetron plasma alone. The enhanced ion bombardment greatly increases the film density and reduces the grain size to a few tens of nanometers. As a result, the coatings exhibit superior properties.

Deposition of MCrAl

Currently, two PEMS systems are available at SwRI, a small one with two magnetrons (as shown in Figure 1.1b) for process development and a large one (1 m^3) with four magnetrons for prototype scale up. The samples for this DOE program have been prepared in the small deposition system. In this system, one magnetron is used for Al deposition while the other is for the MCr deposition. For example, if a 310 SS target is used, a coating with the composition of Fe25Cr20Ni can be obtained. By adjusting the target powers of the 310 SS and Al targets, various compositions in the form of $(Fe25Cr20Ni)_{1-x}Al_x$, where x = 0 to 1, can be obtained. If the 310 SS target is replaced with a different alloy, Ni20Cr for instance, a coating with the composition of $(Ni20Cr)_{1-x}Al_x$ can be obtained.

In this project, rectangular samples with a drilled hole on each end were used. Then the samples were tied using stainless steel wires and hung between the magnetrons. Figure 1.2 is a photograph of the deposition system with samples that are being deposited with Haynes 160 (H160) alloy (Ni29Co28Cr) target on the right and Al target on the left. As can be seen, a total of six chains (columns) are mounted on a main rotary fixture, which rotates at a speed of 6 rpm. In addition, each chain is hung on a sprocket which also rotates around its axis. This double-rotation system is used to increase the uniform coverage of the coating on the samples.

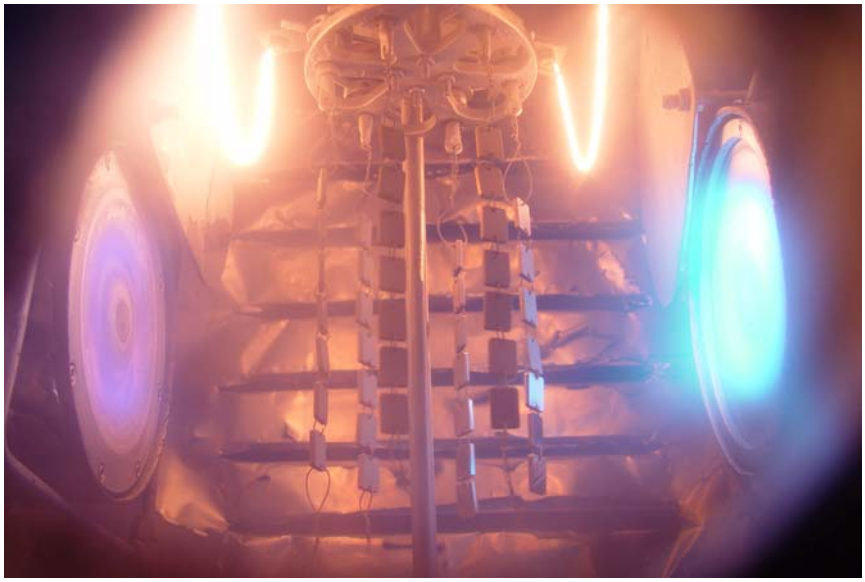

Figure 1.2
Deposition of MCrAl using PEMS process.

Shown in Figure 1.2 are six chains of samples made of three materials (304 SS, P91 and Haynes 230) and two chains for each kind to study the oxidation resistance of the coating on various materials. Hung on each chain are seven samples; therefore a total of 42 samples were being deposited. This setup allows deposition of fairly uniform coating on all six surfaces of each sample except the inner surface of holes and the areas covered by the stainless steel wires. It is evident from Figure 1.2 that the magnetron plasma in front of the H160 target is much stronger than that of the Al target. The strength of the plasma in front of a target is directly related to the sputtering power applied to the target. In this case, a power of 4kW and 1.3 kW was used for sputtering of H160 and Al targets, respectively. The power ratio resulted in deposition of $(Ni29Cr28Co)_{0.89}Al_{0.11}$ coating. As can be seen from the photograph, two W filaments hung from the top of the chamber were used to generate the filament-plasma, while the rotary fixture and hence the parts were biased with a DC power supply at -40V to achieve the enhanced ion bombardment.

Development of Process Variables

In the early stages of the study, the emphasis was placed on understanding the influence of the deposition parameters on the microstructure of the coating. The goal was to obtain dense, uniform coatings. Because there are number of parameters that affect the quality of the coating, the task would be insurmountable if the effect of each parameter were to be studied. The coating deposition process typically consists of two stages; the first one is the ion sputter cleaning of the sample surface and second stage is the coating deposition. Adequate ion sputter cleaning is to guarantee the sample surface free from oxide scale. Presence of the scale adversely affects adhesion of the subsequently deposited coating. Steels and other nickel based alloys typically require 90 minutes ion sputter cleaning using 120V bias at a discharge current of 10A. Therefore, the same parameters were used for cleaning the samples in this study. Our early studies showed that a few processing variables were found to be more critical than the others for the coating

deposition. The critical parameters for the deposition include the deposition time, magnetron power for each target, worktable bias voltage (ion energy delivered to the film surface), and discharge current and the worktable bias current (both for the ion flux). Based on this knowledge, a set of experiments were designed as shown in Table 1.1. Listed in Column 1 is the sample number, Column 2 the deposition duration, Column 3 target 1 material (Al), Column 4 the magnetron power for target 1, Column 5 target 2 material, Column 6 the power for target 2, Column 7 the voltage applied to the worktable, Column 8 the current obtained on the worktable, and Column 9 the discharge current (related to the ion flux).

Table 1.1
Summary of Process Variables Investigated and the Properties of the Coatings Applied using Different Process Variables

Sample No.	Deposit Time (h)	T1 Matl	T1 Pm1 (kW)	T2 Matl	T2 Pm2 (kW)	V bias (V)	I bias (A)	I disch (A)	Thick-ness (μm)	Al (wt%)	Grain Size (nm)	Microstructure
310SS+Al												
DE-1	4	Al	1.1	310SS	4	100	0.11	0	33.8	14.0	9.9	Dense
DE-2	4	Al	1.1	310SS	4	40	0.80	10	35.3	13.6	15.7	Columnar
DE-3	5	Al	1.1	310SS	5	60	1.28	15	38.5	11.6	21.7	Dense
DE-4	9	Al	0.55	310SS	2	40	0.85	10	37.4	12.9	10.1	Columnar
DE-5	8	Al	0.55	310SS	2	60	1.38	15	29.7			Coating dense, interface defects
DE-6	4	Al	1.1	310SS	4	100	0.14	0	29.8			Columnar
DE-7	4	Al	1.1	310SS	4	0	0.00	0	33.1			Columnar
DE-8	2	Al	1.1	310SS	4	150	0.15	0	13.1			
Ni20Cr+Al												
DE-9	4	Al	1.1	Ni20Cr	4	100	0.14	0	35.1	11.0	9.5	Columnar
DE-10	4	Al	1.1	Ni20Cr	4	60	1.38	15	27.8	8.9	24.1	Dense
DE-11	8	Al	0.55	Ni20Cr	2	60	1.30	15	32.2	10.1	14.9	Coating dense, interface defects
304SS+Al												
DE-12	4	Al	1.1	304SS	5	100		0	41.0			
DE-13	4	Al	1.1	304SS	5	60		15	36.3			

Column 10 was the coating thickness obtained from the micrographs of the cross sections of the coated samples, Column 11 the weight percent of Al in the coating determined by performing EDS analysis on the coating, Column 12 the grain size of the coating measured using the width of the most intense x-ray diffraction (XRD) peak, and Column 13 the microstructure observed from the scanning electron microscopy (SEM) study.

Three target materials considered for the initial study include 310SS, Ni20Cr and 304 SS. The stainless steel 310 SS target contains 25 wt.% Cr and 20 wt.% Ni, while Ni20Cr target contains 80 wt.% Ni and 20 wt.% Cr, and 304 SS is a commonly used stainless steel with lower Cr (18 wt.%) and Ni (8 wt.%) than 310 SS.

Evaluation of 310 SS + 10 wt.% Al-Deposited Samples

Following deposition, the coating quality was evaluated to select the process parameters that produce a fairly uniform dense coating. The coated samples were examined in a SEM to assess surface morphology and the coating microstructure. The coating thickness was measured on the SEM micrograph of the cross-section of the coating. Energy dispersive spectroscopy (EDS) was performed at a few locations on the coating to determine the chemical composition of the coating. The coating thickness and Al concentration are shown in Table 1.1. The SEM images of Samples DE1-DE4 are shown in Figure 1.3. It is noted that DE1 samples were processed using the conventional magnetron sputter deposition. During the deposition of DE1 samples, no discharge current (filament-plasma) (Id = 0A) and a higher bias voltage (Vb = 100V) was used. In contrast, samples DE2 through DE4 were processed using the plasma enhanced magnetron sputter (PEMS) deposition. The coating on these samples was deposited using a high discharge current Id = 10 - 15A from the filament-generated plasma. This high discharge current resulted in a high ion flux or the bias current as shown in Table 1.1. A lower bias voltage was used (Vb = 40-80V) to avoid heating the samples to a high temperature during processing and severe sputtering of the coatings. For sample DE4 the magnetron power was reduced to one half while the other processing parameters were the same as for DE2. To compensate for the low deposition rate, the deposition time was increased to 9 hours from 4 hours. The coating surface morphology and microstructure of DE4 seem to be better than that of DE2, but the coating exhibits a columnar structure with defects.

The top-view of the coating on DE1 sample showed typical “cauliflower” features of PVD coatings and the grain boundaries (Figure 1.3). In contrast, the coating surface morphology of DE3 sample reveals the absence of the “cauliflower” features and the grain boundaries. Absence of these features can be attributed to heavy ion bombardment. The morphology of coating on DE3 is preferred to that of DE1.

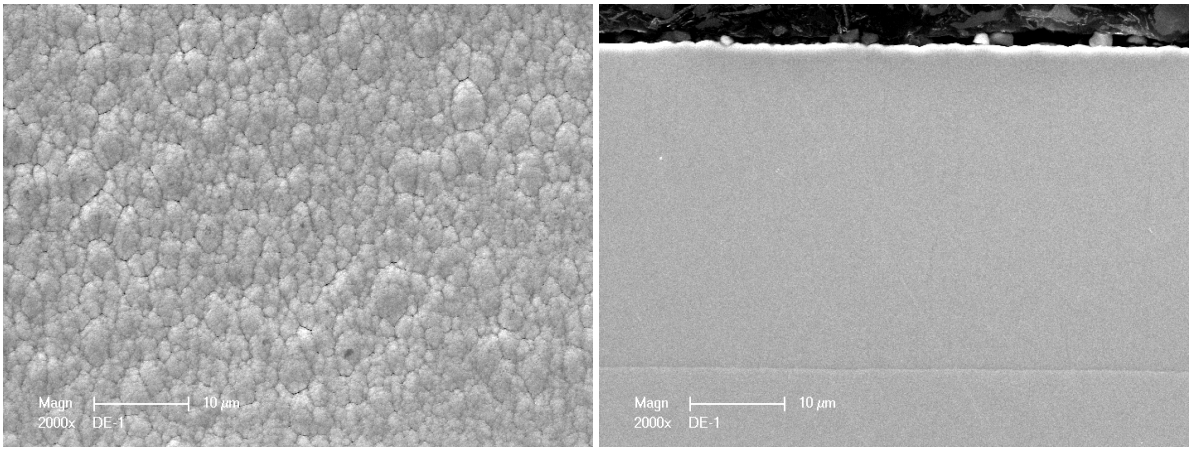

(a) DE1, Vb = 100V, Id = 0A

Figure 1.3
Morphological (left) and cross-sectional (right) SEM images of 310 SS + 10 wt.% Al coatings.

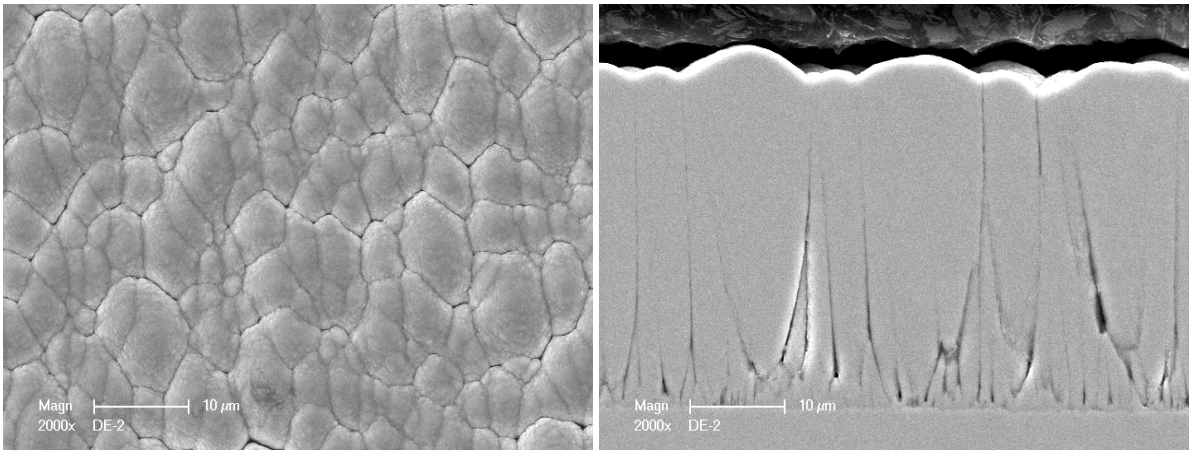

(b) DE2, Vb = 40V, Id = 10A

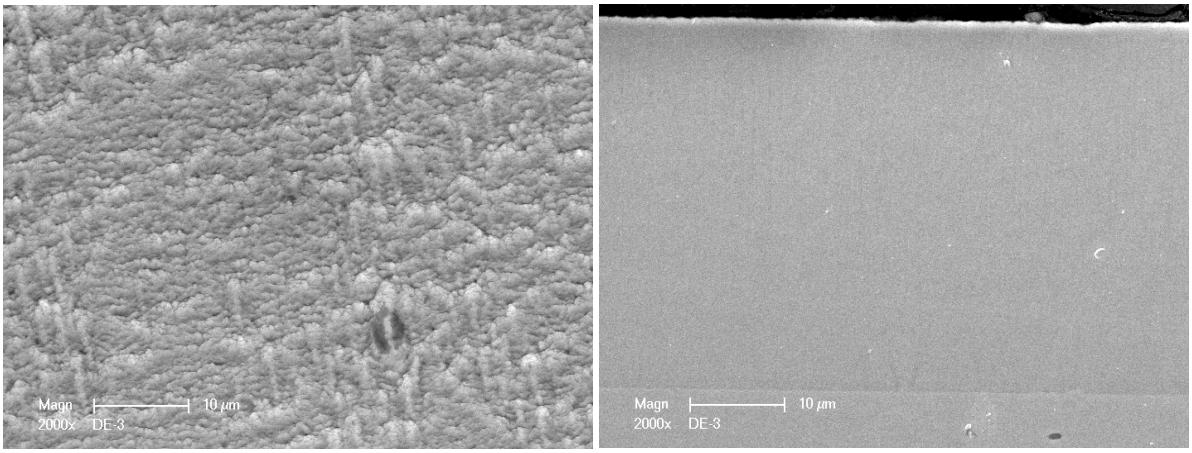

(c) DE3, Vb = 60V, Ib = 15A

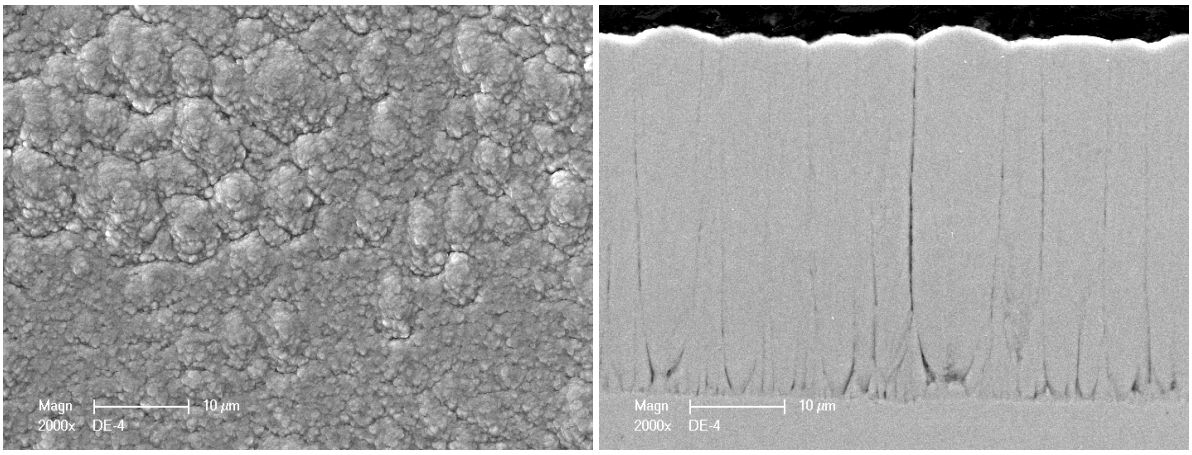

(d) DE4, Vb = 40V, Ib = 10A, ½ magnetron power

Figure 1.3 (cont)
Morphological (left) and cross-sectional (right) SEM images of 310 SS + 10 wt.% Al coatings.

Shown in Figure 1.4 are the coating surface and cross-sectional SEM images of samples DE5-DE8. DE5 was the repeat of DE3 and the coating surface morphology and the microstructure for both coatings were nearly identical except that there were some defects near the interface of DE5, which could be resulted from the improper treatment either at the ion cleaning stage or the initial deposition stage. If the initial sample surface is too rough, or if the ion cleaning is too severe that roughens the surface, the film will grow on an irregular surface, leaving voids and defects. Because all the samples were polished to the same roughness and ion cleaned using the same parameters, it is very unlikely that the problem came from the ion cleaning stage. Even though both DE3 and DE5 were deposited using the same deposition parameters, however, the target condition may be different at the beginning of the depositions. For example, after a number of depositions, dust and coatings may build up on the target surface. When the magnetron is turned on for a new deposition, particles or dust will be sputtered off from the target and then deposited on the sample surface, resulting in defects at the interface. As the target is heating up and running at the steady state, the number of the particles decreases. For DE5, after the initial deposition, the coating was quite dense possibly due to the heavy ion bombardment. In general, the quality of the DE5 coating away from the coating/substrate interface was comparable to that of DE3 and thus, it can be concluded that DE5 was a repeat of DE3.

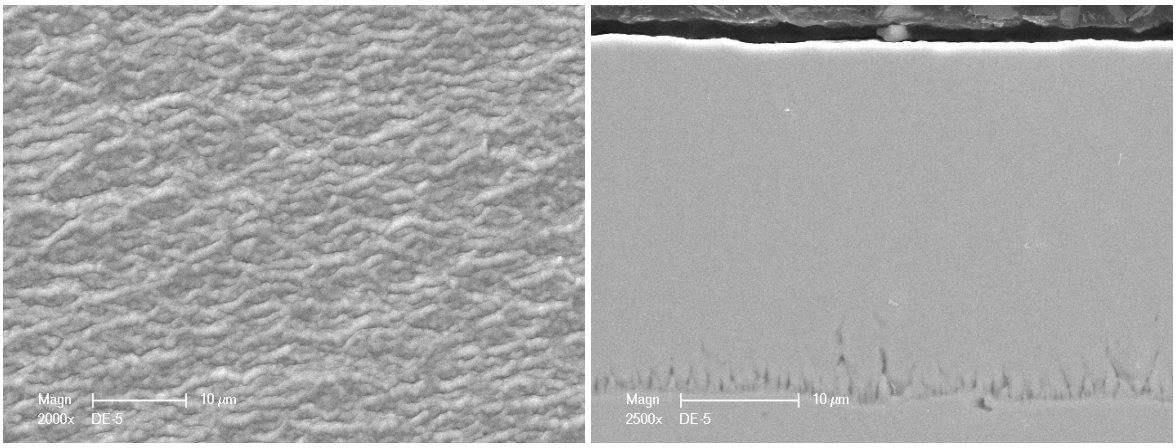

(a) DE5, Vb = 60V, Id = 15A

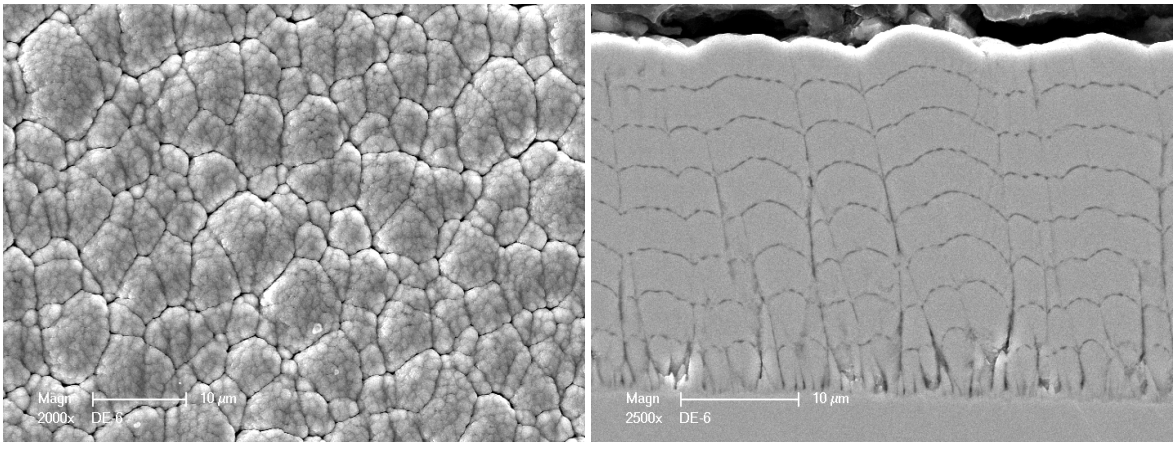

(b) DE6, Vb = 100V, Id = 0A

Figure 1.4
Morphological (left) and cross-sectional (right) SEM images of 310SS+10 wt.% Al coatings.

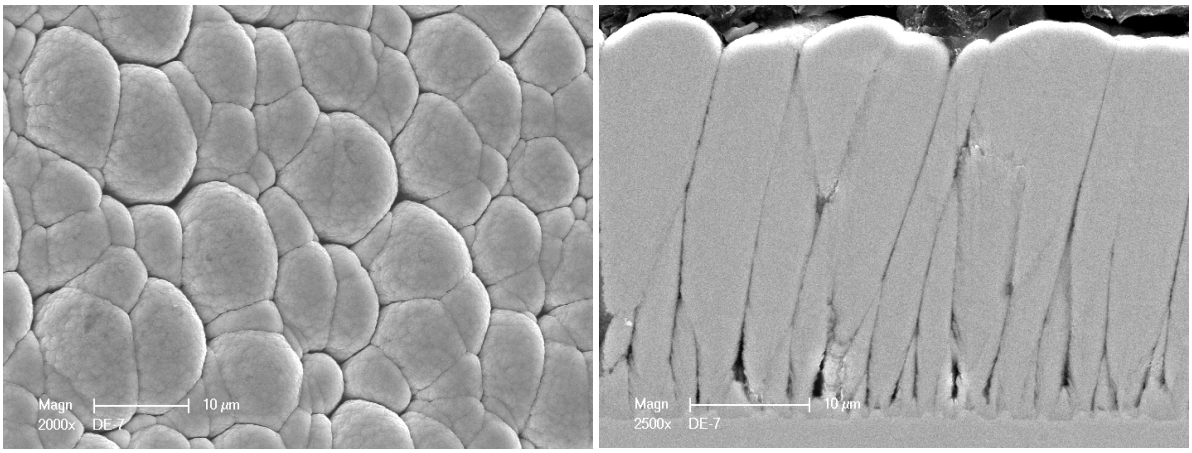

(c) DE7, Vb = 0V, Id = 0A

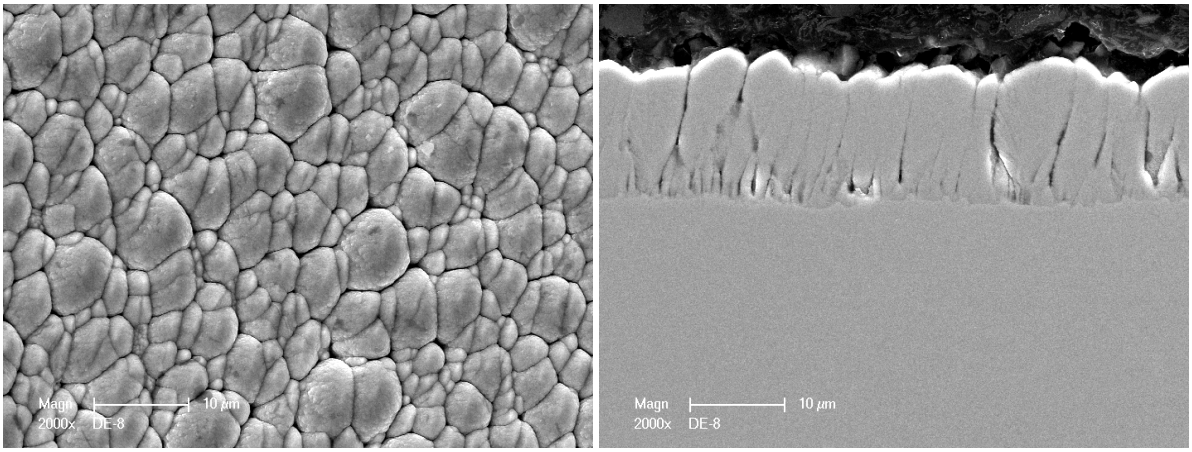

(d) DE8, Vb = 150V, Id = 0A

Figure 1.4 (cont)
Morphological (left) and cross-sectional (right) SEM images of 310SS + 10 wt.% Al coatings.

The process parameters for DE6 were the same as for DE1 (Vb = 100V and Id = 0A), except that DE6 was a multi-layer coating. The objective of the deposition of multi-layer coating was to examine whether or not multi-layered structure interrupts the columnar growth. During the coating deposition, the magnetron power to the 310 SS target was turned off periodically, while the power to the Al magnetron remained the same throughout the process. In this way a multi-layered structure consisting of SS + wt.% Al/Al/SS + 10 wt.% Al layers was deposited. Comparison of the microstructure of DE1 and DE6 samples showed that the coating surface morphologies were very similar. However, the cross-sectional features were quite different. The coating on DE1 sample is quite dense, but on DE6 was columnar. In fact, the columns were extended from the coating/substrate interface to the outer surface of the coating. As for DE7, the bias voltage was 0V implying that no ions were drawn to the surface. As can be seen, the grains of the coating on DE7 samples are larger than that of DE1 and DE6 sample. Hence, ion bombardment is necessary for the formation of a dense coating without the columnar structure and to produce fine grain coating. But if the ion energy is too high as used for DE8 (Vb = 150V, Id = 0A), it is not good either. The use of too high energy leads to formation of columnar structure and reduced coating thickness due to severe ion sputter removal of the as-deposited coating.

After comparisons of the microstructure of all coated sample it was concluded that two sets of deposition parameters (DE1 and DE3) produce the desired dense microstructure. The deposition parameters for these two sets are the conventional magnetron sputter deposition at 100Vb (DE1) and the PEMS process at 60Vb with 15A discharge current (DE3). Further considering the microstructure of the coating on sample DE6, the PEMS process is selected over the conventional magnetron sputter process.

Evaluation of Ni20Cr+10 wt.% Al-Deposited Samples

Three deposition trials were conducted using the Ni20Cr and Al targets to form the Ni20CrAl coatings. The deposition conditions for Ni20Cr + 10 wt.% Al deposition (DE9 to DE11) were listed in Table 1.1. The processing parameters for DE 9 and DE10 were the same as those used for DE1 and DE3. For DE11, the processing conditions were same those used for DE 10, but deposition time was increased from 4 to 8 hours. The measured Al content in the coating varied from approximately 9-11 wt.% among the three samples. The SEM images are shown in Figure 1.5. Comparison of the microstructures of the three coatings showed that the deposition of the coating using the PEMS process resulted in a dense coating without columnar structure.

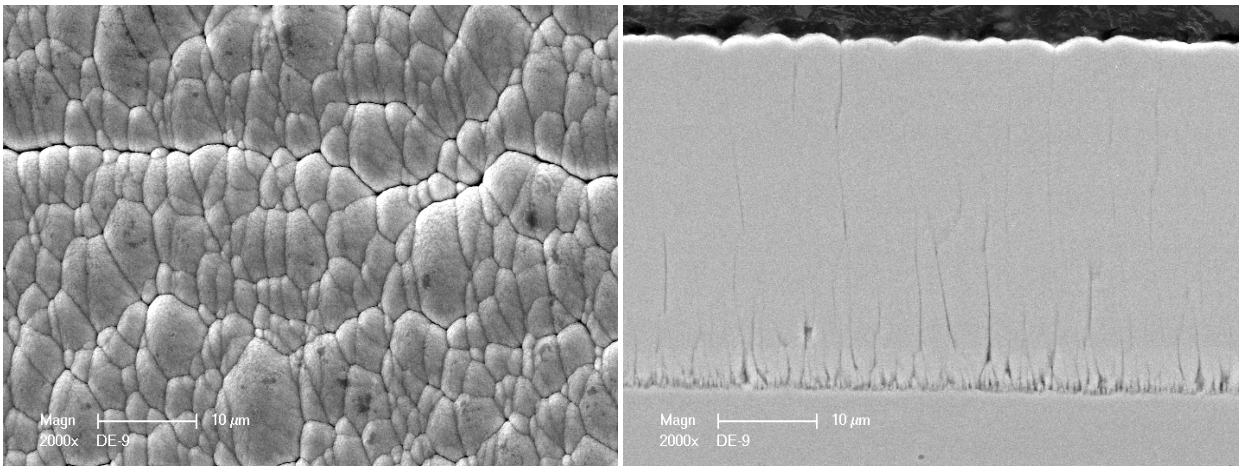

(a) DE9, Vb = 100V, Id = 0A

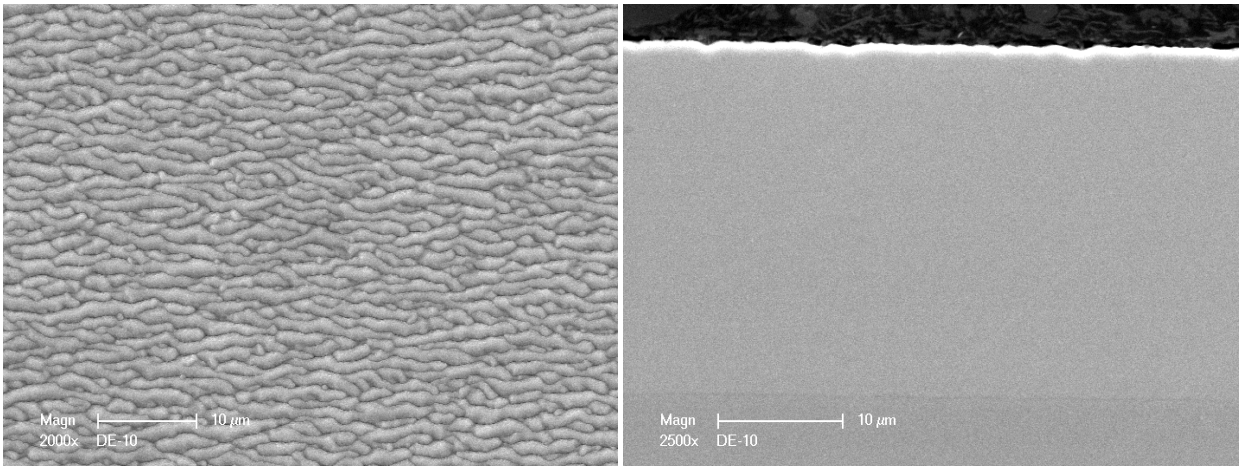

(b) DE10, Vb = 60V, Id = 15A

Figure 1.5
Morphological (left) and cross-sectional (right) SEM images of Ni20Cr + 10 wt.% Al coatings.

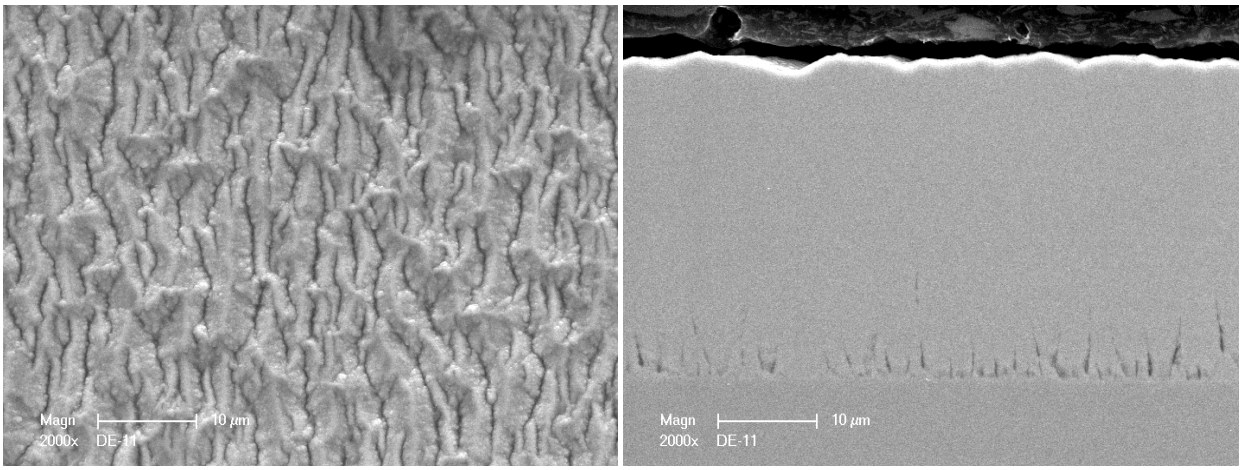

(c) DE5, Vb = 60V, Id = 15A, ½ magnetron power

Figure 1.5 (cont)
Morphological (left) and cross-sectional (right) SEM images of Ni20Cr + 10 wt.% Al coatings.

Evaluation of 304SS + 10 wt.% Al-Deposited Samples

Two deposition trials were conducted using the 304SS and Al targets to form the Fe18Cr8Ni + 10 wt.% Al coatings. The deposition conditions for 304_Al (DE 12 and DE 13) are listed in Table 1.1. Similar to the deposition of 310SS + 10 wt.% Al and Ni20Cr + 10 wt.% Al trials, both conventional magnetron sputter deposition at 100Vb (sample DE12) and PEMS process at 60Vb with 15A discharge current (sample DE13) were used to deposit the coating. The SEM images of the samples are shown in Figure 1.6. Comparison of the cross-sectional images revealed that the microstructure of both samples was similar, but the coating surface morphology of DE13 was slightly better than that of DE12.

Considering the microstructures of all three coatings (310SS + 10 wt.% Al, Ni20Cr + 10 wt.% Al and 304 SS + 10 wt.% Al [SAL]), the PEMS process, with the parameters of DE3, Vb = 60V and Id = 15A was selected for the deposition of advance coatings.

Coating Adhesion

The adhesion of a coating was evaluated using a qualitative standard. Shown in Figure 1.7 is a schematic of the standard. According to the standard, the adhesion test was conducted using Rockwell C scale indentation on a coated sample at 150kg load. The coatings were ranked based on the extent coating cracking and spallation associated with the indentation. The adhesion of a coating is typically ranked into 6 categories. If the indention produces only cracks, the coatings are ranked a “1” and “2” depending on the extent of cracking as illustrated in Figure 1.7. For ranks “3” and “4,” the coating is allowed to spall off near the indent only at couple of locations. If the indentation leads primarily coating spallation, the coatings were ranked 5 or 6 based on the extent of spallation around the indentation and the crater. In general, the coatings with rankings “1” through “4” are considered to be acceptable.

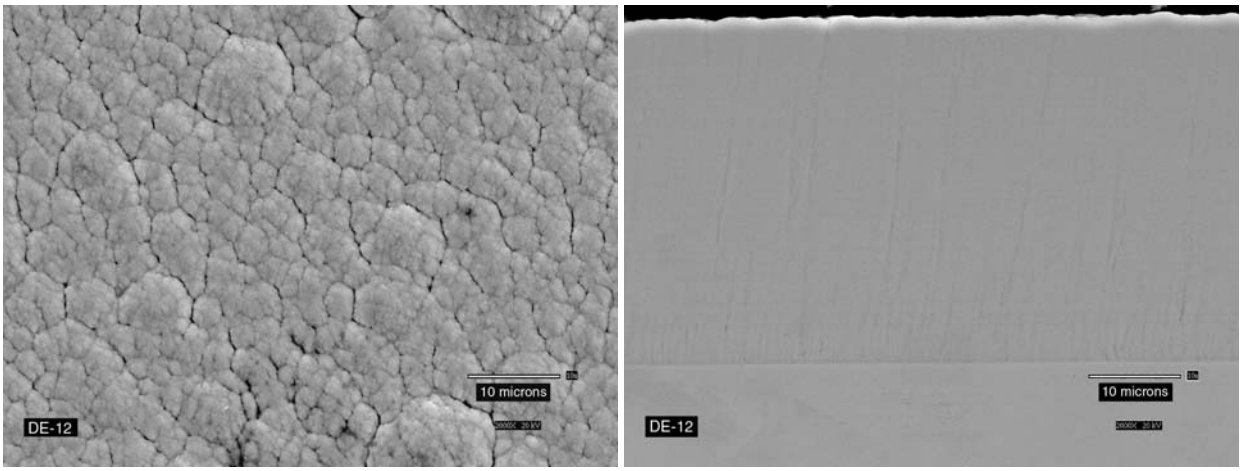

(a) DE12, Vb = 100V, Id = 0A

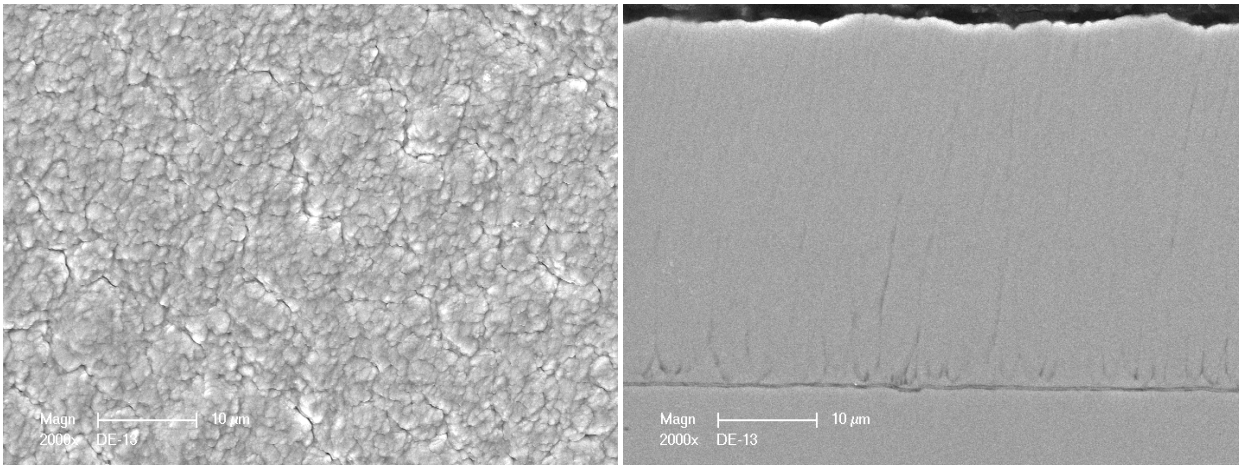

(b) DE5, Vb = 60V, Id = 15A

Figure 1.6
Morphological (left) and cross-sectional (right) SEM images of 304SS + 10 wt.% Al coatings.

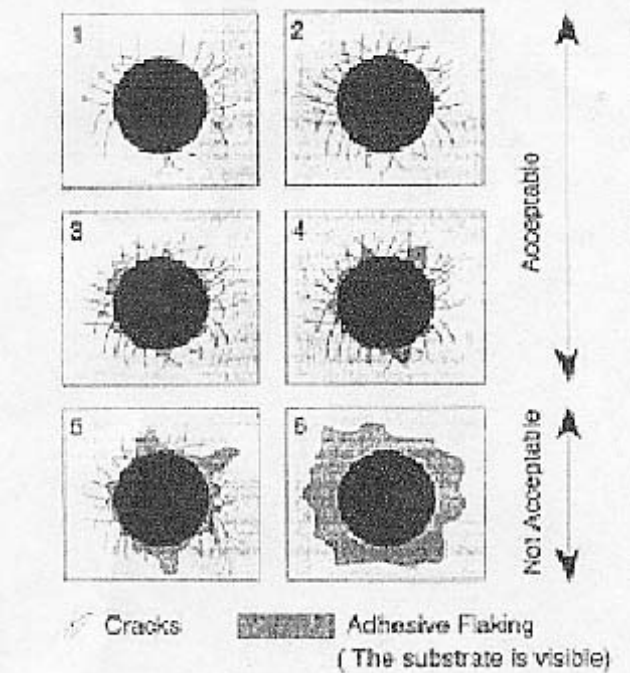

Figure 1.7
Adhesion standard test using Rc indentation.

The Rc indents for sample DE1 through DE4 are shown in Figure 1.8. Using the standard, DE1 through DE 4 coatings were found to either fall within rank "1" or rank "2." Similarly, the indentation data for Ni20Cr + 10 wt.% Al coatings are shown in Figure 1.9 and the adhesion of these coatings were also classified as rank "1" or rank "2." Careful examination of the indents and considering the microstructure results shown in the last sections reveal that the coatings prepared using the PEMS method at Vb = 60V and Id = 15A (DE3 and DE5) show more cracks (but no spallation). This is because these coatings were very dense. In contrast, coatings with columnar structures had fewer cracks because they were more forgiving to the indentation because the columnar can absorb the plastic energy.

Grain Size of As-Deposited Coatings

X-ray diffraction study was performed on selected samples to assess the phases present in the coatings. The diffraction patterns for DE1 and DE3 are shown in Figure 1.10. Besides the major peak of Fe-Cr, Ni-Cr-Fe, AlN, and Al-Fe peaks observed on both samples. It seems that the high ion bombardment using the PEMS process (DE3) suppresses the formation of some of these phases as compared with the conventional magnetron sputtered coating (DE1). Using the width of the most intense XRD peak, the average grain size was determined. The grain-size results are listed in Table 1.1. As can be seen from the table, the grain size of the as-deposited MCrAl coatings varied 10-25 nm. To accurately identify the phases present in the coating and determine the grain size, and evaluate the microstructure, orientation image microscopy and transmission electron microscopy (TEM) work are being conducted on selected samples.

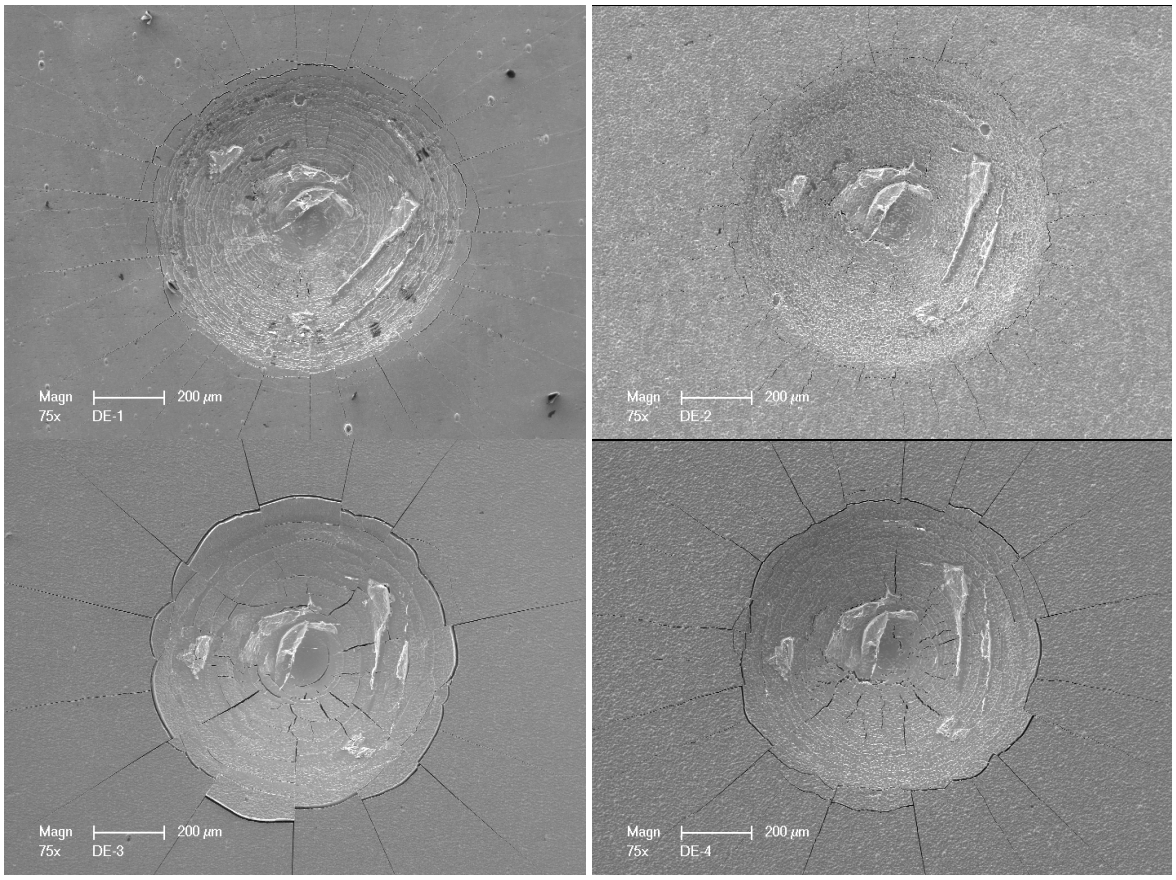

Figure 1.8
Rc indentation of 310 SS + 10 wt.% Al coatings.

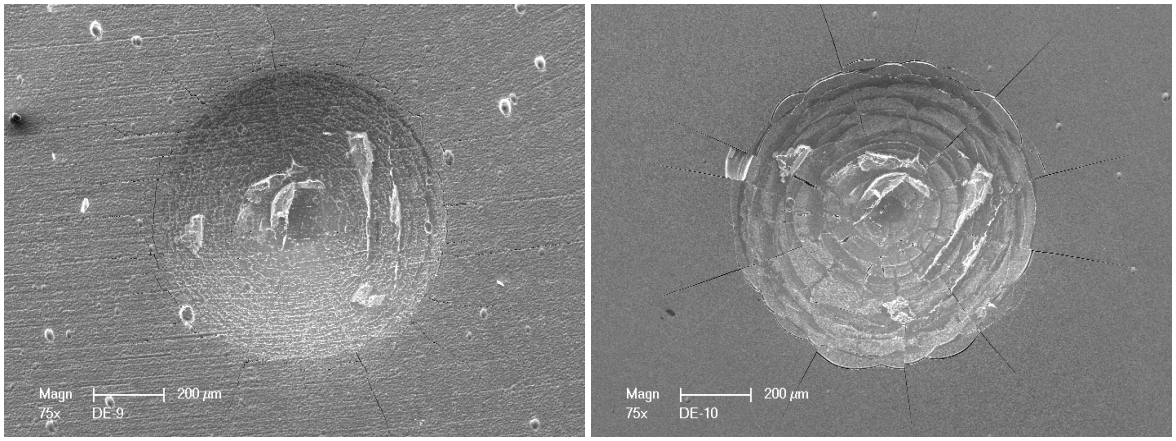

Figure 1.9
Rc indentation of Ni20Cr + 10 wt.% Al coatings.

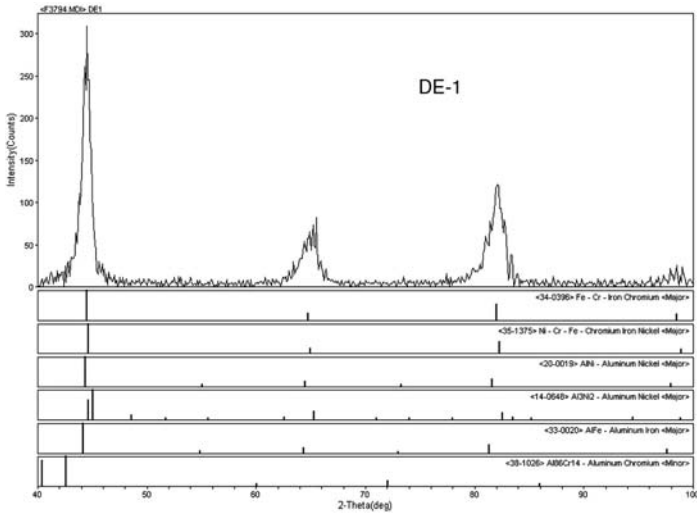

(a)

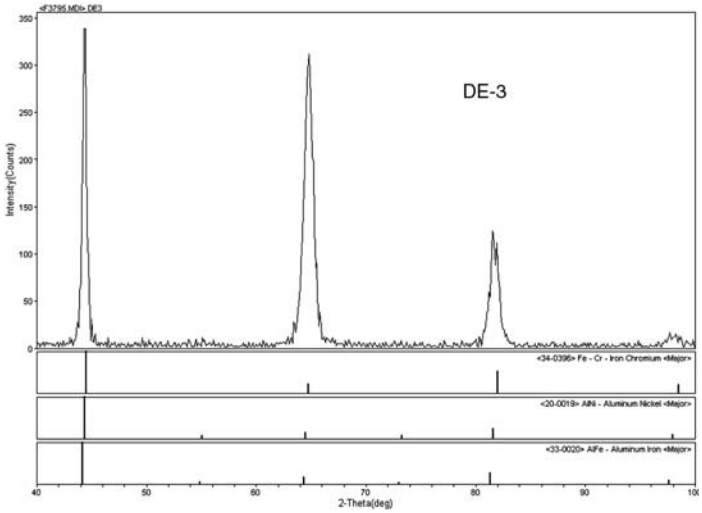

(b)

Figure 1.10
X-ray diffraction spectra of (a) DE1 and (b) DE3.

Selection of Advanced Coating Compositions

Work performed in Task 1 revealed that Fe-18Cr-8Ni-10 wt.% Al and Fe-25Cr-25Ni-10 wt. % Al would not have good oxidation resistance at 750°C. The metallurgical examination of the coating after exposure showed excessive loss of Al from the coating into the substrate by inward diffusion due to high diffusivity of Al in the bcc phase [17]. A possible remedy is to increase the Ni content to 40 wt.%, leading to a coating composition of Fe-25Cr-40Ni-10 wt.% Al. Consistent with the computational results, the results presented by Viswanathan and Purgert [18] showed that Fe-Ni-Cr containing Ni> 25% and Ni-Fe-Cr alloys exhibited better corrosion resistance than Ni based alloys in a simulated boiler environment. With the increased Ni content, the coating becomes predominantly fcc, which would lower diffusivity of Al. Based on the computational results, the suggested compositions for two candidate nanocrystalline coatings are summarized in Table 1.2.

Table 1.2
Summary of Candidate Nanocoating Compositions Suggested by Interdiffusion Computations using DICTRA

Material	Composition in Weight%					Microstructure
	Cr	Ni	Fe	Mo	Al	
Fe-Cr-Ni-Al	20-30	30-50	Bal	0	0-10	bcc + fcc + sigma (depending on Al content)
310SS_Hi Ni	25	25	40	0	0	100 mole% fcc; sigma phase at coating/substrate interface
310SS_Hi Ni + 10 wt.% Al	25	25	40	0	10	bcc + fcc; > 90 mole% fcc

Considering the computation model results and the reliable MCrAl type coatings used for the hot section parts of a gas turbine, two iron base (Fe-Cr-Ni), a nickel base (Ni-Cr-Co), and a cobalt base (Co-Cr-Ni) MCr systems with and without 10 wt.% Al were selected for further evaluation. For deposition of these advanced coatings, four different MCr (310SS, Haynes 120, Haynes 160, and Haynes 188) targets were procured. Nominal compositions of the MCr target materials are given in Table 1.3. For deposition of the base line 304-10 wt.% Al and Ni-20Cr-10 wt.% Al coatings, 304 SS and Ni-20Cr targets were used. The composition of these targets are also included in Table 1.3.

Table 1.3
Chemical Composition of Targets Selected for Deposition of Advanced and Baseline Coatings

Coating Type	Fe	Ni	Cr	Co	Si	W
310 SS	Bal	20	25	--	0.6	--
Haynes 120	Bal.	37.1	24.7	0.8	0.5	< 0.1
Haynes 160	0.5	Bal.	28	30	4	< 0.1
Haynes 188	1.7	23	22	Bal.	0.5	14.
304 SS	Bal.	8	18		0.4	
Ni-20Cr		80	20			

Application of Advanced Coatings

Three substrate materials, 304 SS, P91 steel, and Haynes 230 alloys were selected for application of advanced and baseline coatings. Rectangular samples, with a drilled hole on each end, were machined from the three substrate materials. The samples were polished to a 6 μm finish using standard metallographic techniques. The samples were then tied using SS wires and hung between the magnetrons as shown in Figure 1.2. The parameters for coatings with or without 10 wt.% Al were applied on three substrate alloys, 304 SS, P91, 310 SS with 10 Al was also deposited on P91 and 304 substrate samples. Two magnetrons were used, one for depositing MCr and the other for aluminum. One of the four MCr targets and an aluminum (99.999 pure) target were used to co-deposit MCrAl coating. The samples to be coated were cleaned first using Ar-plasma ions for about 90 minutes to remove oxide scale. To vary the aluminum content from 0 to 10 wt.% in the advanced coatings, the target power for Al deposition was varied from 0 to 1.3 kW. The power for the MCr target was maintained at 4.0 kW. For comparison the baseline 304 SS-10 wt.% Al and N-20Cr-10 wt.% Al coatings were applied on the substrate alloys. The coated samples were shipped to Foster Wheeler Research Center for corrosion testing and evaluation.

Metallurgical Evaluation of As-Deposited Advanced Coatings

Following application of the coating, the chemical composition measurements were conducted on a sample from each set of coatings using EDS and the results are shown in Table 1.4. For comparison, the chemical composition of the baseline 304 SS-10 wt.% Al and Ni-20Cr-10 wt.% Al coatings is shown in Table 1.5.

For microstructural evaluation of advanced coatings in the as deposited condition, a transverse section was removed from a sample of each coating set and metallurgical mounts were prepared from all these sections using standard metallographic techniques. The mounts were examined in a SEM. Typical microstructure of the advanced and baseline nanocrystalline coatings are shown in Figures 1.11 through 1.14.

Table 1.4
Semi-Quantitative Chemical Composition of Advanced Coatings, wt.%

Coating ID	Substrate	Al	Si	Ti	Cr	Fe	Co	Ni	W
DE-16, 310-10 Al	304	11.28	0.58		25.15	47.92		15.07	
DE-16, 310-10 Al	P91	9.56	0.49		25.41	49.46		15.09	
DE-18, H160-10 Al	304	9.53	2.45	0.5	27.43	0.40	28.29	31.40	
DE-18, H160-10 Al	Haynes 230	10.56	2.71	0.42	27.23	0.32	27.78	30.96	
DE-19, H120-10 Al	304	10.02	0.50		25.48	34.07		29.93	
DE-19, H160-10 Al	P91	11.0	0.55		25.33	33.72		29.40	
DE-20, H188-10 Al	304	10.76	--	--	23.87	1.8	35.71	19.60	8.11
DE-20, H188-10 Al	Haynes 230	11.52			22.91	1.30	35.34	19.96	8.36
DE-21, H188	304				25.33	1.97	40.34	21.70	9.49
DE-21, H188	Haynes 230				25.64	1.94	40.65	22.13	9.49
DE-24, H120	304		0.27		27.72	37.33		34.68	
DE-24, H120	P91		0.28		28.15	37.42		34.16	
DE-27, H160	304		1.64	0.45	30.28	0.67	32.33	34.63	
DE-27, H160	P91		1.80	0.46	29.96	0.65	32.46	34.66	

Table 1.5
Semi-Quantitative Chemical Composition of Baseline Nanocrystalline Coatings, wt.%

Coating ID	Substrate	Al	Si	Cr	Fe	Ni
DE-14, 304-10 Al	304	7.42	0.54	18.44	Bal.	6.26
DE-14, 304-10 Al	P91	8.54	0.47	18.26	Bal.	6.51
DE-15, Ni-20Cr-10 Al	Haynes 230	7.66	0.18	18.93	0.44	Bal.

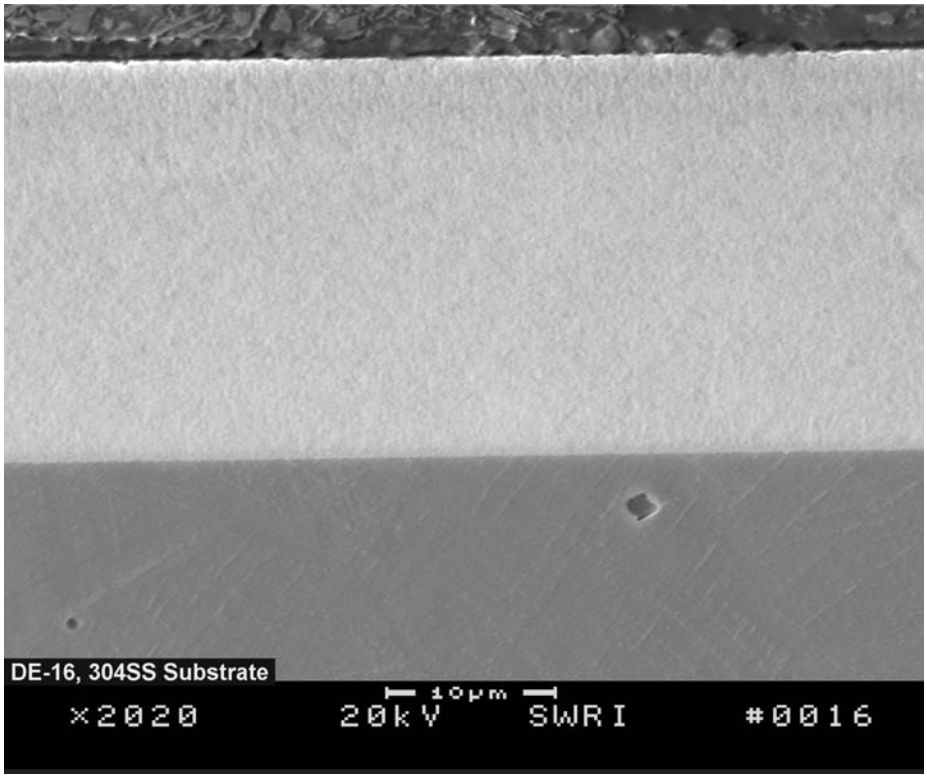

Figure 1.11
SEM micrograph of a cross section of a 310 SS-10 wt.% Al coated specimen (coating thickness ≈ 25 µm).

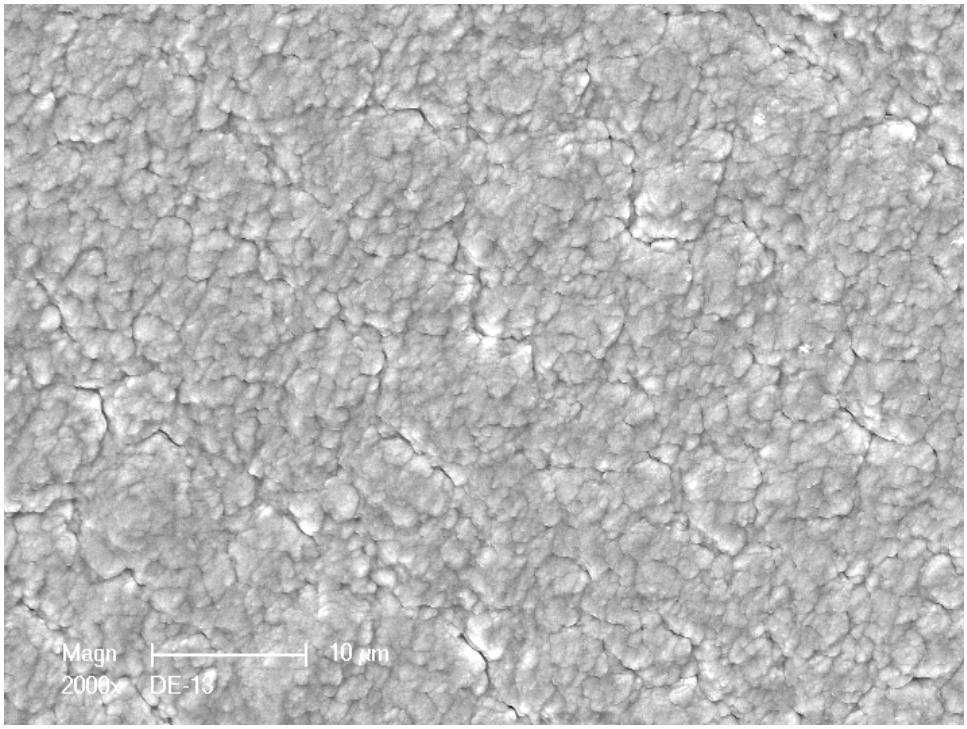

(a)

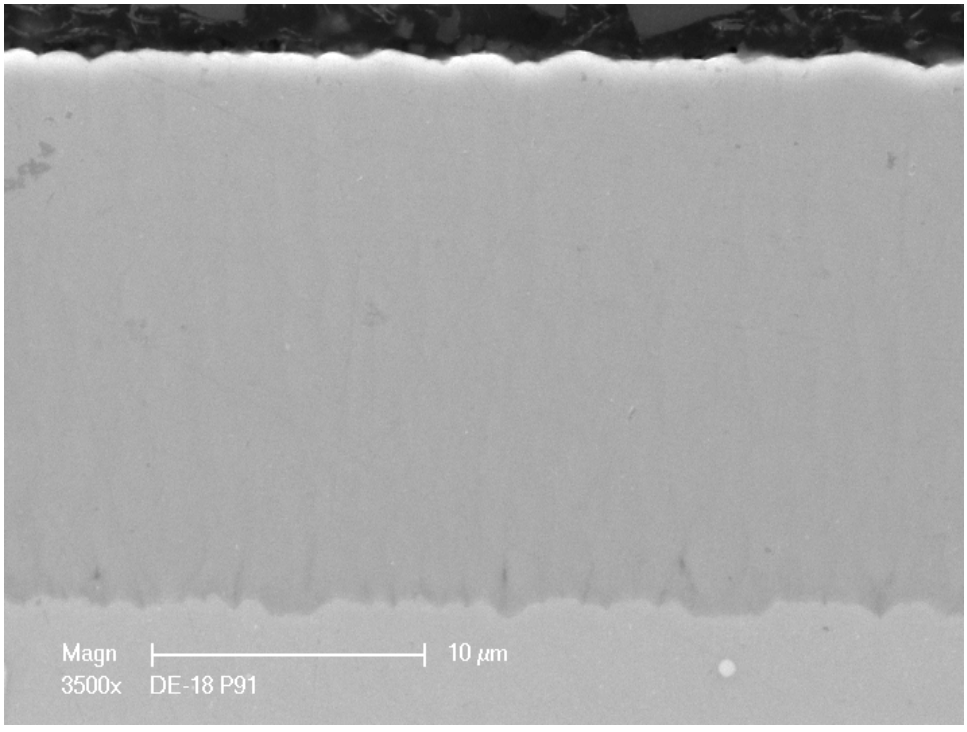

(b)

Figure 1.12
SEM micrographs of a) surface morphology and b) cross section of the H160-10 wt.% Al coated specimen (coating thickness ≈ 21 µm).

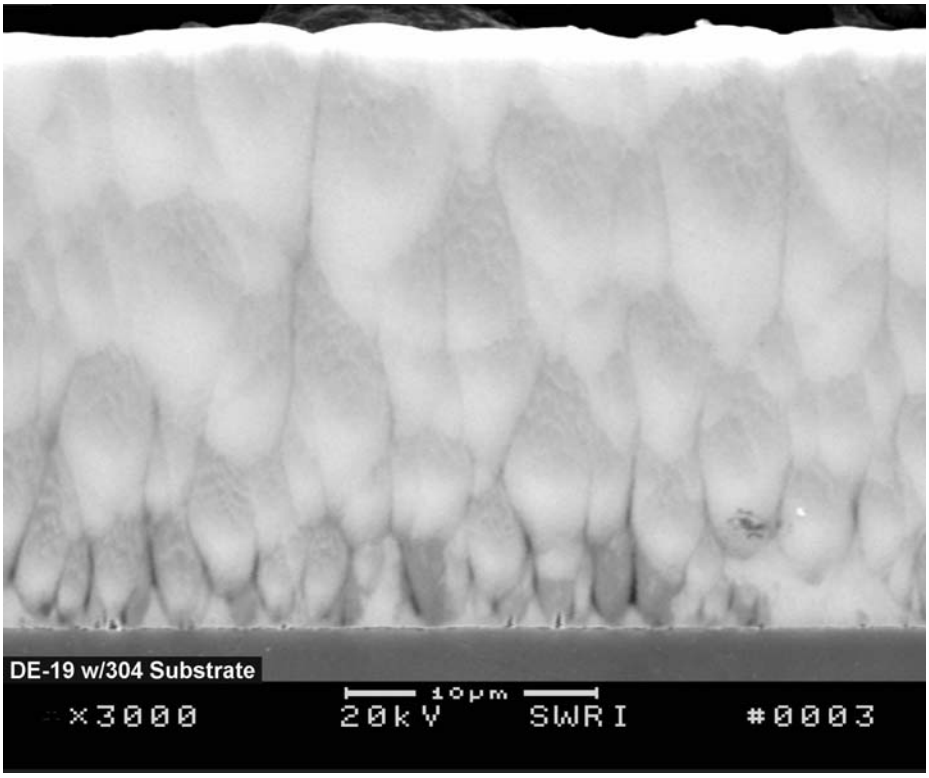

Figure 1.13
SEM micrograph of a cross section of a H120-10 wt.%. Al coated specimen (coating thickness ≈ 24 µm).

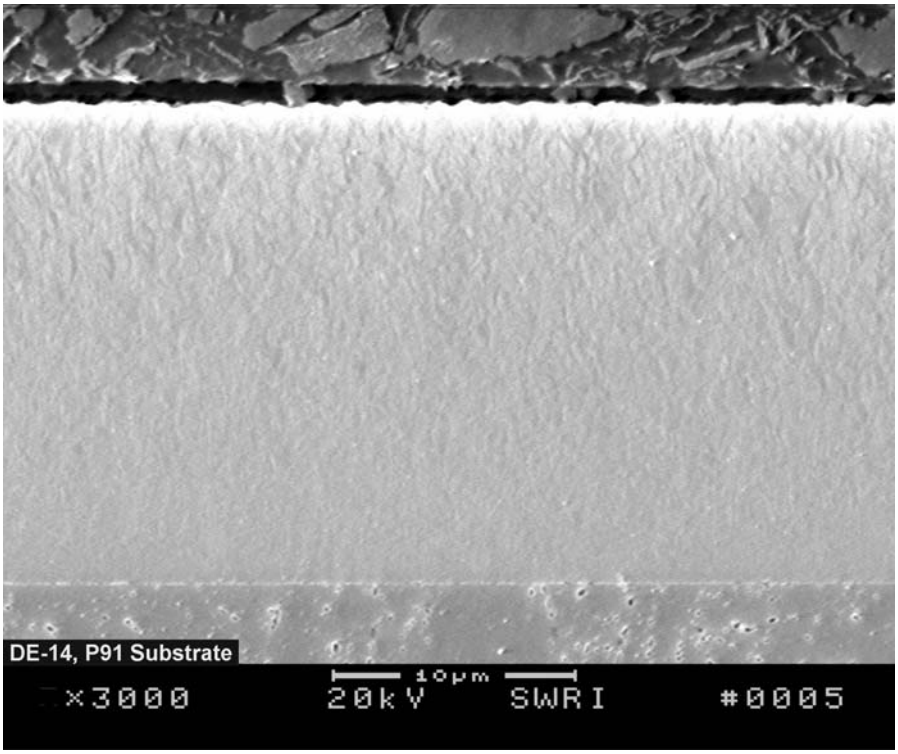

(a)

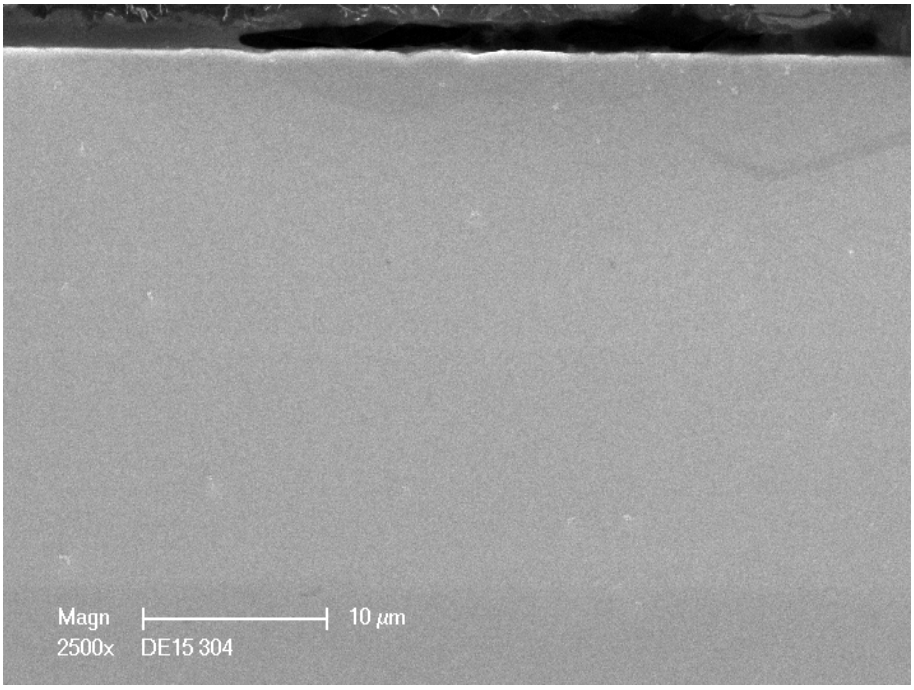

(b)

Figure 1.14
SEM micrographs of cross section of a) 304-10 wt.% Al and b) Ni-20Cr-10 baseline coated specimens.

However, detailed metallographic examination of the as-coated samples revealed cracks in the coatings containing Al. Cracks were seen in the coating on all three substrate materials. Some of these cracks extended through the thickness of the coating. Typical morphology of cracks in the coating is illustrated in Figures 1.15 through 1.17. The coatings without Al showed no cracks, but exhibited coating defects such droplets, or nodules ("cauliflower" or "kennels").

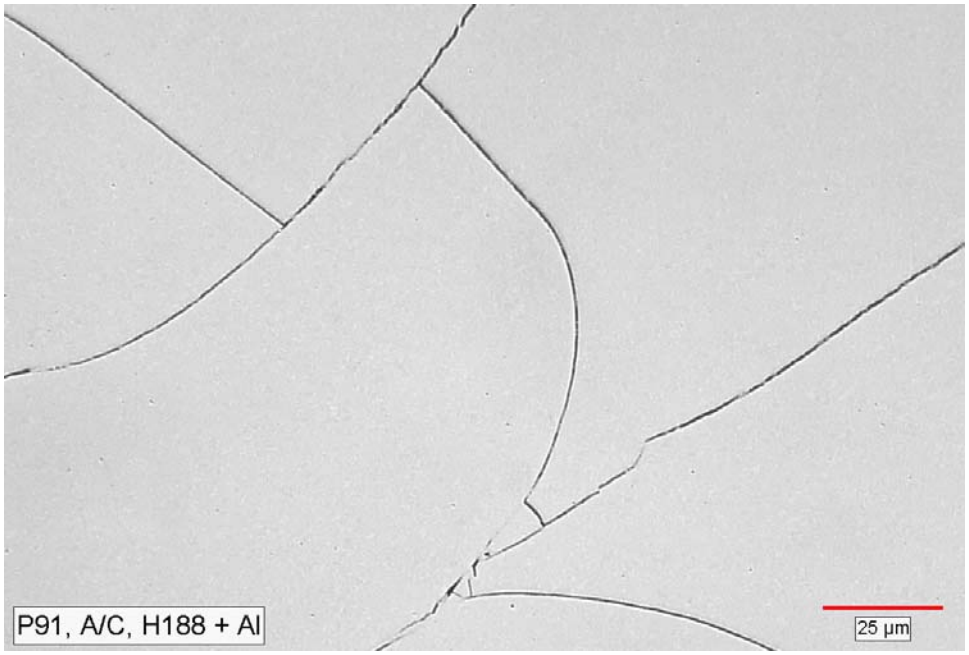

(a)

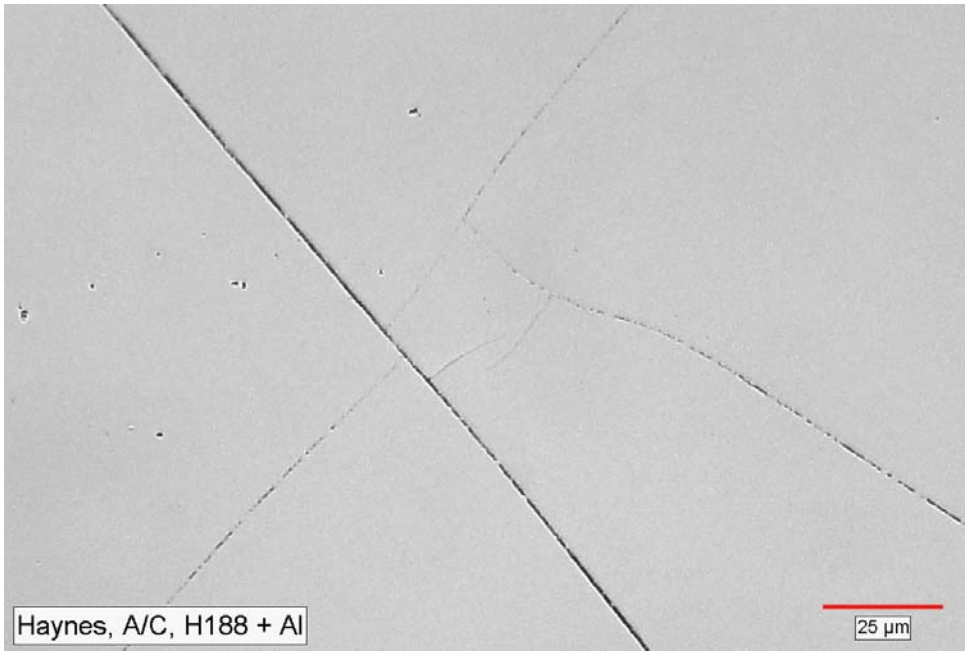

(b)

Figure 1.15
Optical micrographs of top-view of coated samples a) Haynes 188-10 wt.% Al on P 91 and b) Haynes 188-10 wt.% Al on Haynes 230.

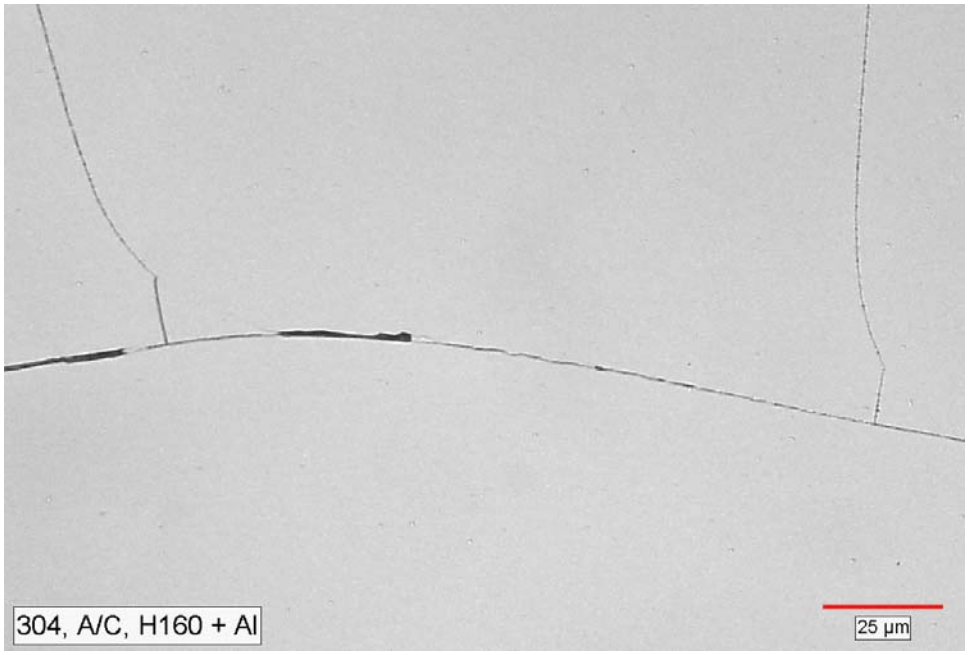

(a)

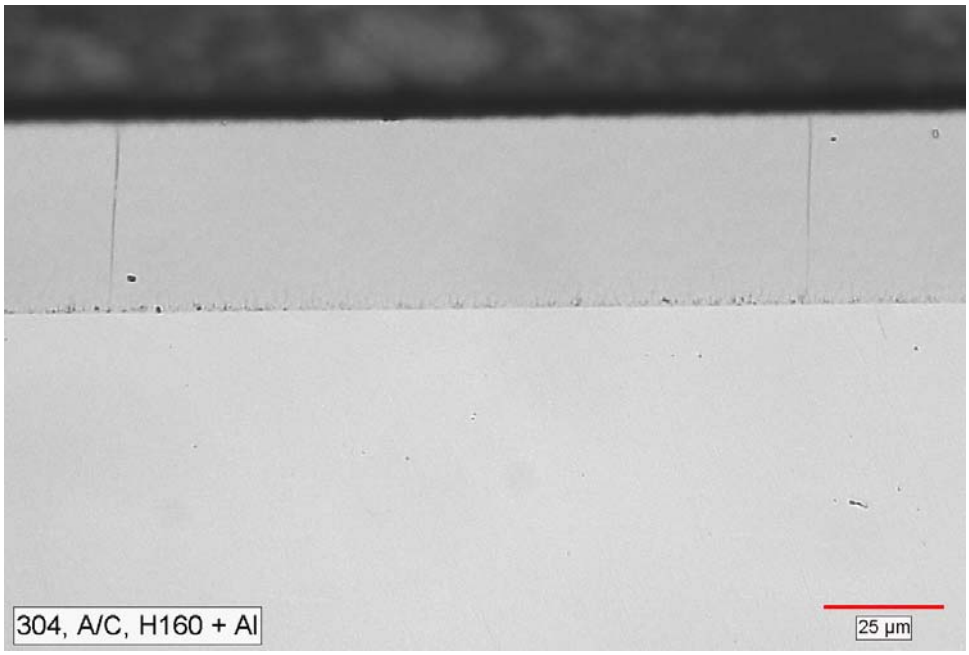

(b)

Figure 1.16
Optical micrographs of a) top-view and b) cross section of a Haynes 160 + 10 wt.% Al coated 304 SS sample.

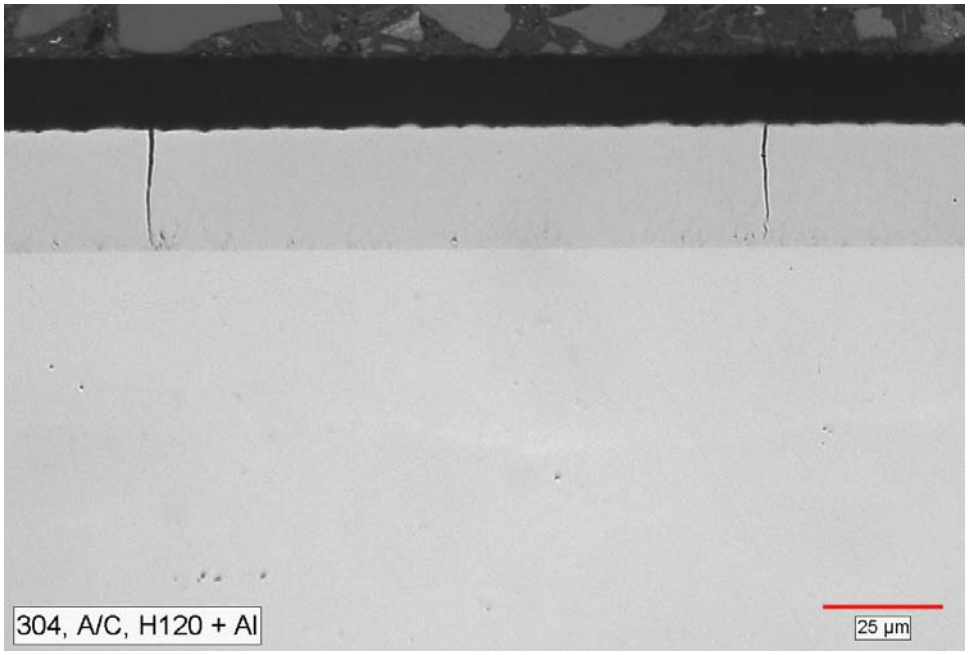

(a)

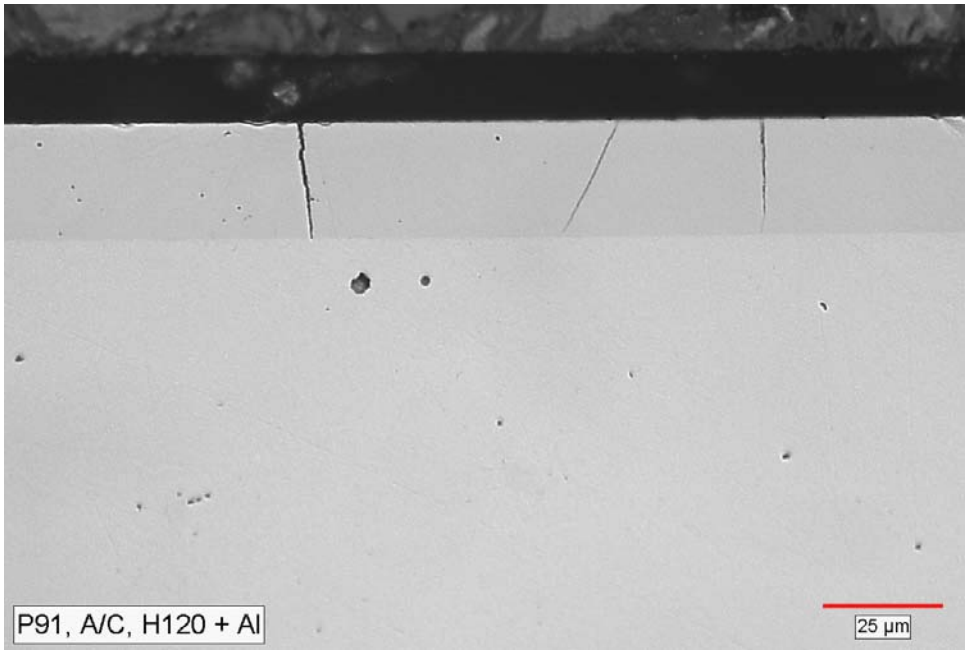

(b)

Figure 1.17
Optical micrographs of cross section of a Haynes 120 + 10 wt.% Al coating on a) 304 SS and b) P-91 steel samples.

Process Optimization Studies

A new deposition method, High Power Impulse Magnetrons Sputtering (HIPIMS), was used to investigate whether this process produces crack free dense coatings. This method utilizes pulsed DC power at a high frequency up to 500 Hz and pulse width of about 200 µs to accomplish the sputtering of a target material. Due to the high pulsed voltage of 1000V, versus ~500V for DC magnetron, it was reported that all metal particles are ionized in the HIPIMS process. In contrast, only a small fraction of the metallic particles (1 to 2 wt.%) are ionized in the DC magnetron sputtering process. When the metal ions come to the surface during deposition, with the application of the electric field, the coating thus formed is very dense.

Since only one high power impulse supply is available at SwRI, it was first used for the 304 SS magnetron as the 304 SS consisted of 90 wt.% of the coating. A conventional DC power supply was used for the Al target. But after a couple of deposition trials using the HIPIMS power supply, it was found that the deposition rate of 304 SS was quite low. To achieve 10 wt.% Al in the coating, the DC magnetron power to the Al target required to reduce form 1 kW to below 0.3 kW at which point the magnetron operation became unstable. The Al content in the as-deposited coating using magnetron power of 0.3 kW was significantly higher than the targeted value of 10 wt.%. As a result, the high power supply was switched to the Al target and the DC power supply was used for the 304 SS target. After a number of trials, the best combination of the power to the Al and the iron based (304 SS or H120), Ni-based (H160), and Co-based (H188) targets were established. The final deposition parameters used for the HIPIMS study are shown in Table 1.6.

Table 1.6
Deposition Conditions for HIPIMS Study

Sample No.	Specimen	Substrate	Number of samples	Total No. of Samples	Target 1/ Par (kW)	Target 2/ Par (kW)	Disc Current (A)	Bias Voltage (V)	QN2 (sccm)	Deposit Time (h)
TiN Barrier Layer + MCrAl, Use HMP power supply on one target and DC on the other target										
TiN	Large	304 SS	6 column x 4	24	Ti/4.0	Ti/4.0	5	40	50	3.5
Use HMP power supply on MCr target, use DC power supply on Al target, deposit AlN for 2hrs then MCrAl										
DED13F	Large	2-uncoated SS, 2-TiN coated 304 SS	2 column x 2	4	304 SS / 0	Al/1.0	0	40	50	2
					304 SS /3.6	Al/3.2	0	40	0	4
DED14A	Large	2-uncoated SS, 2-TiN coated 304 SS	2 column x 2	4	H120 / 0	Al1.0	0	40	50	2
					H120 / 3.6	Al/3.6	0	40	0	5
DED15	Large	2-uncoated SS, 2-TiN coated 304 SS	2 column x 2	4	H160 / 0	Al/1.0	0	40	50	2
					H160 /3.6	Al/3.3	0	40	0	5
DED16	Large	2-uncoated SS, 2-TiN coated 304 SS	2 column x 2	4	H188 / 0	Al/1.0	0	40	50	2
					H188 / 3.6	Al/ 1.0	0	40	0	5
DED16A	Large	2-uncoated SS, 2-TiN coated 304 SS	2 column x 2	4	H188 / 0	Al/1.0	0	40	50	2
					H188 / 3.6	Al/3.1	0	40	0	5
Use MDX-052 DC power supply on both MCr target and Al target, deposit AlN for 2hrs then MCrAl										
DED16B	Large	2-uncoated SS, 2-TiN coated 304 SS	2 column x 2	4	H188 / 0	Al/1.0	0	100	50	2
					H188 / 3.6	Al/ 1.0	0	100	0	5

First TiN was deposited on 24 samples and the deposition parameters are given in Table 1.6. For depositing the MCrAl coatings, 304 SS, H120, H160, H188, and Al targets were used. Only the last successful runs were listed in the Table 1.6. Coating application details are as follows:

As can be seen from the table, for instance test DED13F, coating was deposited on two uncoated 304 SS and two TiN coated 304 SS samples (total of four). After sputter cleaning using standard conditions, all samples were first deposited with AlN. At this time, the power supply to the 304 SS magnetron was off, while Al magnetron power was maintained at 1 kW and bias at 40 V with the nitrogen flow rate at 50 sccm to form AlN for 2 hours. After the AlN deposition, the power to the 304 SS magnetron was increased form 0 to 3.6 kW using the DC magnetron power supply, Al magnetron at 3.2 kW (average) using the HIPIMS power supply, and the bias at 40 V. During the 304 SS + 10 wt.% Al coating deposition. No nitrogen flow was used during the deposition of 304 SS + 10 wt.% Al coating. Using these process parameters, 304 coating with about 10 wt.% Al was successfully deposited on the substrate samples. The deposition time was 4 hrs that resulted in 304 SS + 10 wt.% Al coating thickness of about 20 μm. In this study, two samples with a two-layered coating structure (AlN/304 SS + 10 wt.% Al) and two samples with a three-layered coating structure (TiN/AlN/304SS + 10 wt.% Al) were obtained. Similarly, the other MCrAl coatings on AlN or TiN/AlN coated samples were applied using H120, H160, and H188 targets.

After the MCrAl coating deposition, a transverse section was removed from an each type of coated sample for SEM examination. Figure 1.18 shows selected morphological views at low and high magnifications and cross-sectional views of the 304 SS + 10 wt.% Al coating on AlN/304 SS and AlN/TiN/304 SS. Examination of the samples showed that the coating was dense with no macro-cracks. However, droplets or nodules were observed in the as-deposited coatings. Fine delamination cracks were observed around the periphery of some of these particles as illustrated in Figure 1.18. The coatings deposited using the HIPIMS method seems to have more droplets than coatings processed using the conventional DC deposition process. The presence of these droplets or nodules may not be as detrimental as cracks. However, for long-term durability under oxidizing and corrosive environments, the presence of these droplets or nodules with interface delamination could be as detrimental as cracks.

Comparison of micrographs of cross-sectional views revealed that the AlN adheres well to the 304 SS substrate (left). However, localized delamination was observed between the AlN and TiN interlayers as illustrated in Figure 1.18. The cause for delamination is unknown. However, there may be two reasons for localized delamination. First, after the TiN deposition, the samples had to be removed from the vacuum chamber and the targets had to be replaced for the MCrAl coating deposition. During this time, surface oxidation may occur. After the samples were re-installed back into the deposition system for the AlN deposition and then the 304 SS + 10 wt.% Al deposition, the left over oxide scale on TiN coating after sputter cleaning could be responsible for the observed localized delamination between the AlN and TiN interlayer coatings. Second, the coefficient of thermal expansion of AlN (4.5×10^{-6}/ºC) is lower than that of TiN (9.4×10^{-6}/ºC). During the deposition, the maximum temperature of the samples could reach as high as 400ºC. Upon cooling to room temperature, the AlN coating will be in compression while the TiN coating will be in tension. Using the following parameters (E_{AlN} = 330 GPa, E_{TiN} = 600 GPa, and δT =

400-25 =3 75ºC), thermal stress at the interface is calculated to be -606MPa and +1,102 MPa for the AlN and the TiN coatings, respectively. Such high stresses are likely to cause the coatings to separate. Certainly the other factors such as the CTE difference between the 304 SS + 10 wt.% Al coating and the AlN, as well as the CTE difference between the TiN and the 304 SS substrate could play a role. Finally, the observed delamination at the interface of the AlN/TiN coatings may have occurred during sample preparation for metallographic examination.

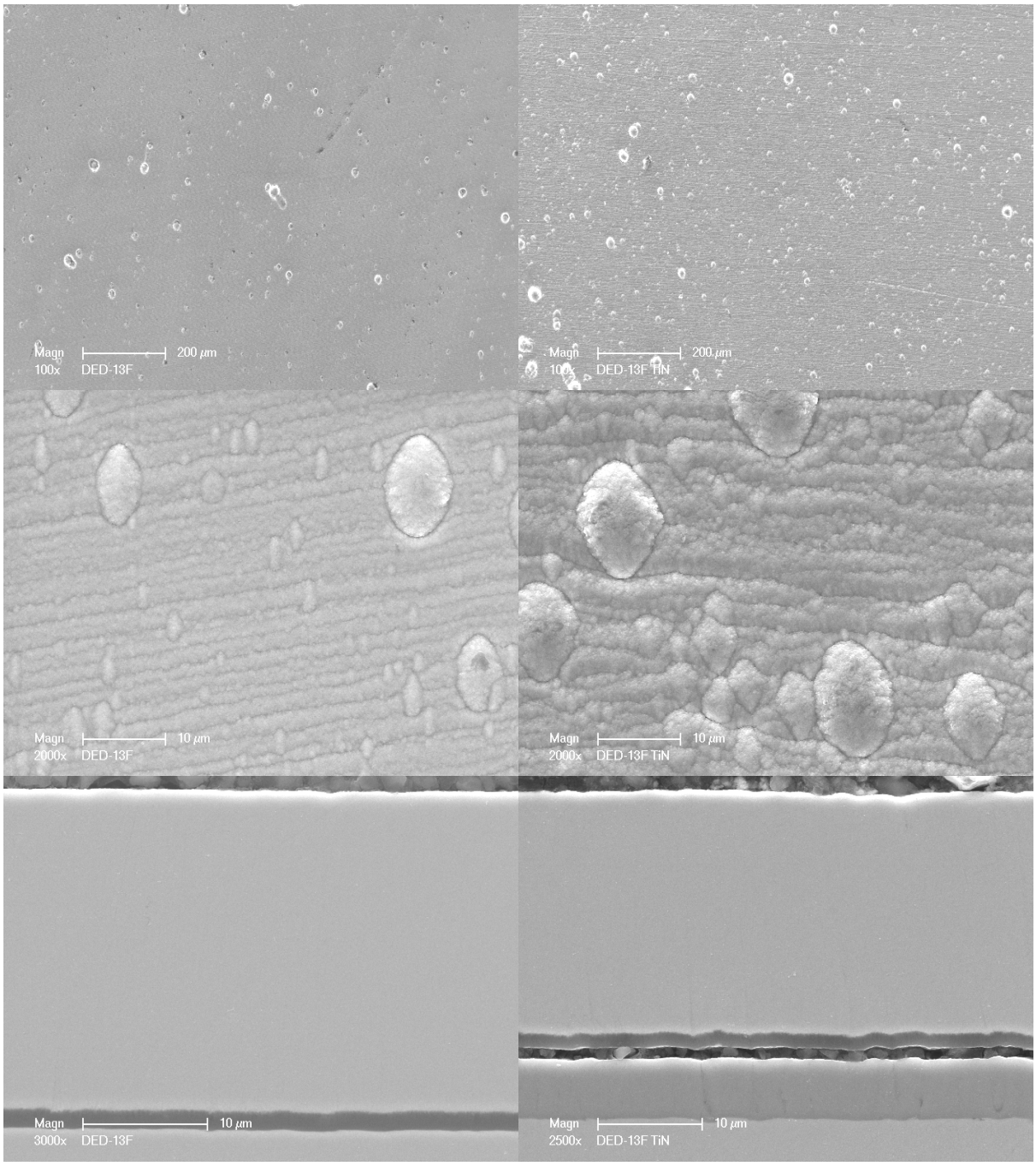

Figure 1.18
Morphological views (top two photographs) and cross-sectional view (bottom photograph) of 304 SS + 10 wt.% Al coating on AlN/304SS (left) and AlN/TiN/304SS (right).

The micrographs of H160 + 10 wt.% Al coating on AlN/304 SS substrate and AlN/TiN/304 SS substrate are shown in Figure 1.19. The morphology of these coatings is similar to the 304 SS + 10 wt.% Al coating as discussed above. In contrast to the 304 SS + 10 wt.% Al coating results, no delamination was observed at the AlN/TiN interface. The H160 + 10 wt.% Al coating also exhibited droplets. It is noted that these droplets, or nodules, grew with the film deposition from the beginning, as shown in Figure 1.20. It was suspected that arcing at the initial stages of the process formed these droplets, or nodules, and caused the abnormal growth.

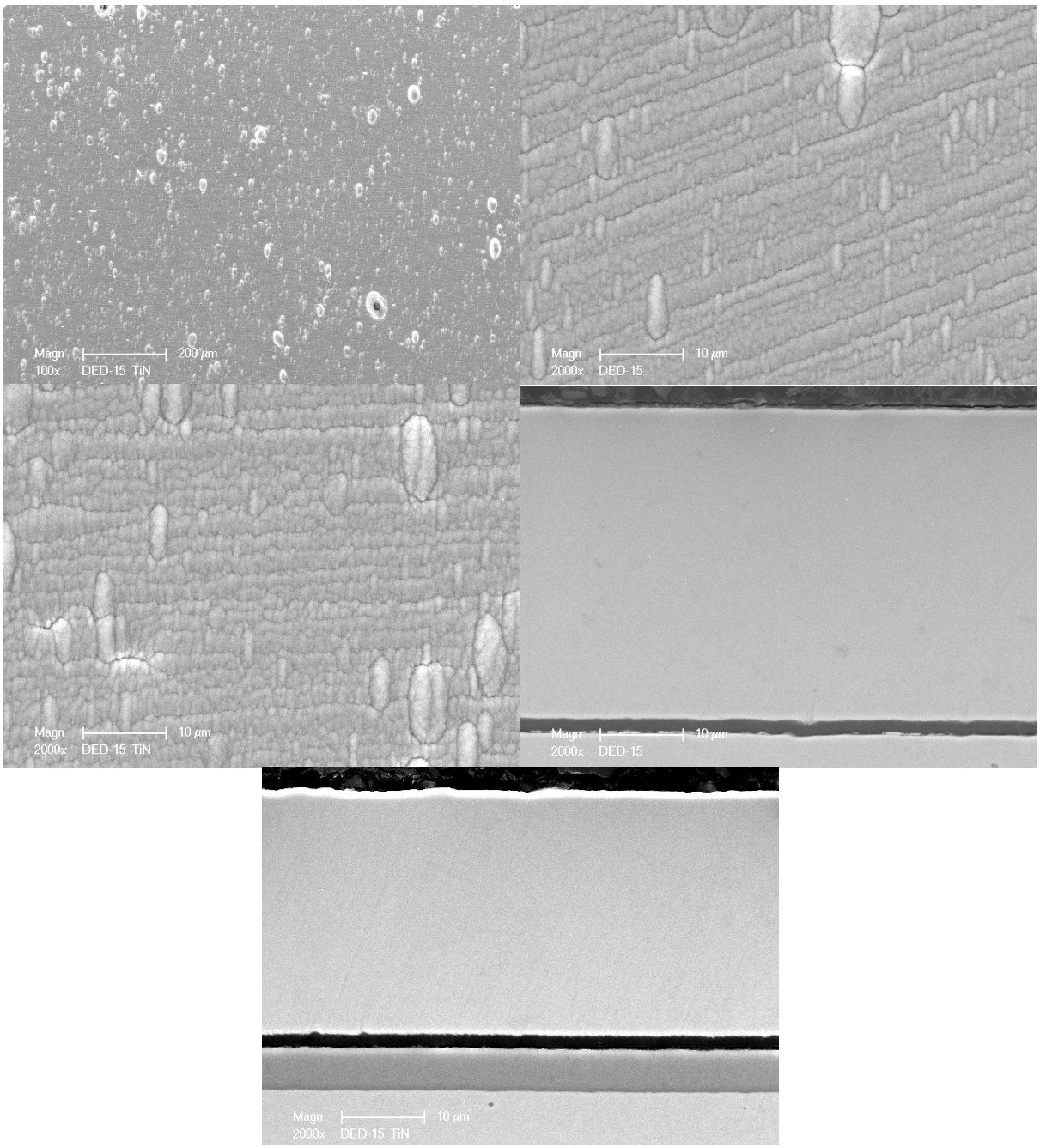

Figure 1.19
Morphological views (top two photographs) and cross-sectional view (bottom photograph) of H160 + 10 wt.% Al coating on AlN/304 SS substrate (left) and AlN/TiN/304SS substrate (right).

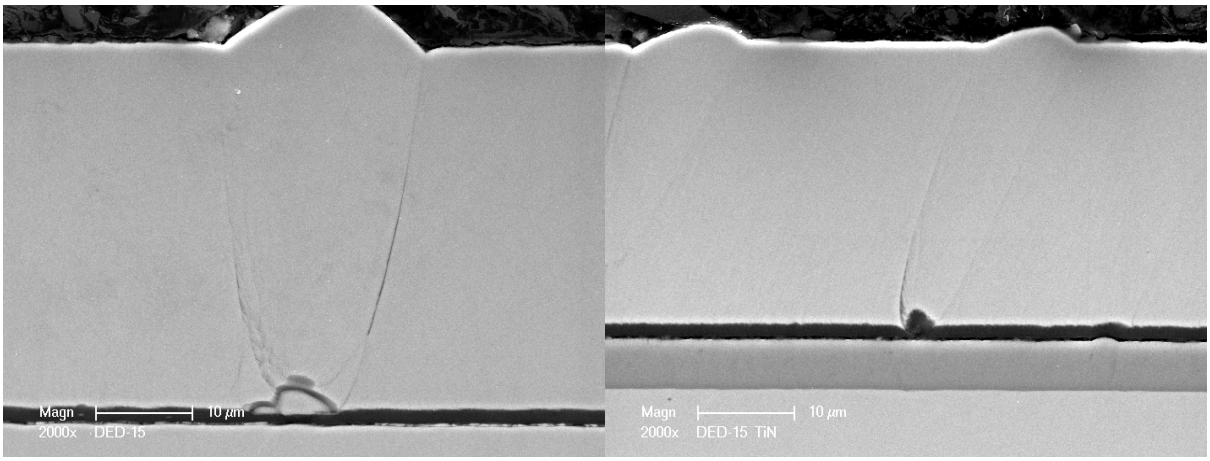

Figure 1.20
High magnification of cross-sectional SEM images of H160 + 10 wt.% Al coating on AlN/304 SS substrate (left) and AlN/TiN/304SS substrate (right) showing the droplet (nodule) formation.

It has been observed from other studies that the coatings produced using the HIPIMS process exhibit high internal stress. One way to evaluate the coating internal stress is by indentation hardness testing using a Rockwell C-scale indenter at 150 kgf load. If the coating delaminates severely, the coating is considered to be brittle and is unsuitable for application on structural components that operate under severe cyclic and thermal loading conditions.

The SEM images of Rc indents on various MCrAl coatings (304 SS + 10 wt.% Al, H120 + 10 wt.% Al, and H160 + 10 wt.% Al) are shown in Figure 1.21. The images on the left are the MCrAl coatings on AlN/304 SS substrate, while the images on the right are the MCrAl coatings on AlN/TiN/304 SS substrate. Comparison of the similar coatings prepared using only DC magnetron sputtering, revealed that the HIPIMS deposited coatings seem to be more brittle. The H160 + 10 wt.% Al coating completely failed. Consequently, the HIPIMS method is not considered to be suitable for the deposition of the MCrAl coatings for structural components that operate under severe loading conditions.

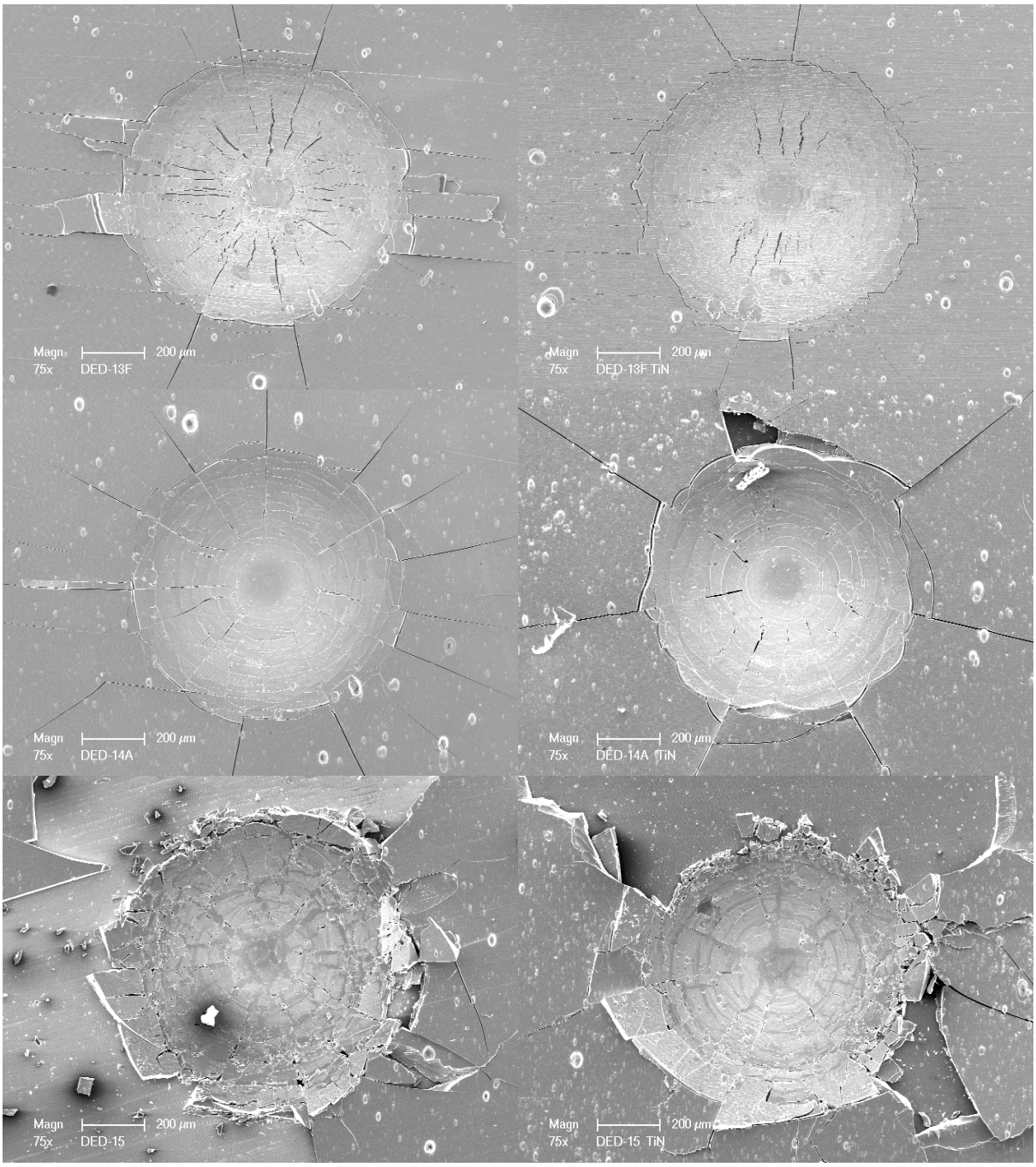

Figure 1.21
SEM images of 304 SS + 10 wt.% Al (top), H120 + 10 wt.% Al (middle) and H160 + 10 wt.% Al (bottom) coatings on AlN/304 SS substrate (left) and AlN/TiN/304 SS substrate (right) after Rc indentation.

For comparison, H188 + 10 wt.% Al coating was deposited on AlN and AlN/TiN coated 304 SS samples using HIPIMS and DC magnetron sputtering process. The processing parameters for the HIPIMS and DC magnetron are shown in Table 1.6. Following application of the coating, the coating surface morphology and the cross section of all specimens were examined in a SEM. The SEM images of the HIMPIS deposited samples the DC magnetron sputtered samples are shown in Figures 1.22 and 1.23, respectively. Comparison SEM micrographs reveal that the HIPIMS deposited coating is very dense and contains relative to the DC magnetron sputtered coating. It is also noted that the high internal stress caused the TiN to crack as illustrated in Figure 1.24 (bottom left cross-sectional image). Comparison of the Rc indentation images (Figure 1.21) show that HIPIMS coating is more brittle relative to the DC magnetron sputtering coating and is less resistant to cracking and spalling. Again, the HIPIMS process seems to generate higher coating stress, which is considered to be responsible for coating delamination.

Currently, the effect of deposition rates and bias voltage (bombardment) on coating quality is being investigated.

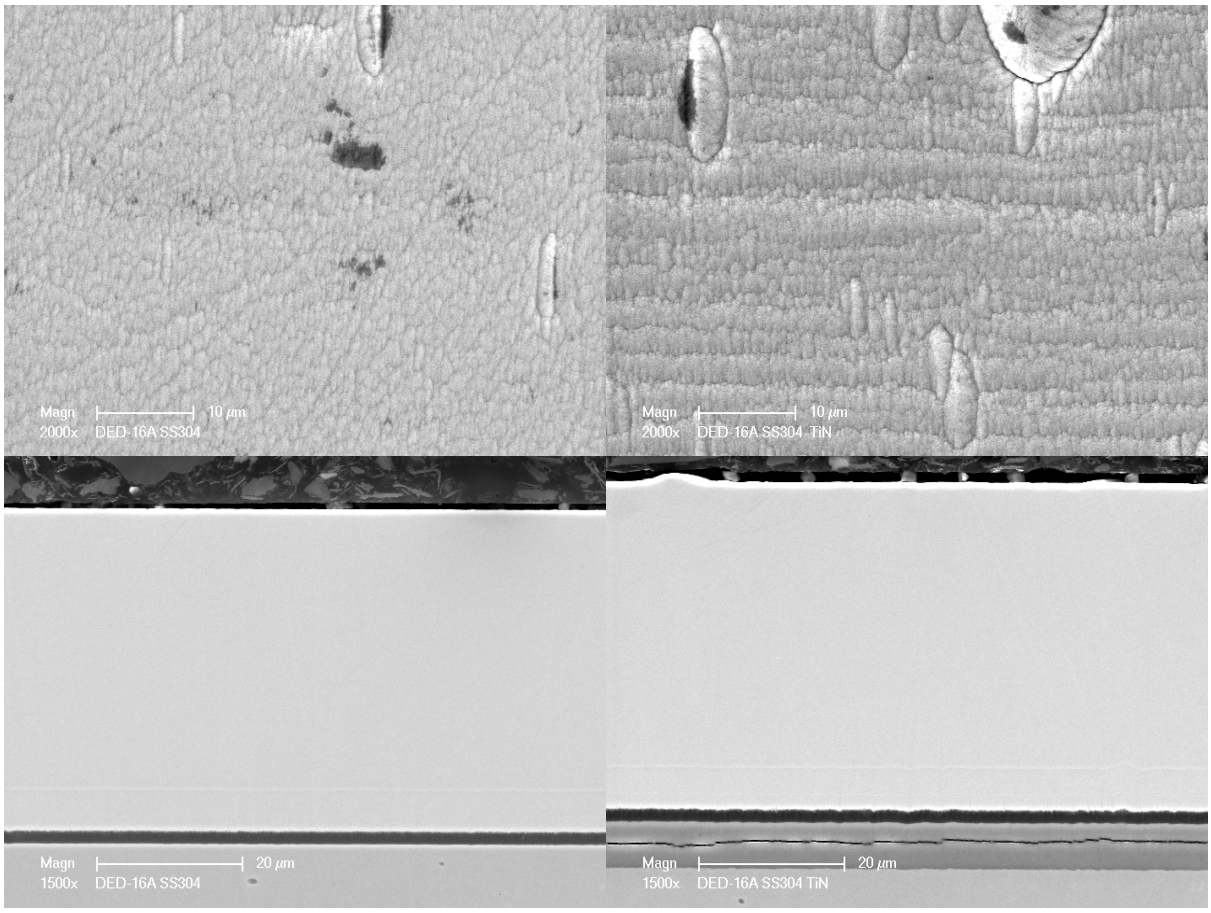

Figure 1.22
Morphological views (top two photographs) and cross-sectional view (bottom photograph) of H188 + 10 wt.% Al coating on AlN/304 SS substrate (left) and AlN/TiN/304 SS substrate (right) deposited using HIPIMS.

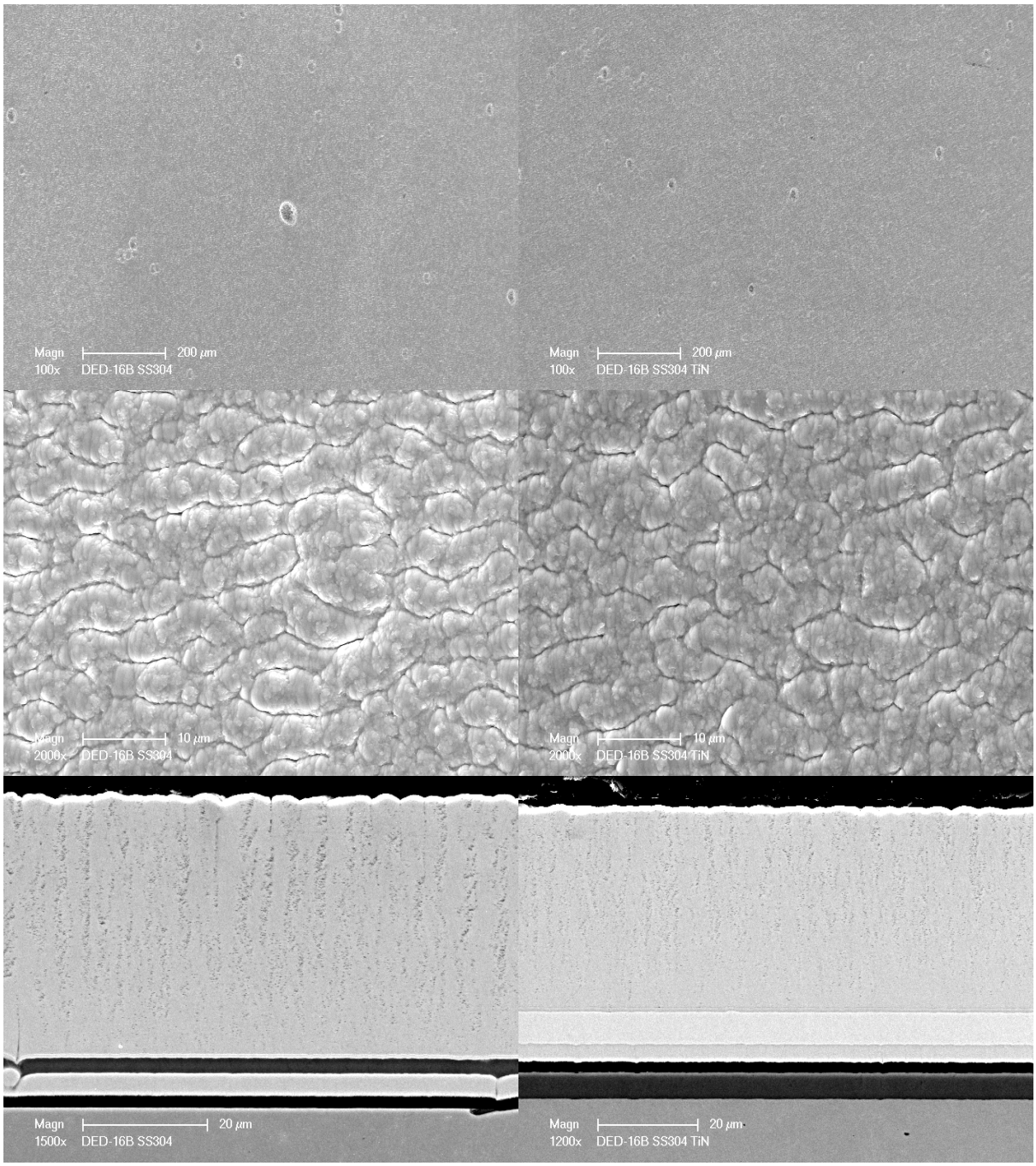

Figure 1.23
Morphological views (top two photographs) and cross-sectional view (bottom photograph) of H188 + 10 wt.% Al coating on AlN/304 SS substrate (left) and AlN/TiN/304 SS substrate (right) deposited using DC magnetron sputtering.

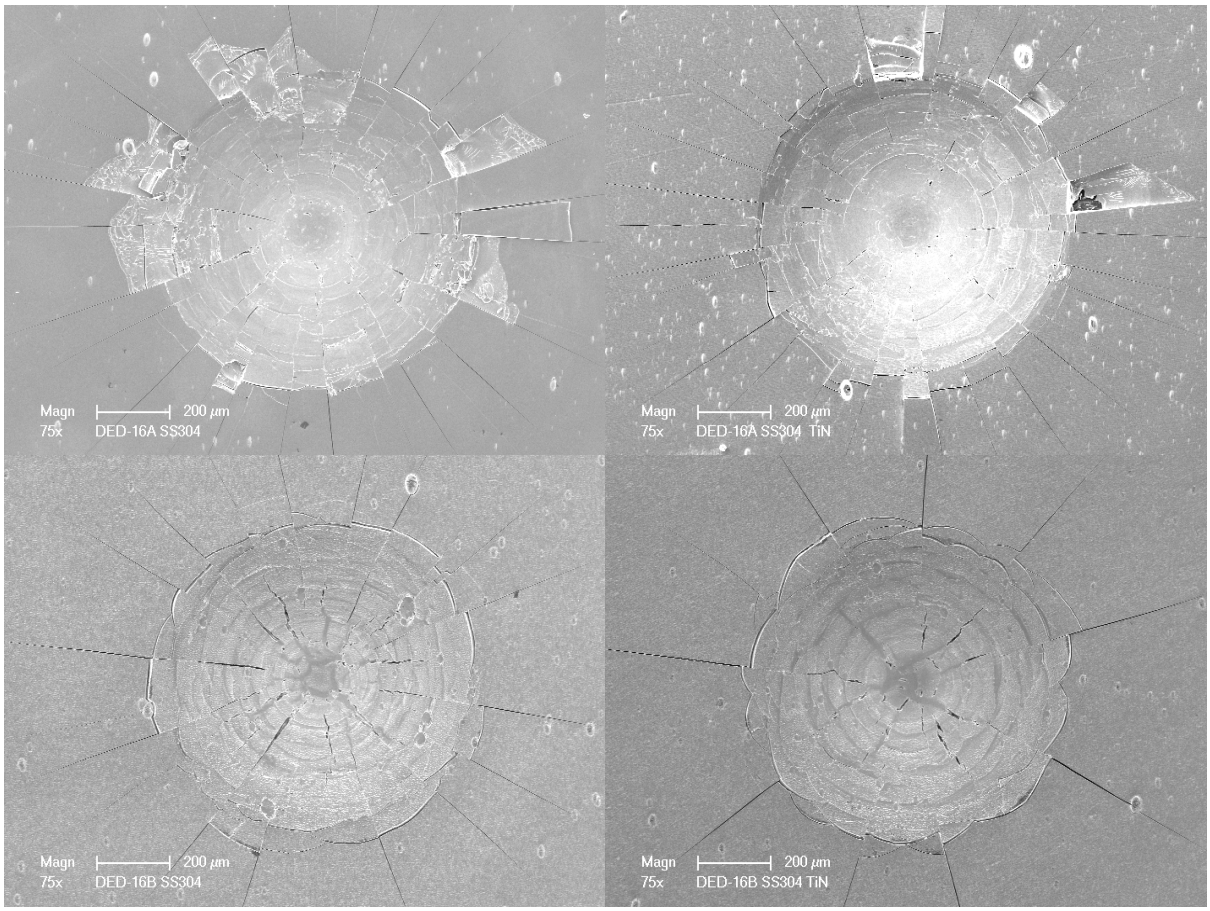

Figure 1.24
Comparison of coating adhesion of HIPIMS (top) and DC magnetron-deposited (bottom), H188 + 10 wt.% Al on uncoated 304 SS (left), and TiN-coated 304 SS (right).

Need for Diffusion Barrier Interlayer Coating

Examination of the cross sections of the Fe-18Cr-8Ni -x Al and Ni-20Cr-xAl nanocrystalline-coated samples revealed that the thermal exposure led to an accelerated loss of Al in the coating due to the inward and outward diffusion of Al [17,19-21]. In relatively short time, the Al content in the Fe-18Cr-8Ni -10 wt.% Al nanocrystalline coating decreased from 10.5 to 3.5 wt.% after exposure of 990 thermal cycles between 750ºC and 25ºC [21]. The rate of Al consumption in the nanocrystalline coatings during thermal exposure was significantly higher than that normally observed in the conventional MCrAl coatings [19,20]. The accelerated rate of Al consumption in these nanocrystalline coatings was due to enhanced grain boundary diffusion. The oxidation life models for these coatings are based on the knowledge of the rate the Al consumption and the amount of Al present in the coating. The accelerated rate of Al consumption limits the oxidation life time of nanocrystalline coatings. Therefore, for the long-term durability of these coatings, it is necessary to minimize Al diffusion from the coating into the substrate. It is well known that a diffusion barrier interlayer coating would normally prevent Al diffusion from the coating into the substrate.

An attempt was made to develop a diffusion barrier coating. A thin barrier (TiN or TiSiCN, or AlN) coating, a few microns thick interlayer, was applied prior to the application of either the Fe-18Cr-8Ni-10 wt.% Al or Ni-20Cr-10 wt.% Al top coating. The coating process parameters were optimized for application of the barrier layer.

Development and Application Diffusion Barrier and MCrAl Coatings

Three ceramic coatings, TiN, TiSiCN and AlN, were selected as the barrier coating. In the service conductor industry, the widely used diffusion barrier coating is TiN. These two coatings are Ti-based coatings and have to be prepared prior to depositing the top coating of 304 SS + 10 wt.% Al or Ni20Cr + 10 wt.% Al. However, from the process point-of-view, AlN is a preferred barrier coating because both AlN and 304SS + 10 wt.% Al (or Ni20Cr + 10 wt.% Al) can be deposited in the same batch without breaking the vacuum.

Shown in Table 1.7 are the first few trials of the barrier coatings. Column 1 lists the test number. Column 2 shows the sample type and pre-treatment. Column 3 shows the deposited coating. For DEB1, there was only one AlN barrier coating. For DEB2, only the SS + 10 wt.% Al coating was deposited and for DEB3, the AlN barrier coating was deposited first then the SS + 10 wt.% Al coating was deposited on top. DEB4 and DEB5 are similar to DEB2 and DEB3, except Ni20Cr was used.

Table 1.7
Processing Parameters for Barrier Coatings

Test No.	Samples	Coating	Deposit Time (h)	T1 Mat'l	P1 (kW)	T2 Mat'l	P2 (kW)	T3 Mat'l	P2 (kW)	T4 Mat'l	P2 (kW)	Q N2 (sccm)	Coating Structure
DEB1	1 SS Small	AlN barrier	1	-	-	Al	1.1	-	-	Al	1.1	75	
DEB2	3 SS, 3 TiN coated, 3 TiSiCN coated	SS+AL	8	304SS	4	Al	1.1	304SS	4	Al	1.1	-	SAL, TiN/SAL, TiSICN/SAL
DEB3	3 SS, 3 TiN coated, 3 TiSiCN coated	AlN barrier SS+AL	1 8	- 304SS	- 4	Al Al	1.1 1.1	- 304SS	- 4	Al Al	1.1 1.1	75 -	AlN/SAL, TiN/AlN/SAL, TiSICN/AlN/SAL
DEB4	3 SS, 3 TiN coated, 3 TiSiCN coated	Ni20Cr +Al	6	Ni20Cr	4	Al	1.1	-	-	-	-	-	NiCrAl, TiN/NiCrAl, TiSICN/NiCrAl
DEB5	3 SS, 3 TiN coated, 3 TiSiCN coated	AlN Barrier Ni20Cr+Al	1 3.5	- Ni20Cr	- 4	Al Al	1.1 1.1	- -	- -	- -	- -	50 -	TiN/AlN/NiCrAl, TiSICN/AlN/NiCrAl

Column 4 shows the deposition time. Typically, the deposition time for AlN is one hour while the deposition time for SS + 10 wt.% Al or Ni20Cr + 10 wt.% Al is much longer. However, during the deposition of DEB5, the target was sputtered through. As a result, the test was terminated. Listed in Columns 5 and 6 are the Target 1 material and the corresponding magnetron power. Similarly, listed in Column 7 through Column 13 are the material and power for Target 2 through Target 4. Column 13 shows the nitrogen flow rate.

It is noted that in Column 2 for Tests DEB2 through DEB5, 3 SS samples without any coating, 3 TiN coated samples and 3 TiSiCN coated samples are used. The TiN and TiSiCN coatings were prepared in a prior batch using SwRI's standard process. Then if we further consider the coatings listed in Column 3, we obtained the multilayered structure as shown in Colum 14 for

samples DEB2 through DEB5. In this way, we are studying the 304SS + wt.% Al coating (abbreviated as SAL) and the Ni-20Cr + 10 wt.% Al coating (Ni-Cr-Al), with and without the diffusion barrier coatings, while the barrier coatings are AlN, TiN, TiSiCN, or TiN/AlN and TiSiCN/AlN.

Coating Characterization

After the deposition, Sample DEB1 was used for the X-ray diffraction to identify the AlN formation. However, the interlayer coating was too thin and no AlN peak could be identified. A specimen from DEB2 through DEB5 was used using SEM to characterize the morphology and the cross-sectional structure. The results are as follows:

Shown in Figure 1.25 are the morphological (left) and cross-sectional (right) SEM images of DEB2 with Figure 1.25a for the SAL only, Figure 1.1b for TiN/SAL, and Figure 1.25c for TiSiCN/SAL. Based on the SEM images, the TiN coating thickness is measured to be about 0.7μm, while the TiSiCN coating thickness is about 0.9μm. Both the morphology and the cross-sectional structure for all the samples are similar as they should be, except that the TiN and TiSiCN diffusion barrier layers have higher contrast to the substrate (304 SS) and the coating (also 304 SS).

Shown in Figure 1.26 are the morphological (left) and cross-sectional (right) SEM images of DEB3 with Figure 1.26a for the AlN/SAL, Figure 1.26b for TiN/AlN/SAL, and Figure 1.26c for TiSiCN/AlN/SAL. The AlN coating thickness cannot be measured due to its low contrast with the substrate and the coating. As in the DEB2 case, both the morphology and the cross-sectional structure for all the samples are similar. Comparing both Figure 1.25 and Figure 1.26, we may note that both morphology and the cross-sectional structure for DEB2 and DEB3 are also similar, as they should be.

Shown in Figure 1.27 are the morphological (left) and cross-sectional (right) SEM images of DEB4 with Figure 1.27a for the Ni-Cr-Al, Figure 1.27b for TiN/ Ni-Cr-Al, and Figure 1.27c for TiSiCN/ Ni-Cr-Al. Upon comparison of the morphology and the cross-sectional structure for all the samples, it appears that the TiN coating and the TiSiCN coating caused the surface roughness to increase; however, the cross-sectional structure for all the coatings was similar. Comparison of the Ni20Cr + 10 wt.% Al coating (Figure 1.27) with the 304SS + 10 wt.% Al coatings (Figures 1.25 and 1.26), we note that the Ni20CrAl coating was much denser with no apparent columnar structure.

Shown in Figure 1.28 are the morphological (left) and cross-sectional (right) SEM images of DEB5 with Figure 1.28a for the AiN/Ni-Cr-Al, Figure 1.4b for TiN/AlN/Ni-Cr-Al, and Figure 1.28c for TiSiCN/AlN/Ni-Cr-Al. The top coating of Ni-Cr-Al was thinner than the other coatings due to the process interruption. Similar to DEB4 (Figure 1.27), the TiN coating and the TiSiCN coating caused some surface roughness to increase, which was also observed in the cross-sectional image.

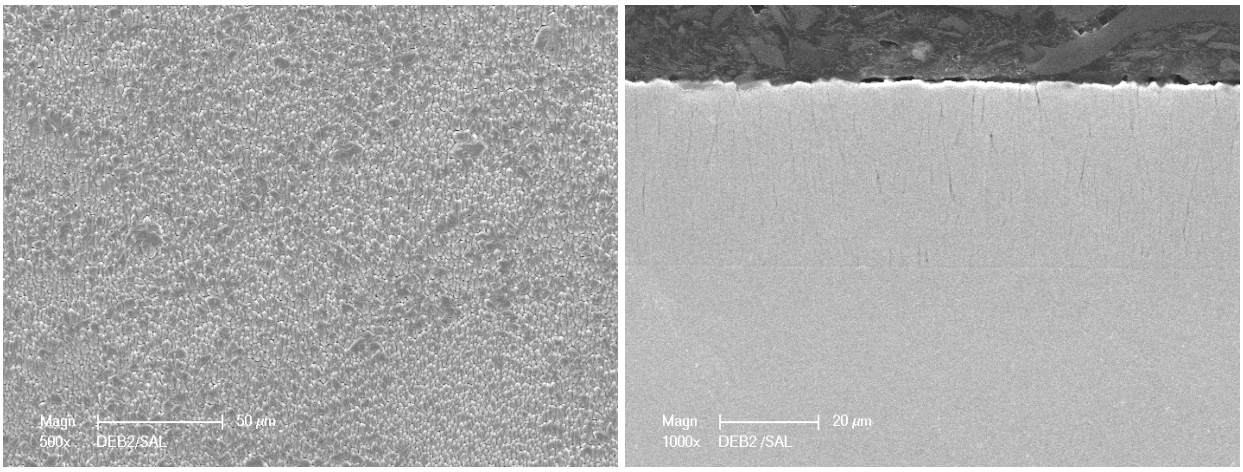

(a)

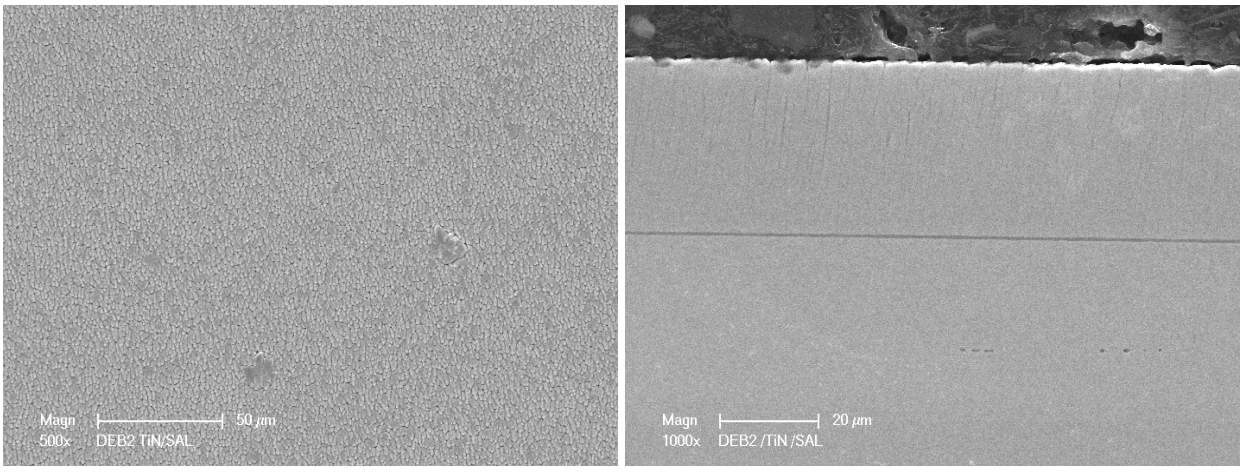

(b)

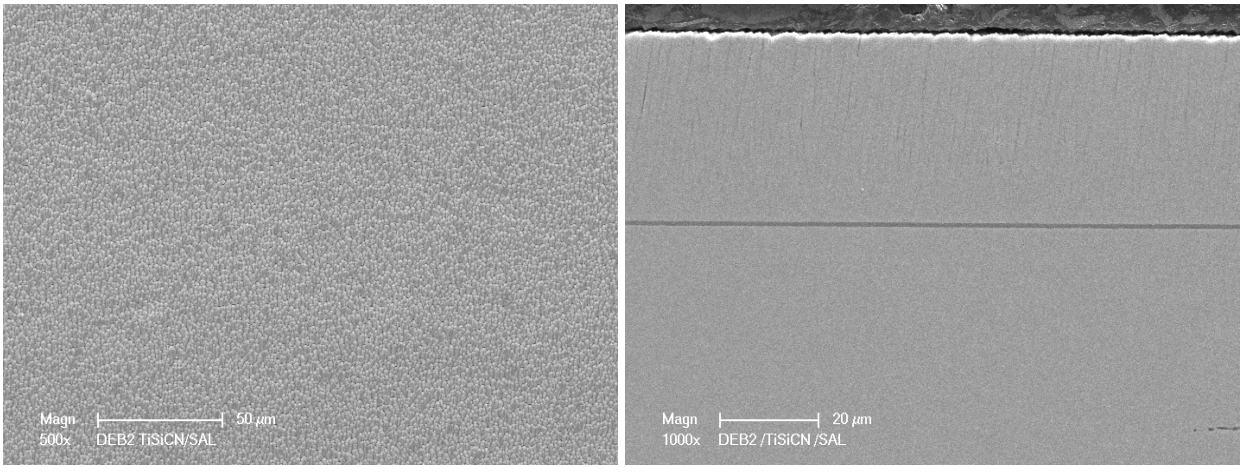

(c)

Figure 1.25
Morphological (left) and cross-sectional (right) SEM images of DEB2.

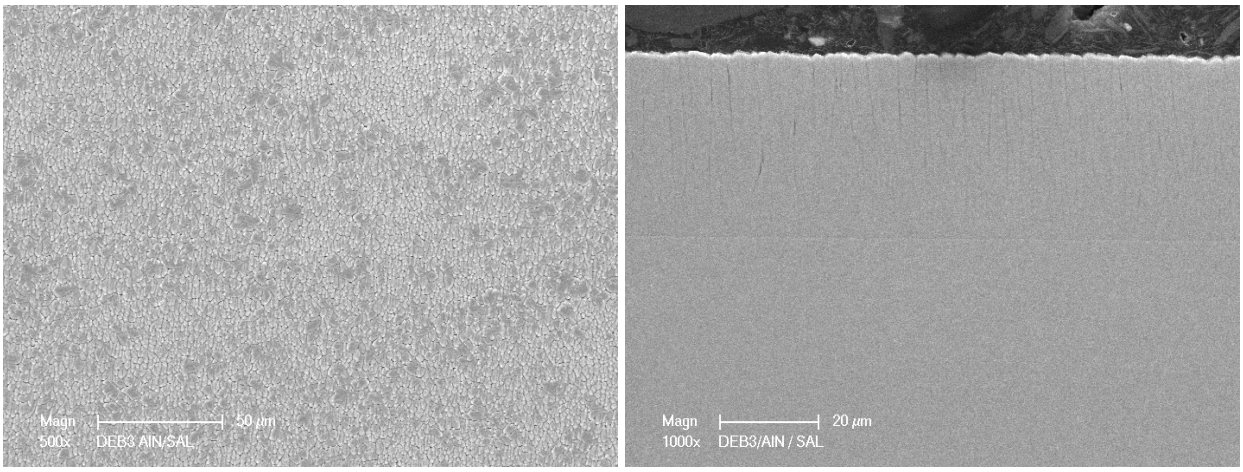

(a)

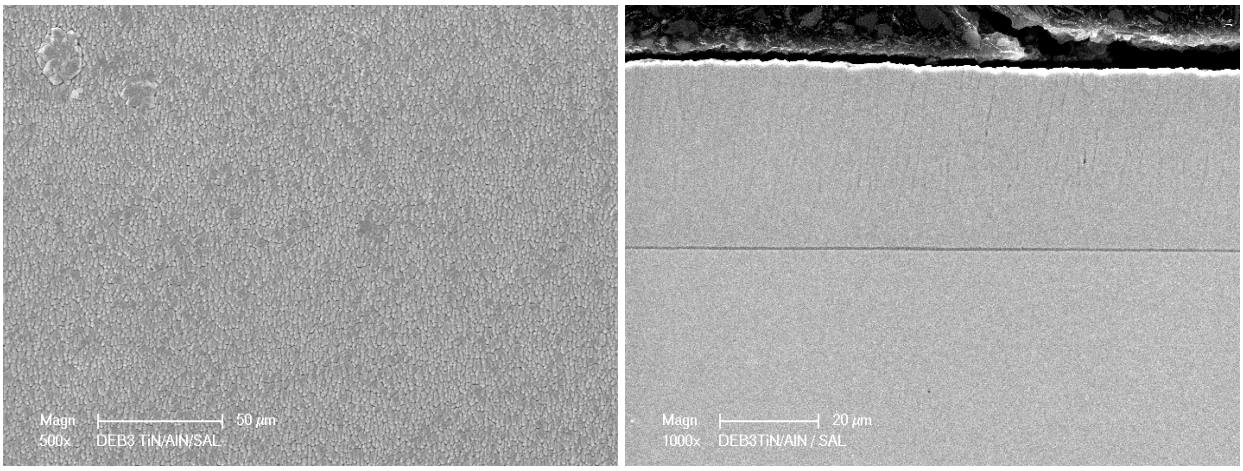

(b)

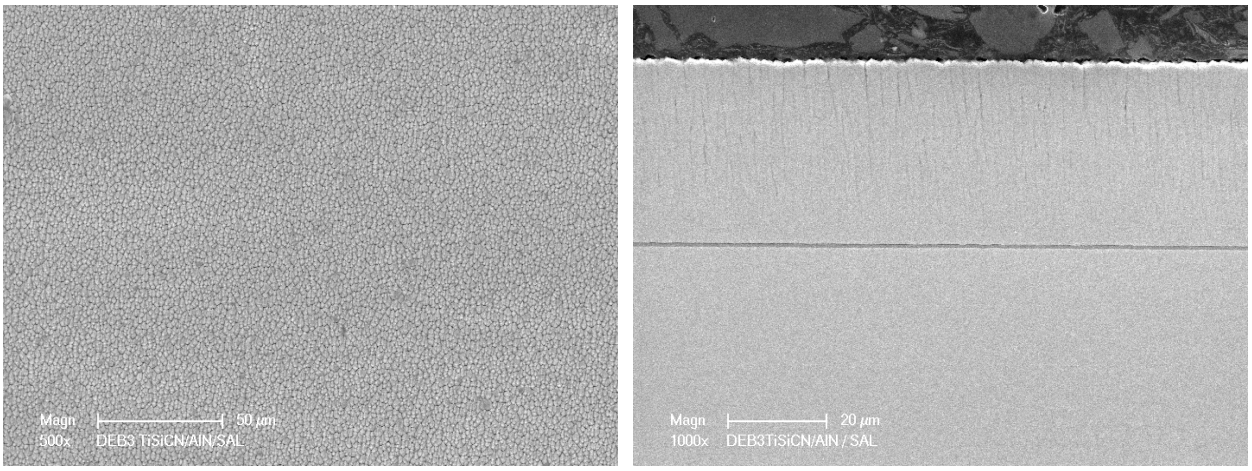

(c)

Figure 1.26
Morphological (left) and cross-sectional (right) SEM images of DEB3.

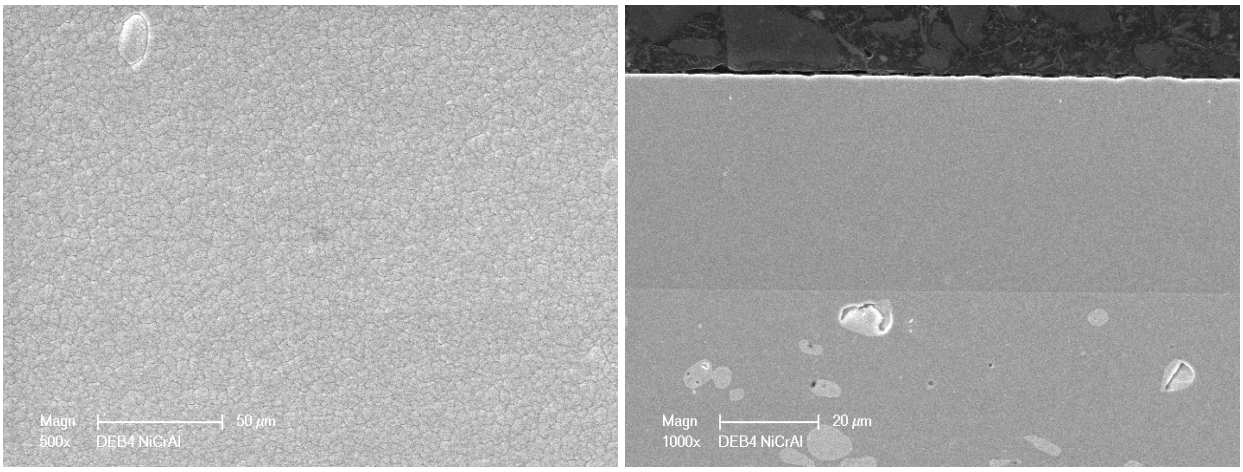

(a)

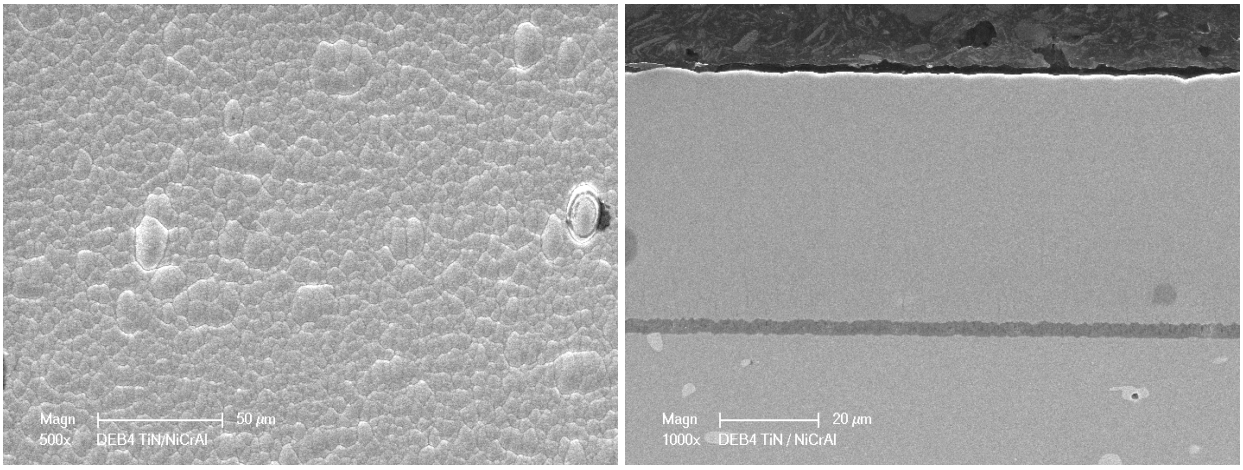

(b)

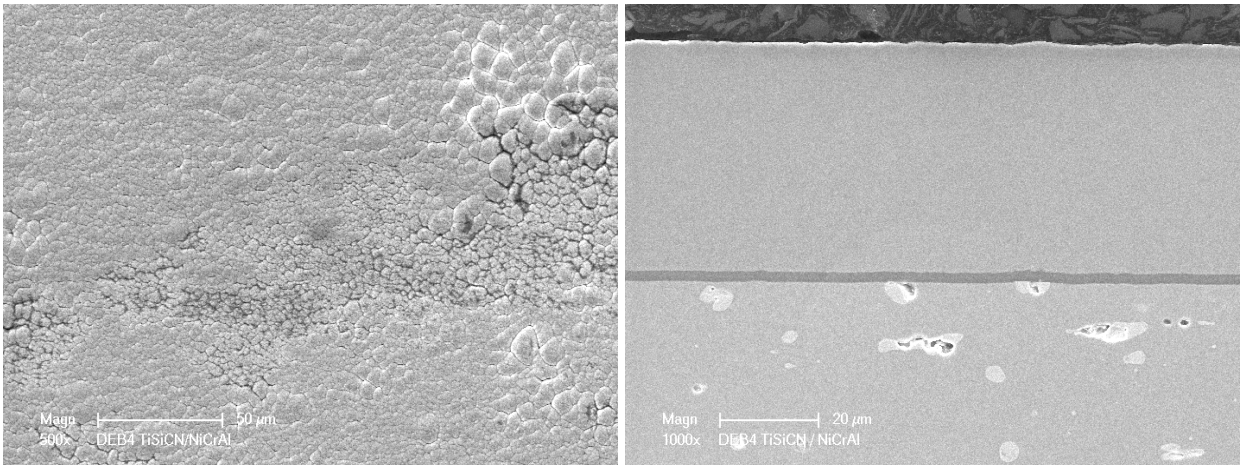

(c)

Figure 1.27
Morphological (left) and cross-sectional (right) SEM images of DEB4.

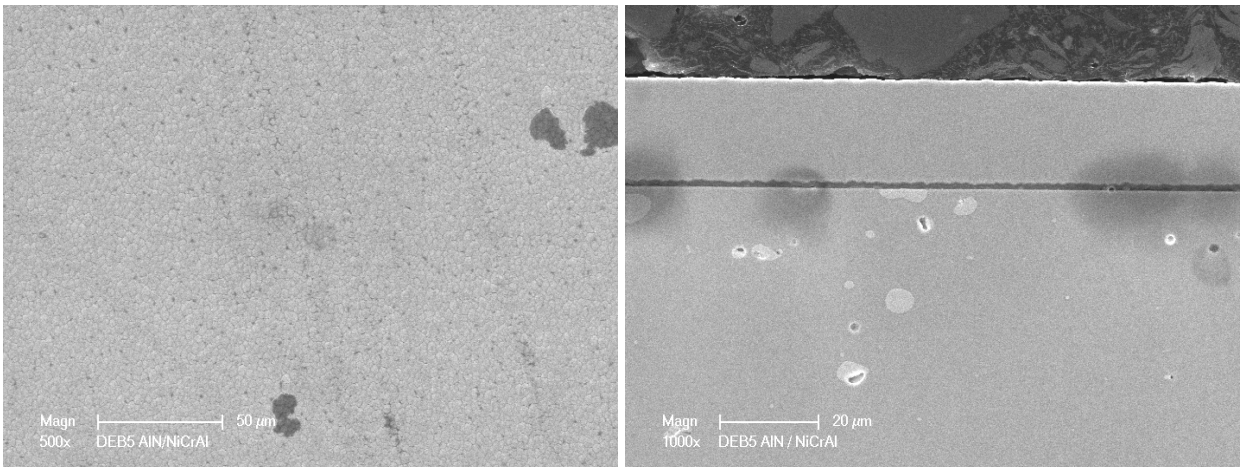

(a)

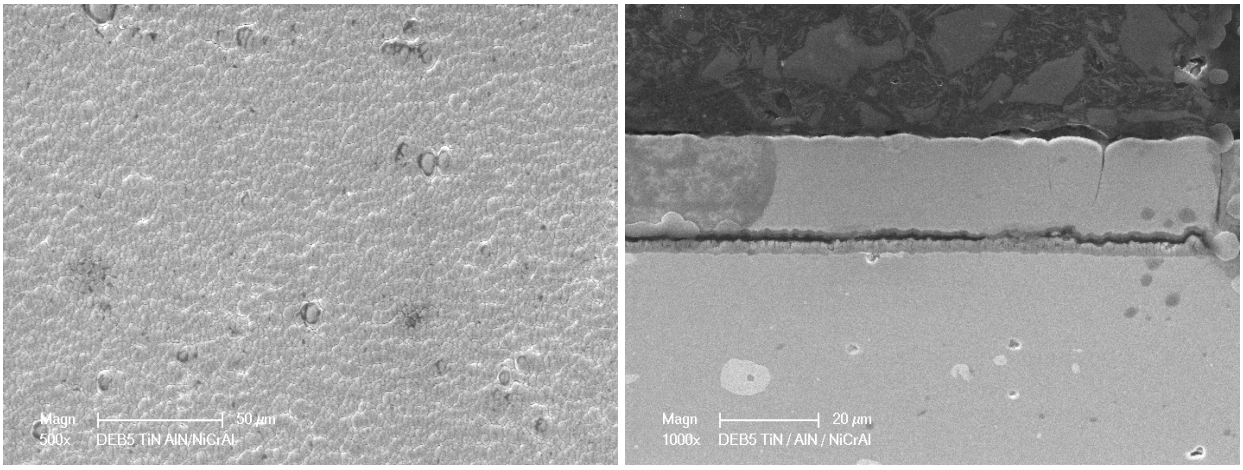

(b)

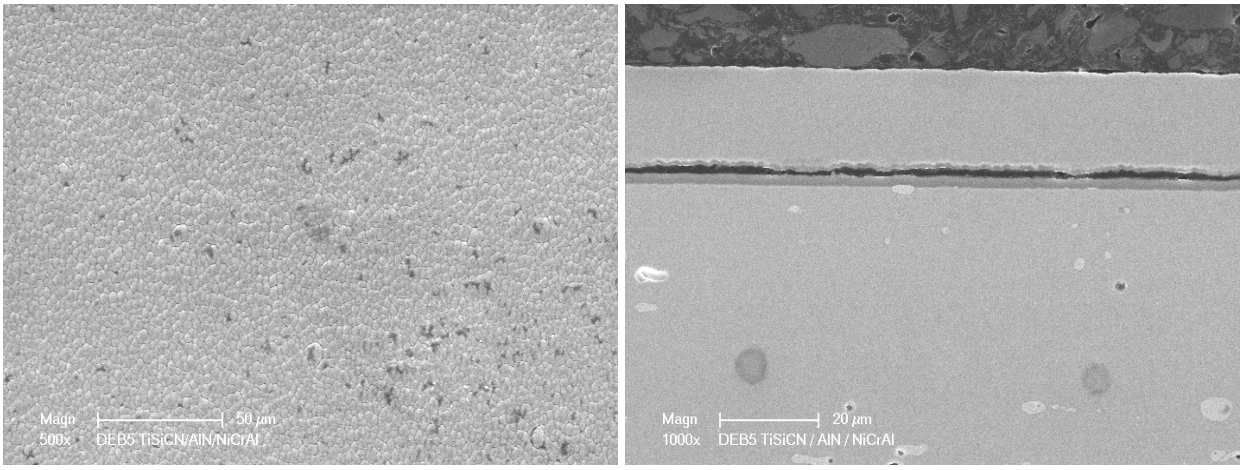

(c)

Figure 1.28
Morphological (left) and cross-sectional (right) SEM images of DEB5.

Characterization of As-Coated Samples

After the preliminary study, a large number of samples were prepared with a diffusion barrier coating and the top MCr coating. A small transverse section was removed from an as-coated sample for microstructural evaluation and metallurgical mounts were prepared from all sections using standard metallographic techniques. The mounts were examined in optical and scanning electron microscopes (SEM). The cross sections of the as-deposited coatings are shown in Figures 1.29 through 1.31. The Ni-20Cr-10 wt.% Al coating thickness over the AlN, TiN, and TiSiCN interlayers were measured to be 18.5, 30.5, and 42 µm, respectively. The Ni-20Cr-10 wt.% Al coating on all three samples was dense and reasonably uniform. The interlayer thickness varied from approximately 1.5 to 2.1 µm among the three coated samples. EDS analysis was performed in the interlayer and the top NiCoCrAlY coatings. As expected, the interlayer showed high levels of Ni and Al or Ti. The chemical composition of the top coating is shown in Table 1.8. It is evident from this table that the Al content among the coatings varied from 11.75 wt.% to 12.14 wt.%. Cyclic oxidation tests were conducted at a peak temperature of 1010ºC on the Ni-20Cr-10 wt.% Al top-coated samples and at 750ºC on the Fe-18Cr-8Ni-10 wt.% Al top-coated samples.

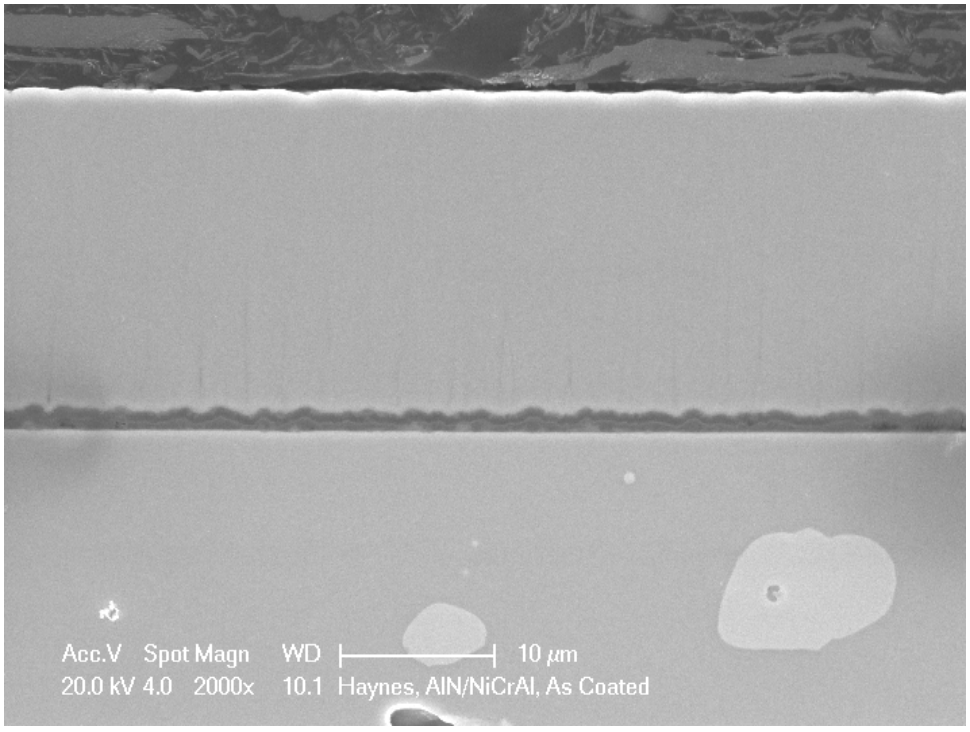

Figure 1.29
Cross section of as-deposited Ni-Cr-Al coating with an AlN diffusion barrier Interlayer.

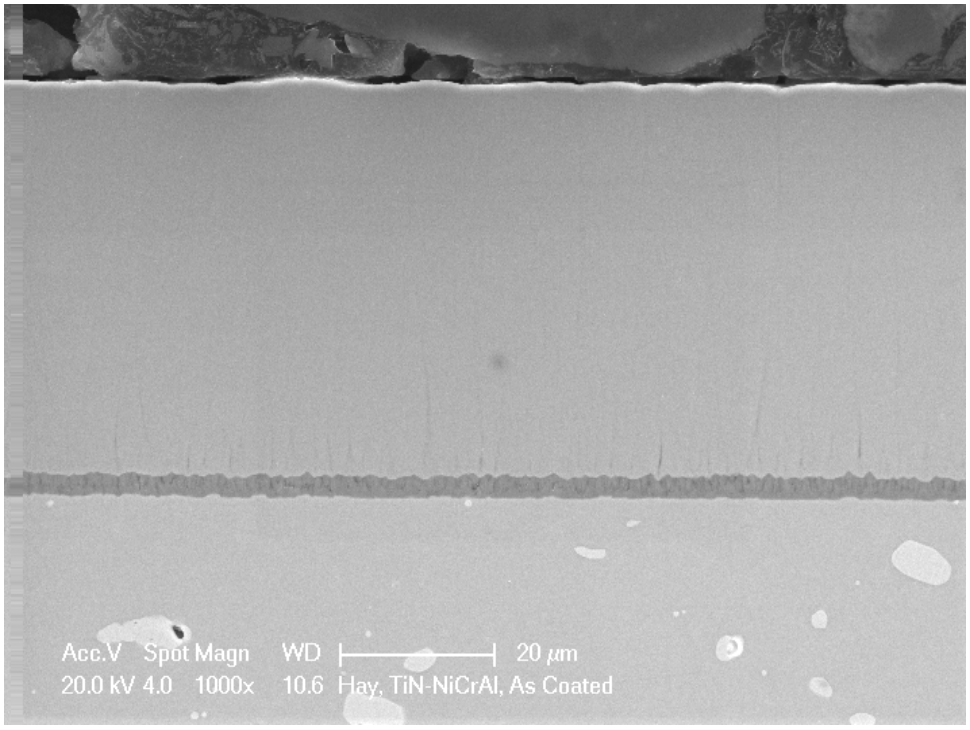

Figure 1.30
Cross section of as-deposited Ni-Cr-Al coating with a TiN diffusion barrier Interlayer.

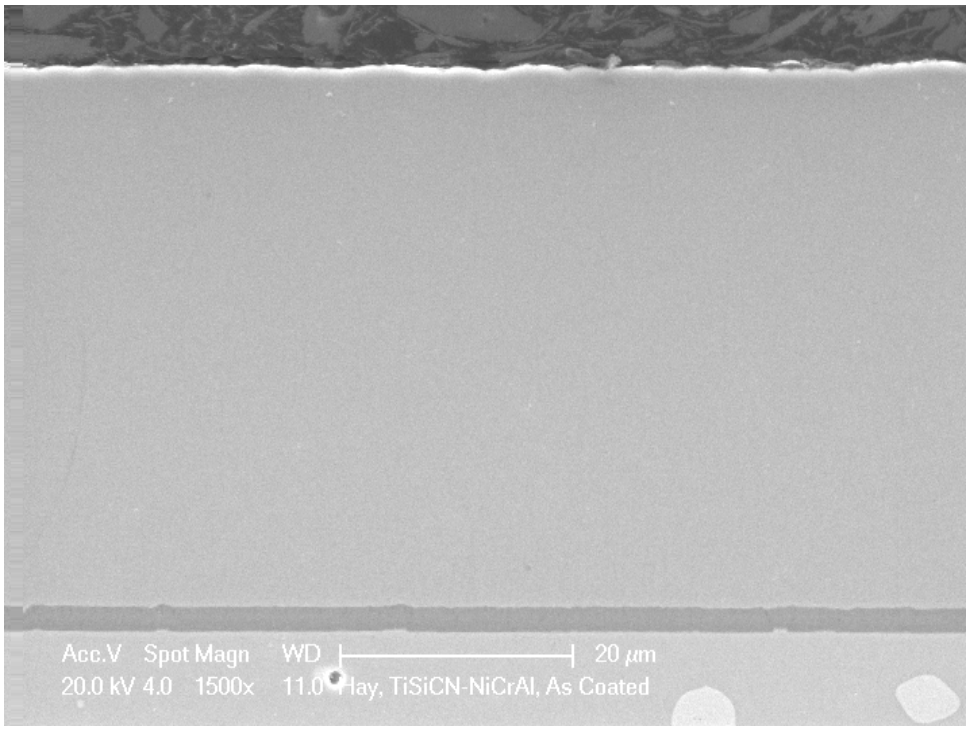

Figure 1.31
Cross section of as-deposited Ni-Cr-Al coating with a TiSiCN diffusion barrier interlayer.

Table 1.8
Semi-Quantitative Chemical Composition of As-Deposited Ni-Cr-Al Coating on the Diffusion Barrier Interlayer, wt.%

Interlayer	Al	Cr	Ni
AlN	12.14	18.66	Balance
TiN	11.75	18.73	Balance
TiSiCN	11.82	18.72	Balance

Oxidation Behavior of Ni-20Cr-10 wt.% Al Coatings with a Diffusion Barrier Interlayer

Cyclic oxidation tests were conducted on the Ni-20Cr-10 wt.% Al coating with a diffusion barrier interlayers on the Haynes 230 samples. The diffusion barrier coatings considered for the evaluation included TiN, TiSiCN, and AlN. The specimens were tested at a peak temperature of 1010ºC. The specimens were thermal cycled in a programmable, automated and bottom drop furnace. For thermal cycling exposure, the specimens were inserted into the furnace which was maintained at the desired peak temperature and held at that temperature for 50 minutes. Following soaking the specimens at the desired peak temperature, the specimens were removed from the furnace for forced air cooling for 10 minutes to room temperature. The samples were then reinserted back into the furnace for another 50 minute cycle. The thermal cycling testing was interrupted at predetermined intervals to weigh the specimens. The mass (weight) change results were documented as a function of number thermal cycles.

The weight change during thermal cycling of coated and uncoated samples at the peak temperature of 1010ºC are compared in Figure 1-32. The cyclic oxidation kinetics of both the uncoated and coated samples initially gained mass for up to 100 thermal cycles. After initial weight gain, the uncoated samples showed evidence of weight loss after approximately 100 thermal cycles. It is clear from the plot that the coated samples showed no evidence weight loss throughout the entire cyclic oxidation test of approximately 2000 thermal cycles between 1010ºC and room temperature. Typically, weight loss of the samples is due to domination of oxide scale spallation during thermal cycling. The cyclic oxidation kinetics of all the coated samples, irrespective of the interlayer composition, appeared to exhibit a parabolic relationship with the number of thermal cycles, suggesting that the protective oxide scale on the coated samples was highly resistant spallation. The cyclic oxidation behavior of all the coated samples with three different interlayers is comparable.

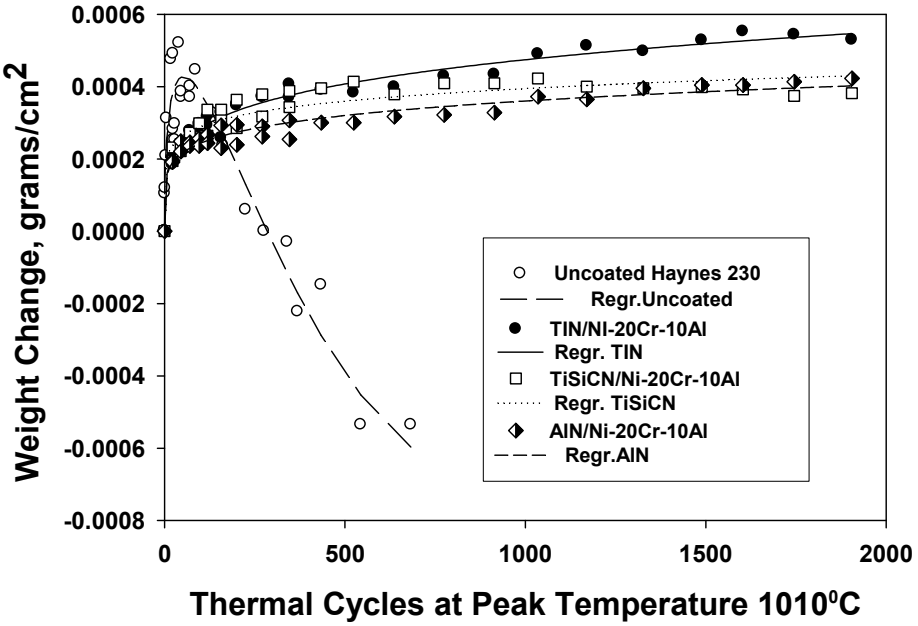

Figure 1.32
Comparison of weight change results of uncoated and sputter-deposited Ni-20Cr-10 wt.% Al coating with different diffusion barrier interlayers on Haynes 230.

Influence of Interdiffusion Layer on Inward Diffusion

Ni-20Cr-10 wt.% Al Coating with Interdiffusion Barrier Interlayer

A transverse section was removed from each coated sample after 346 and 2105 thermal cycles. Metallurgical mounts prepared from these sections were examined and Al content in the overall coating was determined using EDS. Figures 1.33 through 1.35 show the cross sections of the three coatings after 2105 cycles exposure. Examination of the cross sections showed a continuous, uniform Al_2O_3 oxide scale on the external surfaces of all three coatings. The AlN interlayer showed evidence of disintegration after thermal exposure. The TiN and TiSiCN interlayers were continuous after thermal exposure and no degradation was observed. Thermal exposure led to formation of chromium-depleted areas in the Ni-Cr-Al coating adjacent to the AlN interlayer (Figure 1.33), while Cr-rich and Ni-depleted areas in the coating adjacent to the TiN interlayer (Figure 1.34). It is not uncommon for Ni or Cr to segregate to localized areas in highly alloyed Ni-Cr solid solutions. The presence of the TiN interlayer appeared to promote precipitation of Al-rich particles in the coating near the interlayer during thermal exposure. Comparison of the Figure 1.34 and 1.35 micrographs shows the extent of Al-rich particles in the coating was more severe near the TiSiCN interlayer than in the Ni-Cr-Al coating with the TiN interlayer. Al-rich precipitates were observed in the Ni-Cr-Al coated samples at the coating/substrate interface without a diffusion barrier coating interlayer, as illustrated in Figure 1.36.

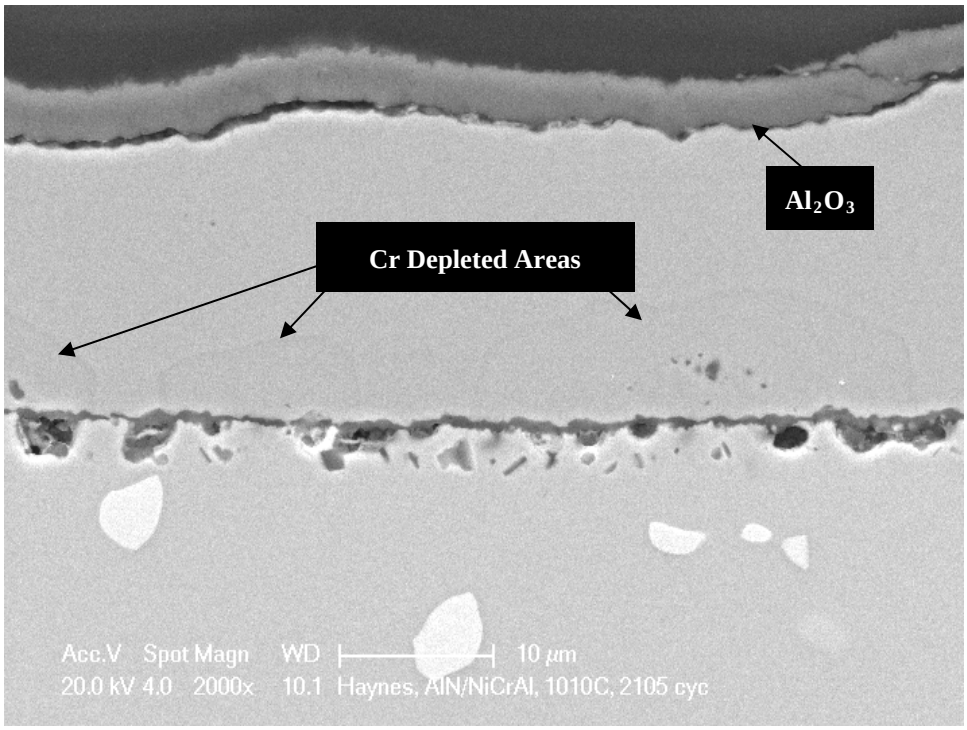

Figure 1.33
Cross section of the Ni-Cr-Al coating with an AlN diffusion barrier interlayer after 2105 cycles exposure.

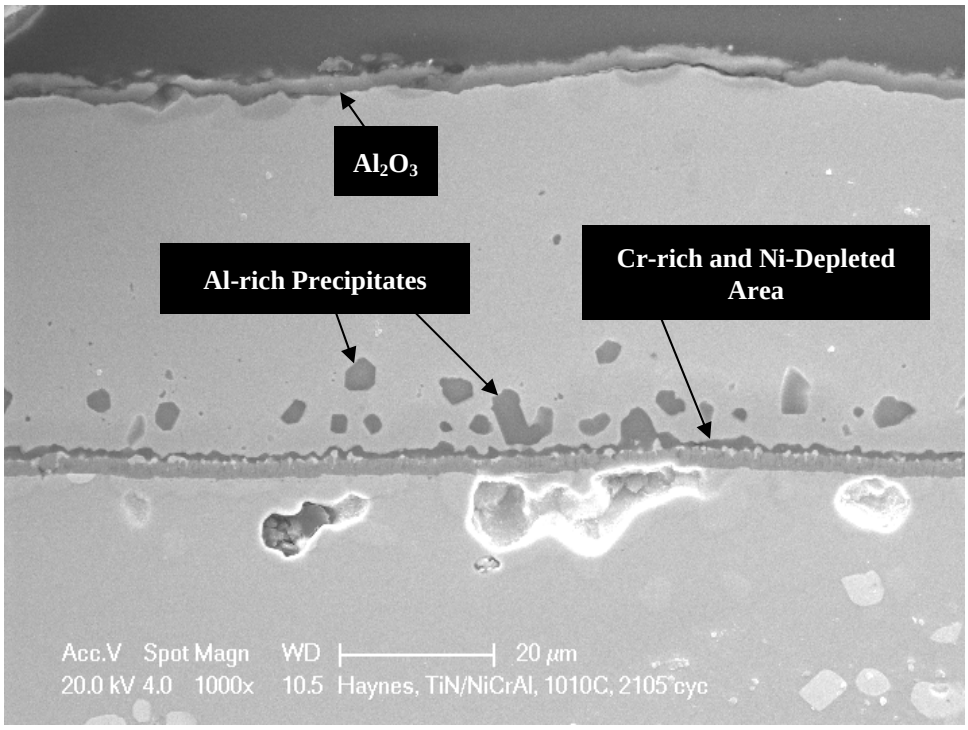

Figure 1.34
Cross section of the Ni-Cr-Al coating with a TiN diffusion barrier interlayer after 2105 cycles exposure.

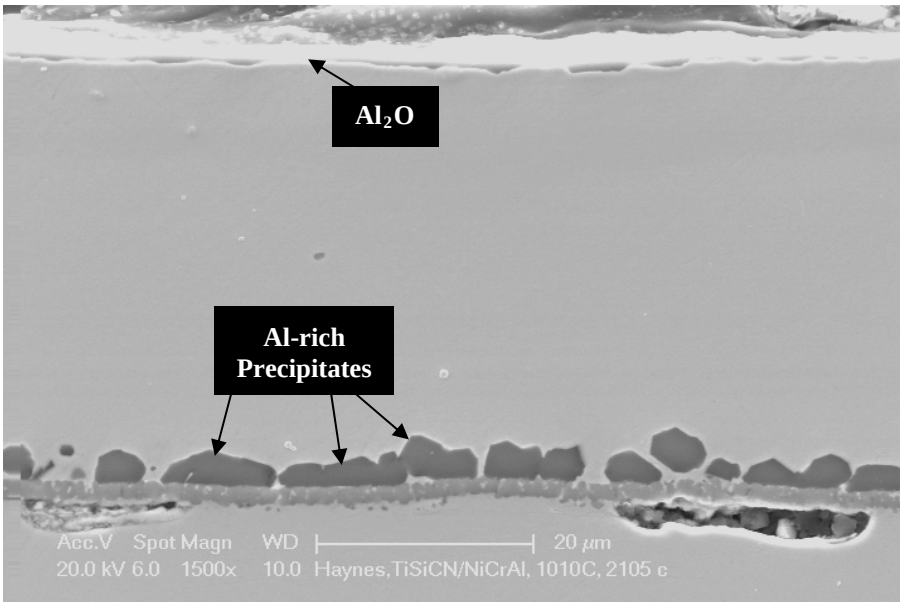

Figure 1.35
Cross section of the Ni-Cr-Al coating with a TiSiCN diffusion barrier interlayer after 2105 cycles exposure.

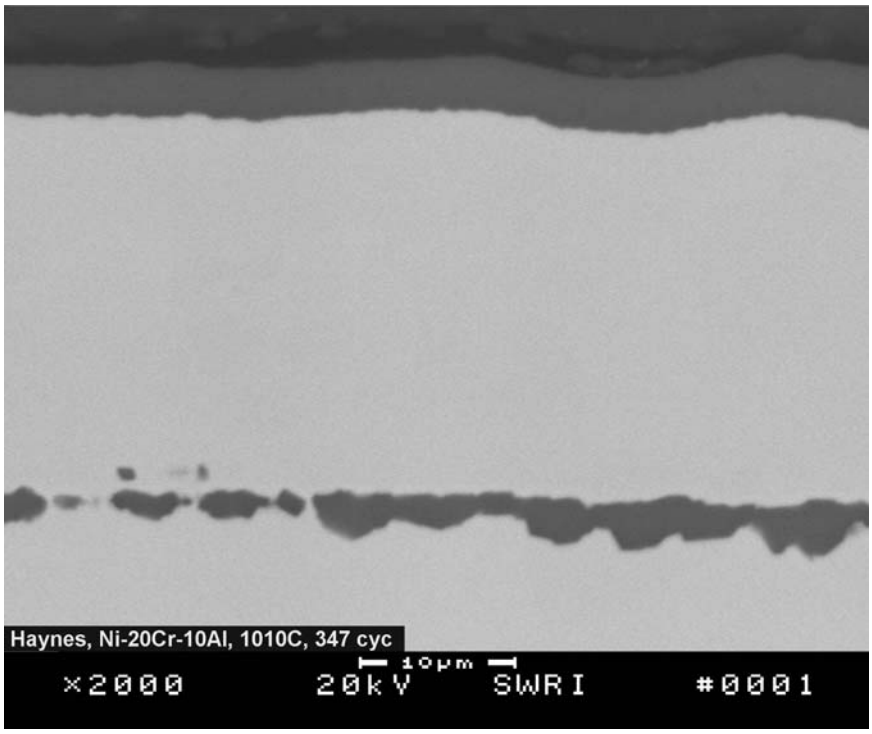

(a)

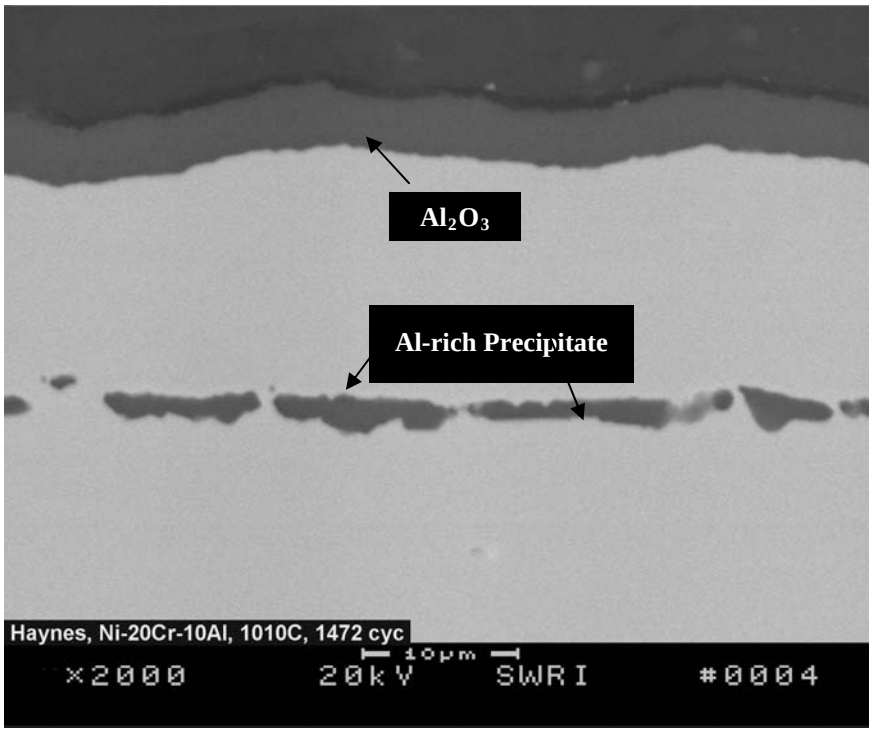

(b)

Figure 1.36
Cross section of the Ni-20Cr-10 wt.% Al coating on Haynes 230 sample without a diffusion barrier interlayer after (a) 347, and (b) 1472 cycles exposure at the peak temperature of 1010ºC.

For chemical composition of the coating, composition measurements were made by EDS at several locations on the overall coating excluding Al_2O_3 scale and Al-rich particles. The Al content in the Ni-Cr-Al coatings with, and without, a diffusion barrier layer after exposure is presented in Table 1.9. The overall Al content in the Ni-Cr-Al coating without a diffusion barrier dropped from 10.56 wt.% in the as-deposited condition to 1.71 wt.% after 347 cycles exposure and to 0.69 wt.% after 1472 cycles exposure. The Al content in the Ni-Cr-Al coating with AlN, TiN, and TiSiCN diffusion barrier interlayer coatings dropped from approximately 12 wt.% in the original as-coated condition to 8.2 wt.%, 8.8 wt.%, and 2.94 wt.%, respectively after 2105 cycles exposure. These results suggest that the AlN and TiN interlayer coatings can be used as a diffusion barrier coating. The metallographic results (Figures 1.34 and 1.35) showed that the TiN interlayer was more stable relative to AlN at 1010ºC.

Table 1.9
Aluminum Content in the Ni-Cr-Al Coating Before and After Thermal Cycling Between 1010ºC and 25ºC

Interlayer	Number of Thermal Cycles	Al Content in the Ni-Cr-Al (wt.%)
No interlayer	0	10.56
No interlayer	347	1.71
No interlayer	1472	0.69
AlN	0	12.14
AlN	346	10.90
AlN	2105	8.22
TiN	0	11.75
TiN	346	11.73
TiN	2105	8.88
TiSiCN	0	11.82
TiSiCN	346	Not Determined
TiSiCN	2105	2.94

Fe-18Cr 8Ni-10 wt.% Al Coating with Interdiffusion Barrier Interlayer

To evaluate the effectiveness of diffusion barrier interlayer coatings on inward diffusion Al from the coating into the 304 SS substrate, the FeCrNiAl (304 SS + 10 wt.% Al) coating was applied on AlN, TiN, TiSiCN, TiN/AlN, and TiSiCN/AlN coated 304 SS samples. The coated specimens were thermal cycled in a programmable, automated, and bottom drop furnace. For thermal cycling exposure, the specimens were inserted into the furnace which was maintained at 750ºC and held at that temperature for 50 minutes prior to air cooling for 10 minutes to room temperature. The samples were then reinserted back into the furnace for another 50-minute cycle. After exposure to 1501-thermal cycles, the samples were sectioned for metallographic examination.

Figures 1.37 through 1.41 show the cross sections of the three coatings after 1051-cycles exposure. The examination of the cross sections showed a continuous uniform Al_2O_3 oxide scale on the external surfaces of all coatings. The FeCrNiAl coating on all specimens was in good condition and no severe oxidation of the coating was noted. However, the AlN interlayer

showed evidence of disintegration after thermal exposure. In the 304 SS substrate FeAl precipitates were observed below the inter layer coating in the interdiffusion zone, suggesting that Al had diffused through the disintegrated AlN layer as illustrated in Figure 1.37. The other interlayer coatings were continuous after thermal exposure and showed no evidence of disintegration. Consistent with this observation, no FeAl precipitates were observed below the inter layer as illustrated in Figures 1.38 through 1.41. For chemical composition of the coating, composition measurements were made by EDS at several locations on the overall coating excluding the Al_2O_3 scale. The Al content in the FeCrNiAl coatings with, and without, a diffusion barrier after exposure is presented in Table 1.10.

It is evident from these results that the overall Al content in the FeCrNiAl coatings without a diffusion barrier dropped from 10.5 wt.% in the as-deposited condition to 3.7 wt.% after 990 cycles exposure at 750°C. The Al content in the FeCrNiAl coating with AlN diffusion barrier interlayer coating dropped from approximately about 10 wt.% in the original as-coated condition to 5.38 wt.%, after 1051 cycles exposure. The Al drop is mostly due to inward diffusion of Al into the substrate and formation of FeAl precipitates in the interdiffusion zone. The Al content in the FeCrNiAl coating with TiN and TiSiCN with or without AlN diffusion barrier interlayer dropped from approximately about 10 wt.% in the original as-coated condition to about 9.5 wt.%, after 1051 cycles exposure, In this case the drop is Al is predominantly due to outward diffusion of Al to form a protective oxide layer at the outer surface of the coated samples. The presence of TiN and TiSiCN with or without AlN interlayer between the FeCrNiAl coating and the substrate either slowed down or prevented inward diffusion of Al from the coating into the substrate. The loss of Al in the FeCrNiAl coating on the AlN-coated 304 sample is consistent with the precipitation of FeAl particles in the interdiffusion zone (Figure 1.25) during thermal exposure. These results suggest that the TiN, TiSiCN, and double interlayer coatings can be used as a diffusion barrier coating.

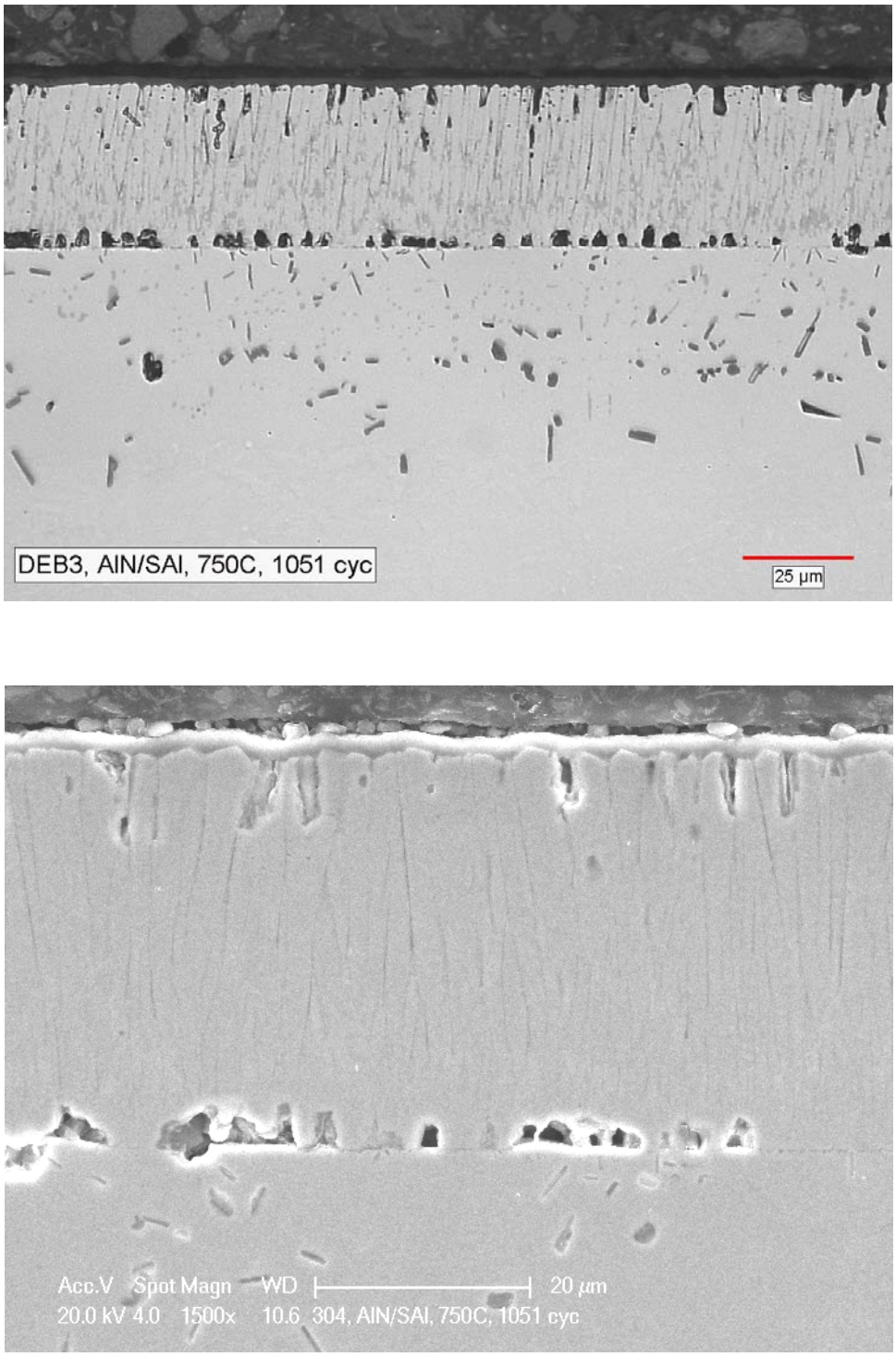

Figure 1.37
Cross section of Fe-18Cr-8Ni-10 wt.% Al coating with an AlN diffusion barrier interlayer after 1051 cycles exposure at 750ºC. Note absence of AlN interlayer and FeAl precipitates in the interdiffusion zone.

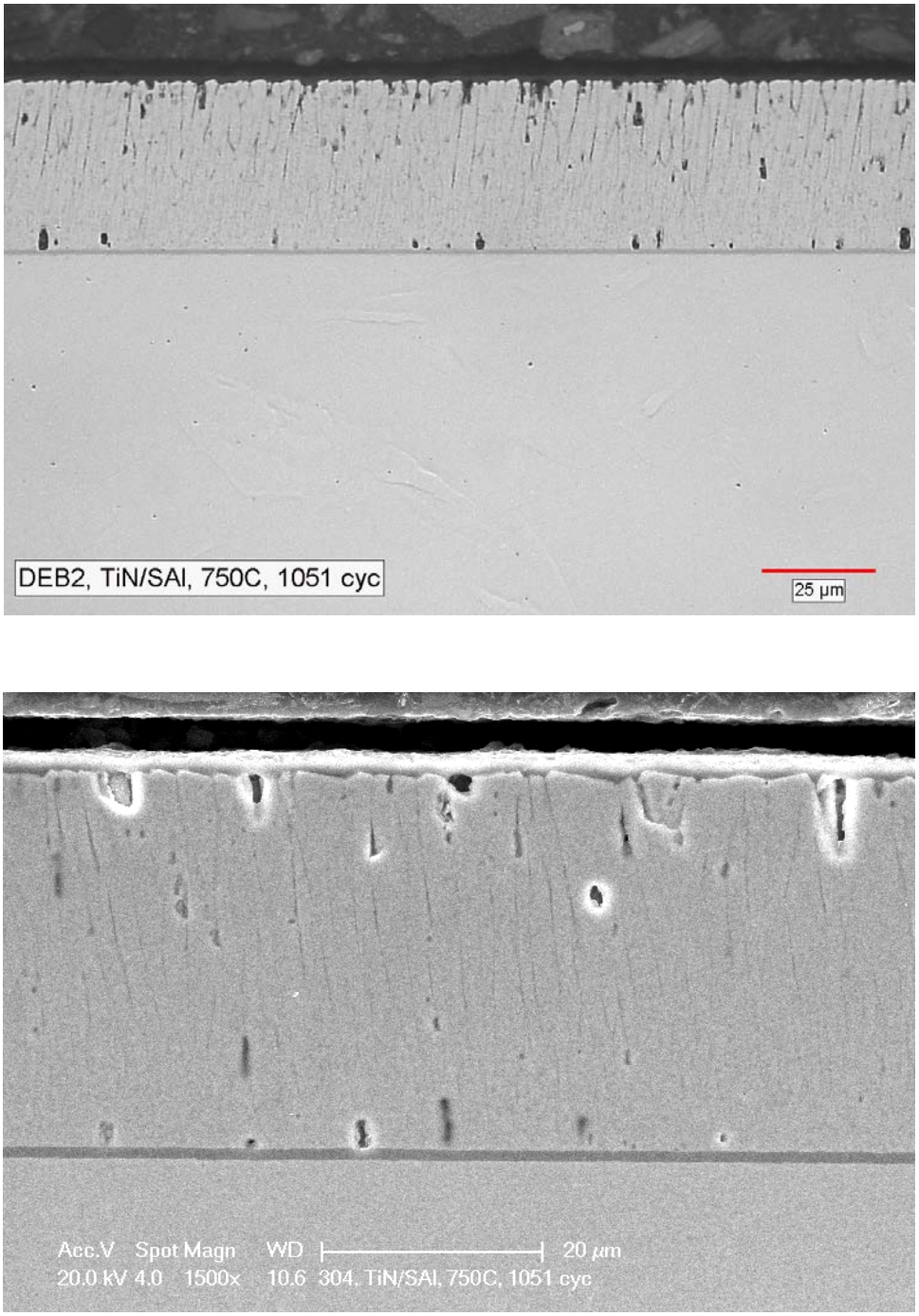

Figure 1.38
Cross section of Fe-18Cr-8Ni-10 wt.% Al coating with a TiN diffusion barrier interlayer after 1051 cycles exposure at 750ºC.

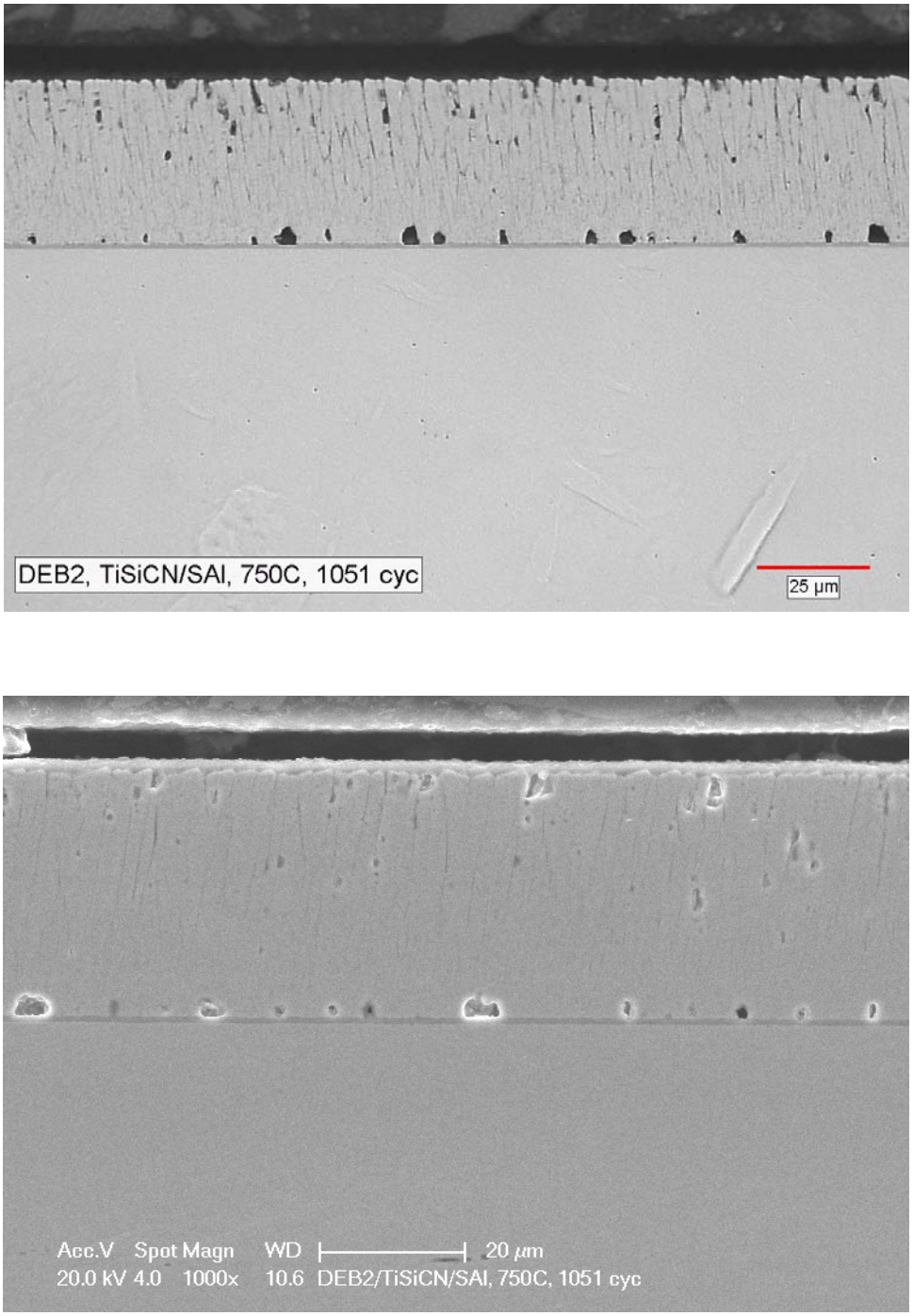

Figure 1.39
Cross section of Fe-18Cr-8Ni-10 wt.% Al coating with a TiSiCN diffusion barrier interlayer after 1051 cycles exposure at 750ºC.

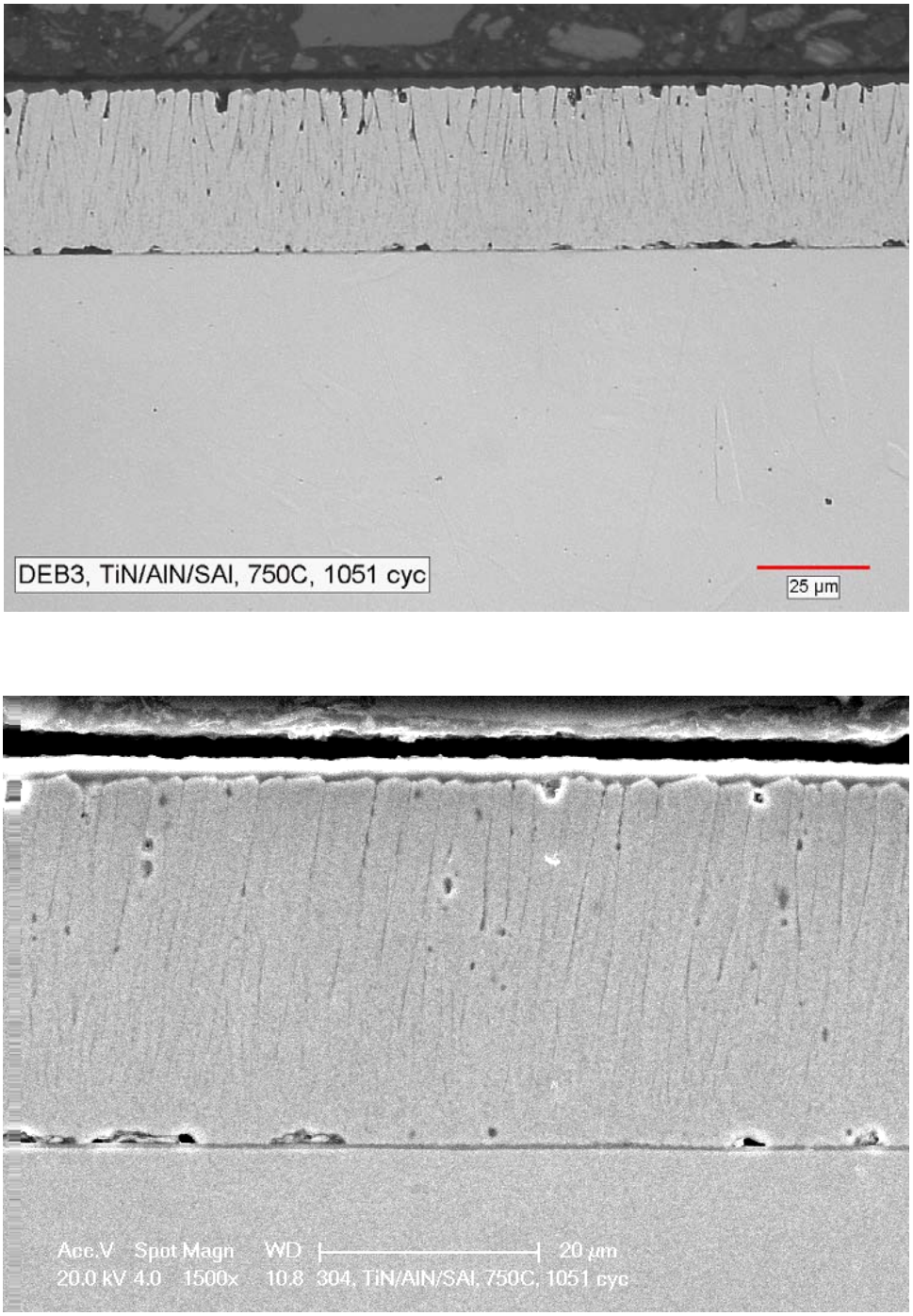

Figure 1.40
Cross section of Fe-18Cr-8Ni-10 wt.% Al coating with a TiN/AlN diffusion barrier interlayer after 1051 cycles exposure at 750ºC.

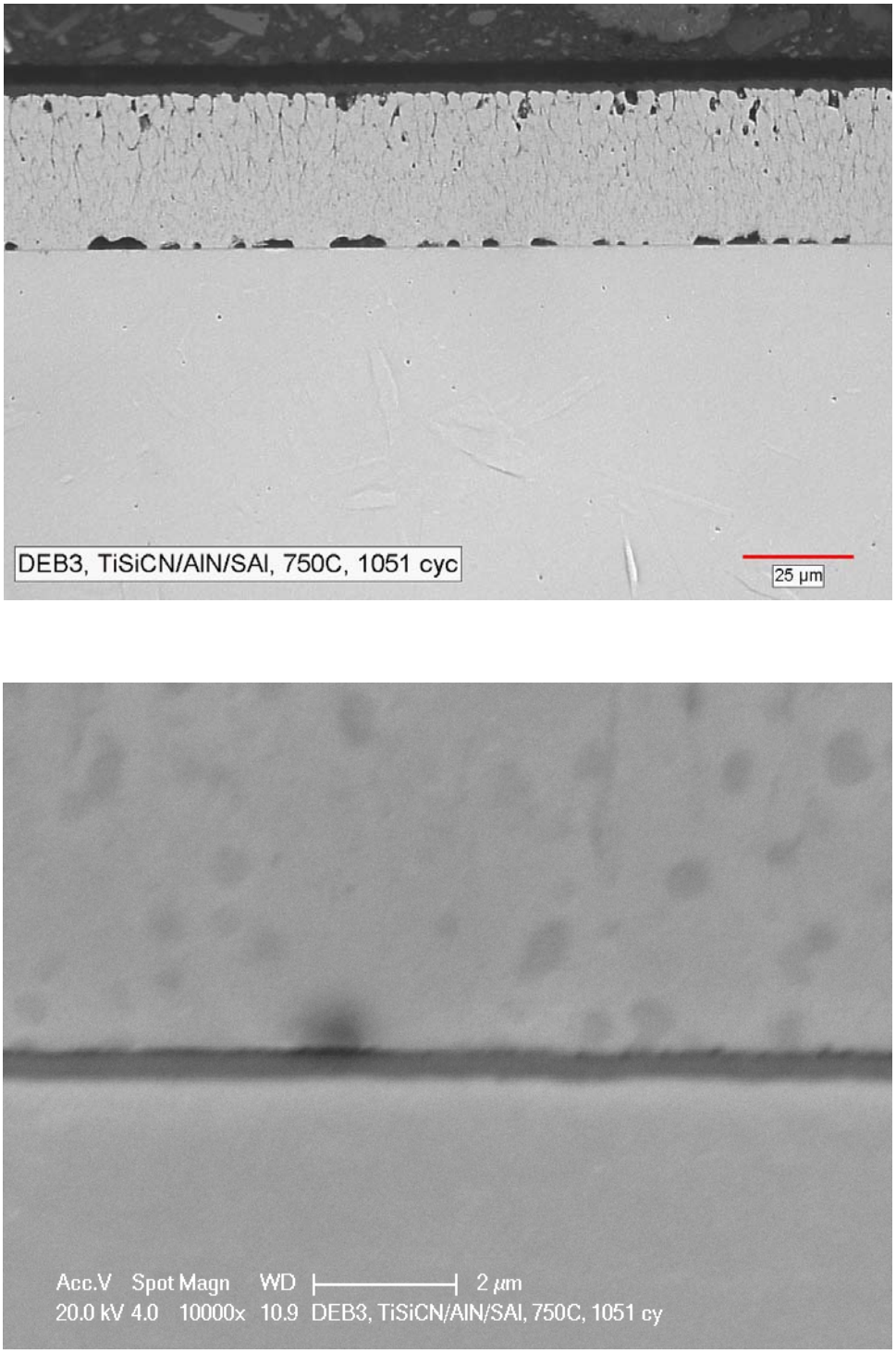

Figure 1.41
Cross section of Fe-18Cr-8Ni-10wt.% Al coating with a TiSiCN/AlN diffusion barrier interlayer after 1051 cycles exposure at 750ºC.

Table 1.10
Aluminum Content in the Fe-Cr-Ni-Al Coating Before and After Thermal Cycling Between 750ºC and 25ºC

Interlayer	Number of Thermal Cycles	Al Content in the FeCrNiAl (wt.%)
No interlayer	0	10.5[1]
No interlayer	990	3.7[1]
AlN	1051	5.38
TiN	1051	9.79
TiSiCN	1051	9.52
TiN/AlN	1051	9.42
TiSiCN/AlN	1051	9.24

Process Optimization of Interlayer Deposition

Diffusion barrier interlayer coating, AlN, was deposited on several 304 SS samples in four coating runs to investigate the effect deposition time on the interlayer coating thickness, microstructure (phase formation), and the quality. The deposition process conditions are shown in Table 1.11. As can be seen from the table, four samples were deposited under the same process conditions (1 kW magnetron power, 100V bias on the sample with the N2 flow rate of 50 sccm) except deposition time.

Table 1.11
Deposition Conditions for AlN Study

Sample No.	Specimen	Substrate	Number of samples	Total No. of Samples	Target 1/ Par (kW)	Target 2/ Par (kW)	Disc Current (A)	Bias Voltage (V)	QN2 (sccm)	Deposit Time (h)
DED5	Large	304 SS	1 column x 2	2	304 SS / 0	Al/ 1.0	0	100	50	0.5
DED6	Large	304 SS	1 column x 2	2	304 SS / 0	Al/ 1.0	0	100	50	1
DED7	Large	304 SS	1 column x 2	2	304 SS / 0	Al/ 1.0	0	100	50	2
DED8	Large	304 SS	1 column x 2	2	304 SS / 0	Al/ 1.0	0	100	50	4

The deposition time was varied from 0.5 to 4 hrs. The thickness of the coating increased with in creasing coating deposition time. After deposition, the samples were characterized using XRD and the XRD pattern are shown in Figure 1.42. An AlN peak near $2\theta = 66.5^{o}$ was observed in all four samples. As expected the AlN peak height increased with increasing deposition time. As the deposition time increased, additional AlN peaks were observed at different 2θ angle positions.

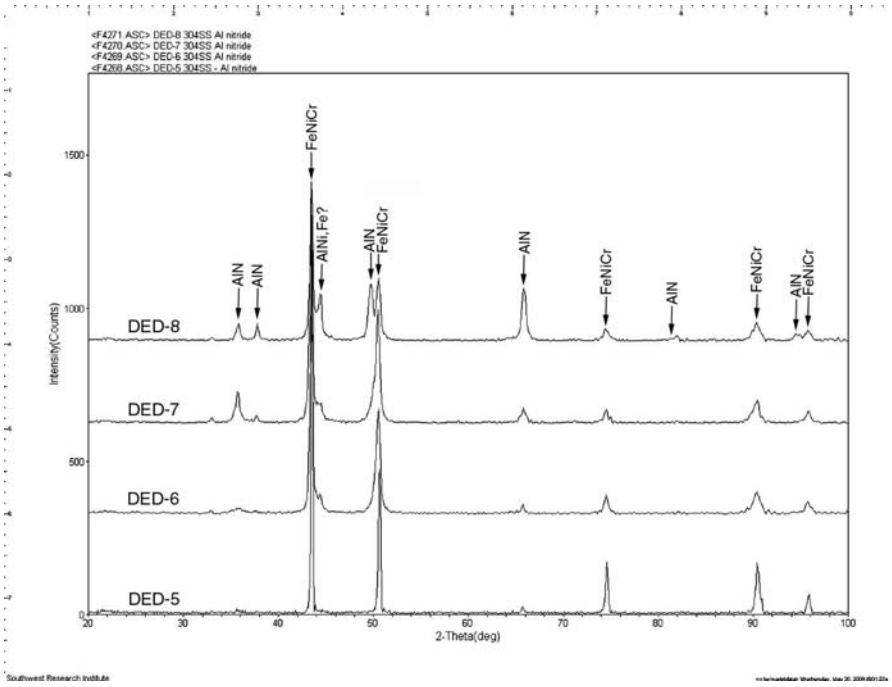

Figure 1.42
XRD data of AlN on four different coated samples DED 5 through DED 8. Note variation AlN peak heights among the four samples.

A transverse section was removed from a sample of each process condition DEB5 through DEB 8. Four sections were mounted and polished using the standard metallographic techniques and the mounts were examined in a SEM for coating quality. The coating on all four samples was dense and free from cracks. The coating/substrate interface was clean and showed no evidence of delamination as illustrated in Figure 1.43. The AlN interlayer coating thickness increased from 0.4 to 3.25 µm as the deposition time increased form 0.5 to 4 hrs. Based on these results, the deposition time of 2 hrs was considered reasonable for AlN deposition of future runs.

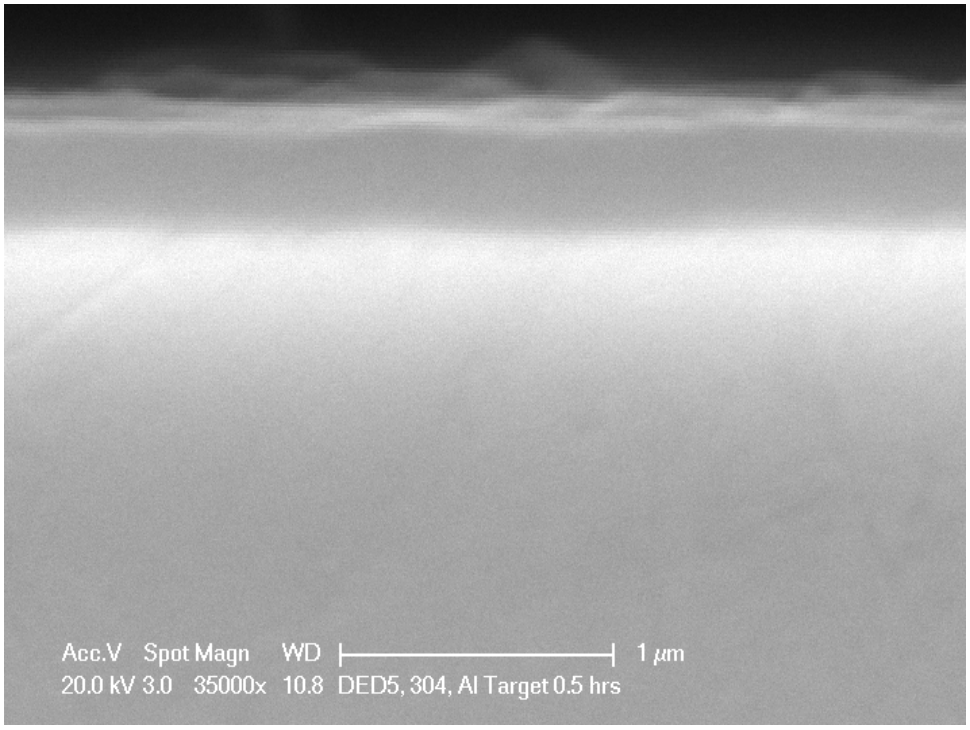

DED 5. Deposition time 0.5 hr. Coating thickness 0.4 μm

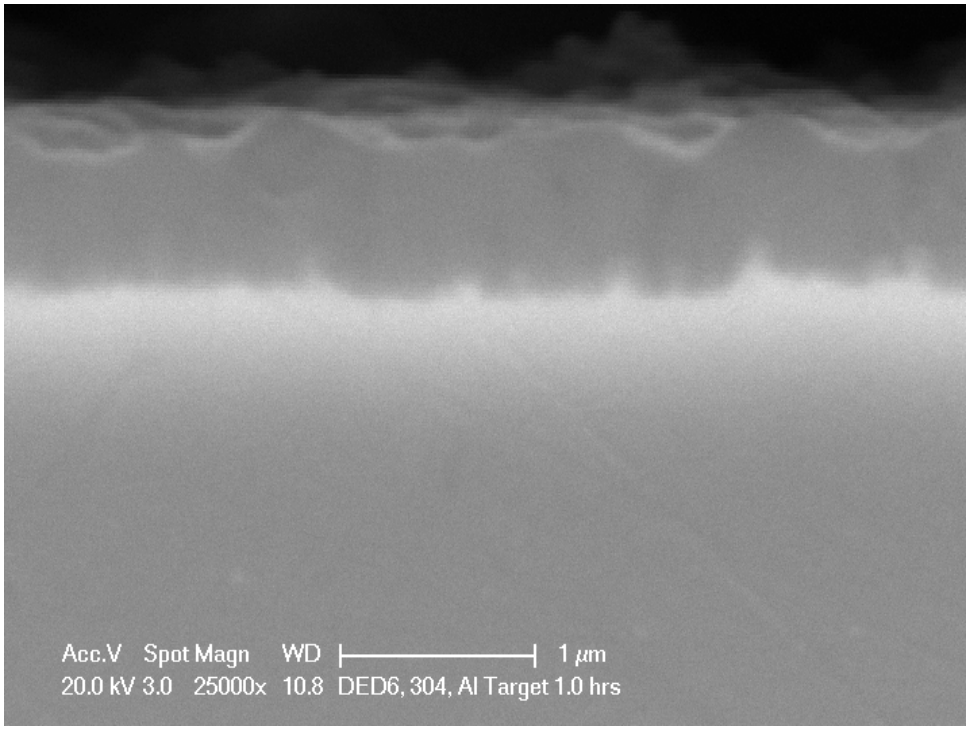

DED 6: Deposition time 1.0 hr. Coating thickness 0.82 μm

Figure 1.43
Transverse sections AlN coated samples showing variation of AlN thickness varying with the deposition time.

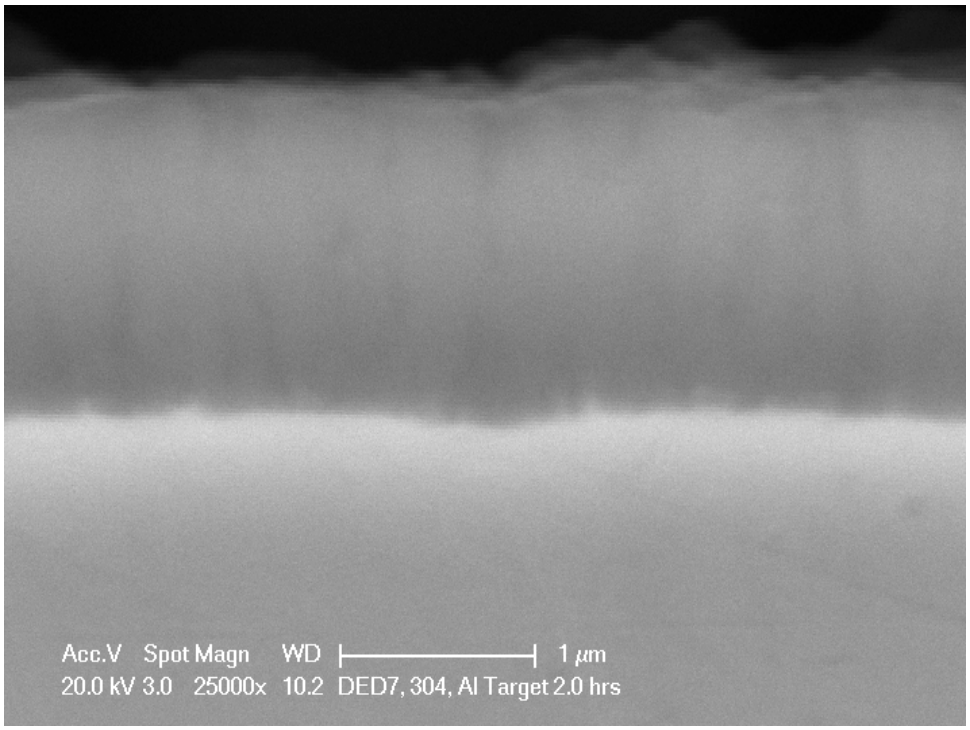

DED 7. Deposition time 2.0 hrs. Coating thickness 1.60 µm

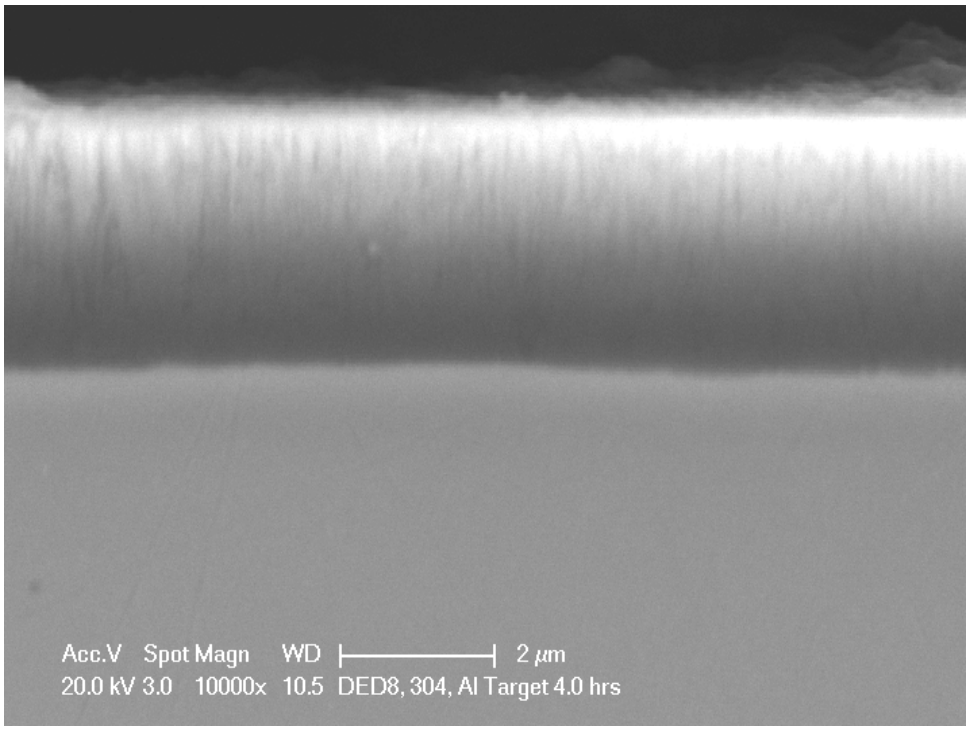

DED 8: Deposition time 4.0 hrs. Coating thickness 3.25 µm

Figure 1.43 (cont)
Transverse sections AlN coated samples showing variation of AlN thickness varying with the deposition time.

Conclusions

The advanced coatings deposited on 304 SS, P91, and Haynes 230 samples using the PEMS method at Vb = 60V and Id = 15A (DE3) exhibited cracks and surface defects.

A new deposition method, High Power Impulse Magnetrons Sputtering (HIPIMS), was evaluated to improve the quality of the coatings. Though this process produced dense and crack-free coatings, the coatings were found to be extremely brittle and unsuitable for long-term application.

A systematic coating deposition study revealed that the coating deposition rate play a major role in controlling the quality of the coating. The effect of deposition rate and bias voltage (bombardment) on the coating quality is being investigated.

Successfully deposited AlN, TiN, and TiSiCN diffusion barrier interlayer coatings on three substrate alloys.

Metallurgical examination of the samples after long-term thermal cycling exposure at 750ºC and 1010ºC showed disintegration of the AlN interlayer, while the other two interlayer coatings showed no evidence of degradation and/or disintegration.

The presence of either TiN or TiSiCN interlayer between the MCr coating and the substrate slowed the rate of Al consumption at both temperatures and prevented inward diffusion of Al from the coating into the substrate. The TiN interlayer is considered to be the best one for both iron- and nickel-based coating systems.

References

1. K. Coleman and D. Gandy; "*Weld Overlay of Waterwall Tubing, Alternate Materials and Distortion,*" EPRI, Palo Alto, CA, 1999, Report # TR-112643.

2. W. Bakker, "*Waterwall Wastage Root Causes: Or How to Predict Wasting Rates from Coal Chemistry,*" EPRI, Palo Alto, CA, 2005, Report # 1004737.

3. W. Bakker, "*Materials Solutions for Waterwall Wastage: An Update,*" EPRI, Palo Alto, CA, 2005, Report # 1009618.

4. W. Bakker, "*Mitigation of Fireside corrosion in Low NO_x Boilers: A State-of-the-Art Assessment of Material Solutions,*" EPRI, Palo Alto, CA, 1999, Report # TR112823.

5. W. Bakker, T. L. Banfield, and J. L. Blough, "*Long-Term Testing of Protective Coatings and Claddings at Allegheny Energy Supply's Ferry # 2 Boiler,*" EPRI, Palo Alto, CA, 2000, Report # 1000186.

6. T. Sherlock, C. H. Wells, R. B. Dooley, and R. Tilley, "*State-of-Knowledge Assessment for Accelerated Corrosion with Low NO_x Burners,*" EPRI, Palo Alto, CA, 1997, Report # TR1007775.

7. K. N. Strafford and R. Manifold, "Effects of Al Additions on the Sulfidation Behavior of Iron," *Oxidation of Metals*, Vol. 5, pp 85, 1972.

8. J. H. DeVan, and P. F Tororelli, "The Oxidation Sulfidation Behavior of Iron Alloy Containing 16-40 wt.% Aluminum," *Corrosion Science*, Vol. 35, pp1065, 1993.

9. S. W. Banovic, J. N. Dupont, and A. R. Marder, "*Evaluation of Low Aluminum Fe-Al Alloys for Use as Weld Overlay Coatings in Reducing Environments,*" Proceedings from the Materials Solution Conference '99 on Joining of Advanced and Specialty Materials, ASM International, Metals Park, OH, pp193, 1999.

10. J. R. Regina, J. N Dupont, and A. R. Marder, "*Weld Overlay Oxy-Fuel Thermal Spray Coatings for Corrosion Protection of Waterwalls in Fossil Fired Plants with Low NO_x Burners,*" ORNL Final Report #ORNL/Sub/95—SU604/04.

11. J. T. Murphy, J.R. Regina, R., M. Deacon, J. N. DuPont, and A. R. Marder, "*High Temperature Corrosion Resistance of Candidate FeAlCr Coatings in Low NO_x Environments,*" 19th Annual Conference on Fossil Energy Materials, May 14-16, 2005, Knoxville, TN.

12. *Lehigh Energy Update*, Vol. 22, July 2004.

13. N. S. Cheruvu, K. S. Chan, and R. Viswanathan, "Evaluation, Degradation, and Life Assessment of Coatings for Land-Based Turbines," *Energy Materials*, Vol. 1, pp 33, 2006.

14. D.J. Branagan, M. Britsameter, B. E. Meacham, and V. Belashchen, *"High Performance Nanoscale Composite Coatings for Boiler Applications,"* Submitted for journal publication.

15. Z. Liu, W. Gao, and Y. He; "Oxidation behavior of nanocrystalline Fe-Ni-Cr-Al alloy coatings, *Materials Science and Technology*, Vol. 15, pp 1447, 1999.

16. C. Zhang, X. Peng, J. Zhao, and F. Wang; "Hot Corrosion of an Electrodeposited Ni-11 wt.% Cr Nanocomposite Under Molten Na2SO4- K2SO4-NaCl," *Journal of the Electrochemical Society*, Vol. 152, pp B321, 2005.

17. N. S. Cheruvu, K. Chan, and R. Wei, "*Program on Technology Innovation: Computational Modeling and Assessment of Nanocoatings for Ultra Supercritical Boilers,"* EPRI Palo Alto and the U.S. Department of Energy, Pittsburgh, PA: 2008 Report # 1016181.

18 R. Viswanthan and R. Purgert, *"U.S. Program PM Materials and Technology for Ultra-Super-Critical Coal Fired Steam Power Plants,"* Proceedings of Creep 8, Eighth International Conference on Creep and Fracture at Elevated Temperatures, July 22-26, San Antonio, TX, Paper CREEP2007-26826, 2007, pp 1.

19. N. S. Cheruvu, R. P. Wei, M. R. Govindaraju, and D. Gandy, "Cyclic Oxidation Behavior and Microstructure of Nanocrystalline Ni-20Cr-4Al Coating," Accepted for publication, *Oxidation of Metals*.

20. N. S. Cheruvu, R. P. Wei, M. R. Govindaraju, and D. Gandy, "Evaluation of Nanocrystalline Coatings for Coal Fired Ultra-Supercritical Boiler Tubes," Proceedings of PVP-2009, ASME 2009 Pressure Vessel and Piping Conference, July 26-30, 2009, Prague, Czech Republic, Paper PVP2009-77092.

21. N. S. Cheruvu, R. P. Wei, M. R. Govindaraju, and D. Gandy, *"Microstructure and Oxidation behavior of Nanocrystalline 304SS-Alx Coatings,"* Presented at 36th International Conference on Metallurgical Coatings and Thin Films, IMCTF 2009, April 27–May 1, San Diego, CA.